

Study of charm/bottom ratio in non-photonic electron
 $\sqrt{s} = 200$ GeV(RUN6) via electron-hadron correlation
(PPG94)

Y .Morino, Y .Akiba^a, M. Leitch^c, K. Ozawa^b and S. Butsyk^c

CNS, University of Tokyo

a RIKEN

c LANL

b University of Tokyo

Contents

List of Figures	xiii
List of Tables	xvi
1 Introduction	1
2 Run and Track selection	3
2.1 Data files	3
2.2 Event and track cuts	3
2.2.1 Global cuts	3
2.2.2 hadron cuts	4
2.2.3 Normal electron cuts	4
2.2.4 Tight electron cuts	4
2.3 Good Run Selection	5
2.3.1 Hadron good run at MB data set	5
2.3.2 Electron good run at MB data set	6
2.3.3 Electron good run at PH trigger events	7
2.3.4 Electron good run in converter runs at RUN5	9
2.4 Momentum calibration for RUN6	14
3 Measurement of Heavy Flavor Electron	17
3.1 Invariant Yield	17
3.1.1 Integrated Luminosity	18
3.1.2 BBC Trigger Bias	18
3.2 Electron Identification	18
3.2.1 Detector Response	18
3.3 Inclusive Electron Spectrum	22
3.3.1 Reconstruction Efficiency for Electron	23
3.3.2 Trigger Efficiency	24
3.3.3 Hadron Contamination	25
3.3.4 Invariant Cross Section of Inclusive Electron	28
3.3.5 Systematic Errors	29
3.3.6 Absolute Normalization	32
3.4 Comparison with PPG65	33

4	Measurement of electrons from heavy flavor decays	39
4.1	Cocktail Method	39
4.1.1	Neutral Pions	40
4.1.2	Other Light Mesons	41
4.1.3	K_{e3} Decay	41
4.1.4	Photon Conversions	41
4.1.5	Direct Photon	42
4.1.6	Quarkonium and Drell-Yan	43
4.1.7	Implemented Cocktail in RUN5 and RUN6	43
4.1.8	Systematic Errors	43
4.2	Converter Method	48
4.2.1	Method to Subtract Photonic Electrons	49
4.2.2	R_γ and the Blocking Factor	49
4.2.3	R_{CN}	51
4.2.4	Converter Method for RUN6	51
4.2.5	Systematic Errors	52
4.3	Comparison of the Results from Two Methods	52
4.3.1	Photonic Electrons	52
4.3.2	Normalization of Cocktail	53
4.4	Results	54
4.4.1	RUN5 and RUN6 Results	54
4.4.2	Combined Result	54
5	Correlation analysis	61
5.1	Extraction Method	61
5.2	Electrons from e^+e^- Creation	63
5.3	Correlation Analysis at Real Data	63
5.4	Used Cut for the Correlation Analysis	64
5.5	Calculation of ϵ_{data}	65
5.5.1	Count of N_{tag}	65
5.5.2	Number of Electrons from Heavy Flavor	67
5.6	Systematic Error of ϵ_{data}	67
5.6.1	Subtraction of Like Sign Entries	68
5.6.2	Subtraction of Remaining Electron Pairs	69
5.6.3	Count of Electrons from Heavy Flavor	69
5.6.4	Other Contributions to N_{tag} Background	70
5.7	Results of ϵ_{data}	71
5.8	Simulation Study for Correlation Analysis	76
5.9	Simulation Overview	76
5.9.1	PYTHIA Simulation	76
5.9.2	EvtGen Simulation	76
5.9.3	PISA Simulation	77
5.10	Calculation of ϵ_c and ϵ_b	77

5.11	Systematic Errors for ϵ_c and ϵ_b	80
5.11.1	Geometrical Acceptance	80
5.11.2	Production Ratios of Charmed and Bottomed Hadrons	80
5.11.3	Branching Ratio	81
5.11.4	$b \rightarrow c \rightarrow e$ Process	81
5.11.5	Momentum Distribution of Charmed and Bottomed Hadrons	82
5.11.6	PYTHIA Uncertainty	83
5.11.7	Summary of Systematic Error for PYTHIA and EvtGen	84
5.12	ϵ_{data} , ϵ_c and ϵ_b	84
6	Result	91
6.1	$(b \rightarrow e)/(c \rightarrow e + b \rightarrow e)$ Results	91
6.1.1	BLUE Method in Correlation Analysis	91
6.1.2	Physical Constraint	92
6.1.3	Lower and Upper Limit	93
6.1.4	The Combined Result	93
6.2	Comparison of the Data with Simulation	94
6.3	Cross Section of Bottom	99
6.3.1	Invariant Cross Section of Electrons from Charm and Bottom	99
6.3.2	Total Cross Section of Bottom	99
A	Data Tables	109
B	Comparison Between Real Data and Simulation in RUN6	113
B.1	eID variables	113
B.2	Geometrical Acceptance	114
C	Correlation Function of Electron and Hadron	119
C.1	Correlation Function in Real Data	119
C.2	PYTHIA tuning status	120
D	Details of ϵ_c and ϵ_b	123
E	Air Conversion	127
F	Used RUN	133
F.1	RUN5	133
F.2	RUN6	135

List of Figures

2.1	Hadron yield in 0.4-5.0 GeV/ c per MB event at RUN5. black points show good runs and red points show bad runs.	6
2.2	Hadron yield in 0.4-5.0 GeV/ c per MB event at RUN6. black points show good runs and red points show bad runs.	7
2.3	Electron yield in 0.5-5.0 GeV/ c per MB event at RUN5. black points show good runs and red points show bad runs.	8
2.4	Electron yield in 0.5-5.0 GeV/ c per MB event at RUN6. black points show good runs and red points show bad runs.	9
2.5	The distribution of the ratio at RUN5, $Ratio_{PHMB} = (\text{number of MB\&PH triggered events in ERT data}) / (\text{number of MB\&PH triggered events in MB data})$	10
2.6	The distribution of the ratio at RUN6, $Ratio_{PHMB} = (\text{number of MB\&PH triggered events in ERT data}) / (\text{number of MB\&PH triggered events in MB data})$	10
2.7	PH triggered electron yield in 1.6-5.0 GeV/ c per sample MB event at RUN5. black points show good runs and red points show bad runs.	11
2.8	Dead map of EMCAL east in PH triggered events	11
2.9	Dead map of EMCAL east in PH triggered events	12
2.10	PH triggered electron yield in 1.6-5.0 GeV/ c per sample MB event at RUN6. black points show good runs and red points show bad runs.	12
2.11	Electron yield in 0.5-5.0 GeV/ c per MB event at RUN5 converter runs. black points show good runs and red points show bad runs.	13
2.12	PH triggered electron yield in 1.6-5.0 GeV/ c per sample MB event at RUN5 converter runs. black points show good runs and red points show bad runs. . . .	13
2.13	J/Ψ peak in RUN5 p+p	15
2.14	J/Ψ peak in RUN6 p+p without private correction	15
2.15	J/Ψ peak in RUN6 p+p with private correction	16
3.1	The distribution of n_0 with the standard eID cut without n_0 cut and the $0.5 < p_T < 5$ GeV/ c cut in the real data (square) and simulation (circle).	20
3.2	The distribution of $disp$ with the standard eID cut without $disp$ cut and the $0.5 < p_T < 5$ GeV/ c cut in the real data (square) and simulation (circle).	20
3.3	The distribution of $chi^2/npe0$ with the standard eID cut without $chi^2/npe0$ cut and the $0.5 < p_T < 5$ GeV/ c cut in the real data (square) and simulation (circle).	21

3.4	The distribution of <code>emcsdphi_e</code> with the standard eID cut without <code>emcsdphi(z)_e</code> cut and the $0.5 < p_T < 5$ GeV/ c cut in the real data (square) and simulation (circle).	21
3.5	The distribution of <code>emcsdz_e</code> with the standard eID cut without <code>emcsdphi(z)_e</code> cut and the $0.5 < p_T < 5$ GeV/ c cut in the real data (square) and simulation (circle).	22
3.6	The distribution of <code>prob</code> with the standard eID cut without <code>prob</code> cut and the $0.5 < p_T < 5$ GeV/ c cut in the real data (square) and simulation (circle).	23
3.7	The mean value of <code>ecore/mom</code> distribution with the standard eID cut as a fiction of electron p_T in the real data (square) and simulation (circle).	24
3.8	The sigma value of <code>ecore/mom</code> distribution with the standard eID cut as a fiction of electron p_T in the real data (square) and simulation (circle).	25
3.9	The distribution of <code>phi</code> with the standard eID cut and the $0.5 < p_T < 5$ GeV/ c cut in the real data in RUN5 (square) and simulation (circle).	26
3.10	The distribution of <code>zed</code> with the standard eID cut and the $0.5 < p_T < 5$ GeV/ c cut in the real data in RUN5 (square) and simulation (circle).	27
3.11	Electron efficiency as a function of electron p_T . Red points are electron efficiency and blue points are positron in RUN5. Black points are efficiency of electron and positron. Green line is a fit function of efficiency of electron and positron.	28
3.12	Electron efficiency as a function of electron p_T . Red points are electron efficiency and blue points are positron in RUN5. Black points are efficiency of electron and positron. Green line is a fit function of efficiency of electron and positron.	29
3.13	The ratios the number of electron in $0.8 < \text{ecore/mom} < 1.4$ with tight eID cut over that with standard eID cut as a function of electron p_T in RUN5.	30
3.14	The ratios the number of electron in $0.8 < \text{ecore/mom} < 1.4$ with tight eID cut over that with standard eID cut as a function of electron p_T in RUN6.	30
3.15	Raw spectra of electrons in RUN5 MB data. Blue circles show all electrons in MB data and red squares show 4X4c fired electrons.	30
3.16	Raw spectra of electrons in RUN6 MB data. Blue points show all electrons in RUN6 MB data and red squares show 4X4c fired electrons.	30
3.17	Trigger efficiency of 4x4c trigger in RUN5.	31
3.18	Trigger efficiency of 4x4c trigger in RUN6.	31
3.19	The distributions of <code>ecore/mom</code> in RUN5 MB data were used to study hadron contamination in $0.5 < p_T < 4.0$ GeV/ c	32
3.20	The <code>ecore/mom</code> distribution of electrons with tight eID cut and estimated that of hadron as described above in RUN5. Black points show the distribution of electron and blue points show estimated that of hadron.	33
3.21	Invariant cross section of inclusive electrons in RUN5 MB and PH triggered events. Blue circles show electrons in MB events and red squares show electrons in PH triggered events with standard eID cut. Green triangles show electrons in PH triggered events with tight eID cut.	34

3.22	Invariant cross section of inclusive electrons in RUN6 MB and PH triggered events. Blue circles show electrons in MB events and red squares show electrons in PH triggered events with standard eID cut. Green triangles show electrons in PH triggered events with tight eID cut.	35
3.23	The invariant $e^+ e^-$ mass peak in data sample.	35
3.24	The production of conversion electrons.	35
3.25	e^+e^- mass distribution in RUN5 PH fired events. Black points show the mass distribution when both electrons are applied all cuts and red points show the one when one electron is applied all cuts and the other is applied all cuts except n0 cut.	36
3.26	The ratio of invariant cross section of inclusive electrons in this analysis over PPG65 result.	36
3.27	The ratio of raw spectra in (1) over that in (2). See the text for the detail. . . .	37
3.28	the ratio of raw spectra in (1) over that in PPG65 analysis. See the text for the detail.	37
3.29	The ratio of invariant cross section of inclusive electrons in this analysis over PPG65 result with 1.03 correction.	38
4.1	Invariant differential cross section of (blue symbols at low p_T) and π^0 s (red symbols) together with a fit according to π^\pm Eq. 4.1 (left panel). Ratio of the data to the fit (right panel).	40
4.2	Measured direct photon spectrum (large symbols shown in red) compared with the cocktail parameterization (histogram indicated by small 'datapoints') for p+p collisions.	42
4.3	Invariant cross section of electrons from all sources considered in the RUN5 p+p cocktail	45
4.4	Invariant cross section of electrons from all sources considered in the RUN6 p+p cocktail	46
4.5	Individual contributions to the cocktail systematic error. The total error is depicted by the data points which are shown together with a fit.	47
4.6	Invariant yields of inclusive electrons in coveter and non-converter runs. Open symbols show the spectra in the converter run and closed symbols show the spectra in the non-converter run. Red squares show the results in PH data set and blue circles show the results in MB data set.	48
4.7	The ratios of the electron yield in the converter run over the non-converter run (R_{CN}) as a function of electron p_T in RUN5 MB data. The black line is $R_\gamma(p_T)$	51
4.8	The ratios of the electron yield in the converter run over the non-converter run (R_{CN}) as a function of electron p_T in RUN5 PH data. The black line is $R_\gamma(p_T)$	51
4.9	The ratio of measured/cocktail photonic electron spectra in RUN5. Blue circles show the ratios at MB data and red squares show the ratios in PH data. Dotted line show systematic error of the cocktail.	53

4.10	The ratio of measured/cocktail photonic electron spectra in RUN6. Blue circles show the ratios at MB data and red squares show the ratios in PH data. Dotted line show systematic error of the cocktail.	53
4.11	The systematic error of the cocktail. Black line show the total systematic error of the cocktail before the normalization of the cocktail.Red line shows the systematic error after the normalization.	54
4.12	The invariant cross section of electrons from heavy flavor decay in RUN5 MB and PH data. Circle points show the result from converter method and triangle points show the result from cocktail method. Open symbols show the result at MB data and closed symbols show the result at PH data. Closed squares show the result at PH data with tight eID cut.	57
4.13	The invariant cross section of electrons from heavy flavor decay in RUN6 MB and PH data. Circle points show the result from converter method and triangle points show the result from cocktail method. Open symbols show the result at MB data and closed symbols show the result at PH data. Closed squares show the result at PH data with tight eID cut.	58
4.14	The invariant cross section of electrons from heavy flavor decay in RUN6 PH data. Red points show the results from cocktail method and black points show the result at high p_T extension.	59
4.15	The invariant cross section of electrons from heavy flavor decay in RUN6 PH data. Red points show the results from cocktail method and black points show the result at high p_T extension.	59
4.16	The spectrum of the single non-photonic electrons in RUN5 and RUN6 with FONLL calculation [38].	60
5.1	A conceptual view of invariant mass distributions of unlike sign pairs and like sign pairs.	62
5.2	The invariant mass distribution of electron-hadron pairs in $ y < 0.4$, when the trigger electron is photonic electron. In left panels, black lines are unlike charge sign pairs and red lines are like charge sign pairs. Subtracted invariant mass distribution of electron-hadron pairs was shown in the right panels.	63
5.3	Phase spaces of positive charged hadron with the geometrical cut in RUN5.	64
5.4	M_{ee} distribution of unlike sign and like sign pairs of the selected electron and hadron in RUN6. Black points show unlike charge sign pairs and red points show like charge sign pairs.	65
5.5	Invariant mass distribution from trigger electrons and associated hadrons in RUN5. Black lines are unlike charge sign pairs and red lines are like charge sign pairs.	66
5.6	Invariant mass distribution from trigger electrons and associated hadrons in RUN6. Black lines are unlike charge sign pairs and red lines are like charge sign pairs.	67
5.7	Subtracted M_{eh} distribution of electron-hadron pairs (black points) and estimated M_{eh} distributions of the remaining electron pairs (red points) in RUN5.	68

5.8	Subtracted M_{eh} distribution of electron-hadron pairs (black points) and estimated M_{eh} distributions of the remaining electron pairs (red points) in RUN6.	69
5.9	Subtracted invariant mass distribution of electron-hadron pairs after subtraction of estimated remaining electron pairs in RUN5.	70
5.10	Subtracted invariant mass distribution of electron-hadron pairs after subtraction of estimated remaining electron pairs in RUN6.	71
5.11	The fraction of electron from heavy flavor decay in inclusive electrons in RUN5 as a function of electron p_T	72
5.12	The fraction of electron from heavy flavor decay in inclusive electrons in RUN6 as a function of electron p_T	72
5.13	The ratio of (unlike sign)/(like sign) M_{eh} distribution in mixing events in RUN5.	73
5.14	A conceptual view of the simulation study	76
5.15	Electron energy spectrum at $B \rightarrow e\nu X$ of EvtGen and CLEO [23].	78
5.16	Subtracted and normalized invariant mass distributions of electron-hadron pairs in charm and bottom production. Red points show charm case and blue points show bottom case. p_T range of trigger electrons is 2.0-3.0 GeV/c.	79
5.17	Subtracted and normalized invariant mass distributions of electron-hadron pairs in charm and bottom production. p_T range of trigger electrons is 3.0-4.0 GeV/c.	79
5.18	Subtracted and normalized invariant mass distributions of electron-hadron pairs in charm and bottom production. p_T range of trigger electrons is 4.0-5.0 GeV/c.	79
5.19	Subtracted and normalized invariant mass distributions of electron-hadron pairs in charm and bottom production. p_T range of trigger electrons is 5.0-7.0 GeV/c.	79
5.20	The spectra of the single electrons from charm and bottom at PYTHIA and FONLL [38]. Dark orange line and magenta line show the spectra from charm and bottom at PYTHIA. Green line and cyan line show the spectra of the electrons from charm and bottom at PYTHIA with weighting factor. Red line and blue lines show the spectra from charm and bottom at FONLL.	82
5.21	Conceptual view of the procedure to estimate contribution of jet fragmentation simulated by PYTHIA. Blue particles are D mesons and baryons simulated by EvtGen and green particles are jet fragmentation simulated by PYTHIA.	84
5.22	The correlation function of electrons and hadrons, when the trigger electrons were from heavy flavor. Black points show the result in RUN5 data obtained at SectionC and various lines show the result at PYTHIA with the parameter sets.	85
5.23	ϵ_c , ϵ_b and ϵ_{data} as a function of electron p_T in RUN5.	86
5.24	ϵ_c , ϵ_b and ϵ_{data} as a function of electron p_T in RUN6.	86
6.1	$(b \rightarrow e)/(c \rightarrow e + b \rightarrow e)$ in the electrons from heavy flavor as a function of electron p_T in RUN6 and RUN5 with FONLL calculation. Black points show the result in RUN6 and RUN5. Red lines are FONLL prediction and pink solid and dotted lines are uncertainty of FONLL prediction.	94
6.2	Comparison of the data with PYTHIA and EvtGen simulation about subtracted invariant mass distributions in RUN5. Electron p_T range is 2.0-3.0 GeV/c.	96

6.3	Comparison of the data with PYTHIA and EvtGen simulation about subtracted invariant mass distributions in RUN5. Electron p_T range is 2.0-3.0 GeV/c. . . .	96
6.4	Comparison of the data with PYTHIA and EvtGen simulation about subtracted invariant mass distributions in RUN5. Electron p_T range is 3.0-4.0 GeV/c. . . .	97
6.5	Comparison of the data with PYTHIA and EvtGen simulation about subtracted invariant mass distributions in RUN5. Electron p_T range is 3.0-4.0 GeV/c. . . .	97
6.6	Comparison of the data with PYTHIA and EvtGen simulation about subtracted invariant mass distributions in RUN5. Electron p_T range is 4.0-5.0 GeV/c. . . .	98
6.7	Comparison of the data with PYTHIA and EvtGen simulation about subtracted invariant mass distributions in RUN5. Electron p_T range is 4.0-5.0 GeV/c. . . .	98
6.8	Upper panel:Invariant cross sections of electrons from charm and bottom with FONLL calculation. Lower panel: The ratios of data points over FONLL prediction as a function of electron p_T	103
6.9	Invariant cross sections of electrons from bottom from FONLL calculation and PYTHIA. The simulations include electron from $b \rightarrow c \rightarrow e$ and $b \rightarrow e$. Black line show FONLL calculation. Other lines show PYTHIA with $1.5 < k_T < 10$ GeV/c. Dotted lines show electron from $b \rightarrow e$	104
6.10	Rapidity distribution of B hadron and electrons from bottom at PYTHIA. Black points show the distribution of electrons and blue points show that of B hadron.	104
6.11	Ratios of the rapidity distributions shown at Fig.6.10	104
6.12	$d\sigma^{b \rightarrow e}/dy _{y=0}$ with FONLL prediction as a function of rapidity.	105
6.13	$d\sigma_{b\bar{b}}/dy _{y=0}$ with FONLL prediction as a function of rapidity.	105
6.14	Rapidity distribution of bottom quark at HVQMNR using CTEQ5M as parton distribution function.	106
B.1	The distribution of <code>n0</code> with the standard eID cut without <code>n0</code> cut and the $0.5 < p_T < 5$ GeV/c cut in the real data (square) and simulation (circle).	113
B.2	The distribution of <code>disp</code> with the standard eID cut without <code>disp</code> cut and the $0.5 < p_T < 5$ GeV/c cut in the real data (square) and simulation (circle).	114
B.3	The distribution of <code>chi2/npe0</code> with the standard eID cut without <code>chi2/npe0</code> cut and the $0.5 < p_T < 5$ GeV/c cut in the real data (square) and simulation (circle).	114
B.4	The distribution of <code>emcsdphi_e</code> with the standard eID cut without <code>emcsdphi(z)_e</code> cut and the $0.5 < p_T < 5$ GeV/c cut in the real data (square) and simulation (circle).	115
B.5	The distribution of <code>emcsdz_e</code> with the standard eID cut without <code>emcsdphi(z)_e</code> cut and the $0.5 < p_T < 5$ GeV/c cut in the real data (square) and simulation (circle).	115
B.6	The distribution of <code>prob</code> with the standard eID cut without <code>prob</code> cut and the $0.5 < p_T < 5$ GeV/c cut in the real data (square) and simulation (circle).	116
B.7	The mean value of <code>ecore/mom</code> distribution with the standard eID cut as a function of electron p_T in the real data (square) and simulation (circle).	116
B.8	The sigma value of <code>ecore/mom</code> distribution with the standard eID cut as a function of electron p_T in the real data (square) and simulation (circle).	117

B.9	The distribution of ϕ with the standard eID cut and the $0.5 < p_T < 5$ GeV/ c cut in the real data in RUN6 (square) and simulation (circle).	117
B.10	The distribution of z_{ed} with the standard eID cut and the $0.5 < p_T < 5$ GeV/ c cut in the real data in RUN6 (square) and simulation (circle).	118
C.1	The $\Delta N/\Delta\phi$ distribution per the number of the trigger electrons, when the trigger electrons were the inclusive electrons. Black points shows the $\Delta N/\Delta\phi$ in real events and red points show the background.	120
C.2	The $\Delta N/\Delta\phi$ distribution per the number of the trigger electrons, when the trigger electrons were the photonic electrons. Black points shows the $\Delta N/\Delta\phi$ in real events and red points show the background	120
C.3	The correlation function of electron-hadrons when the trigger electrons are inclusive (black), photonic (red) and heavy flavor (blue).	121
C.4	The correlation function of electrons and hadrons at the tuned PYTHIA, when the trigger electrons were from charm and bottom. Red line shows the correlation function in the case of charm production and blue line shows that in the case of bottom production.	122
C.5	The correlation function of electrons and hadrons, where the trigger electrons are from heavy flavor. Black points show the result at RUN5 data obtained and green line shows the result at PYTHIA when we set R_b to 0.15.	122
E.1	Di-electron invariant mass distribution in RUN5 and RUN6 CNT ERT.	127
E.2	Invariant cross section of generated inclusive photon (black), photon from $\pi^0 \rightarrow \gamma\gamma$ (red), photon from $\eta \rightarrow \gamma\gamma$ (green) and direct photon (blue).	128
E.3	The p_T distribution of electrons from photon conversion. Normalization of p_T distribution was not done at this step.	129
E.4	$1 - \sigma_{conv}(k)/\sigma_{conv}(inf)$. Red points show the value taken from [13]. Black line show interpolate line	130
E.5	Invariant cross section of electrons from increasing air conversion due to the absence of He bag. Blue points show the electrons from increasing air conversion and green line shows the electrons from air conversion at $r < 30$ cm. Black line shows the total background electrons implemented as cocktail.	131
E.6	Invariant cross section of electrons from all sources considered in the RUN6 p+p cocktail	132

List of Tables

2.1	The measured mass and width, which was obtained from Gaussian fit, of J/Ψ at RUN5 and 6.	14
3.1	The eID cut used for the comparison of the variables.	19
3.2	The ratio of the number of entries at the simulation over that at real data	22
3.3	Estimated hadron contamination	27
3.4	Estimated hadron background	29
3.5	The efficiency of eID parameter at real data and the simulation	36
4.1	Radiation length (L) of each material near the interaction point. Conversion probability (P^{Conv}) is calculated for the case of electrons emitted from photon with $p_T = 1.0$ GeV/ c	50
4.2	Summary of error source	55
5.1	Result of fit for (mixing unlike sign)/(mixing like sign) by constant	69
5.2	ϵ_{data} and used values at each electron p_T range(RUN5)	74
5.3	ϵ_{data} and used values at each electron p_T range(RUN6)	75
5.4	PYTHIA tuning parameters	77
5.5	Result of ϵ_c	79
5.6	$D^+/D^0, D_s/D^0, \Lambda_c/D^0$ ratios from other experiments [16, 17, 18] and PYTHIA (default and tuned)	80
5.7	$B^+/B^0, B_s/B^0, B$ baryons/ B^0 ratios from other experiment [17] and PYTHIA (tuned)	81
5.8	Detail of charm and bottom decay for electron p_T 2-3 GeV/ c	87
5.9	The effect of $D^+/D^0, D_s/D^0, \Lambda_c/D^0$ changes on ϵ_c	88
5.10	The effect of B_s/B^0 and B baryons/ B^0 changes on ϵ_b	88
5.11	Branching ratio of D and B hadrons in P.D.G and EvtGen. The assigned uncertainties for the branching ratios and these effect on the ϵ_c and ϵ_b electron p_T 2-3 GeV/ c	89
5.12	Inclusive resonance D production in B decays at PDG and EvtGen	90
5.13	Summary of ϵ_c and ϵ_b	90
5.14	$\epsilon_{data}, \epsilon_c$ and ϵ_b	90
6.1	Summary of error source	92
6.2	Result of $(b \rightarrow e)/(c \rightarrow e + b \rightarrow e)$ in RUN5 and RUN6	95
6.3	χ^2/ndf (theoretical uncertainty is NOT included)	95

6.4	Invariant cross section of electrons from charm and bottom	99
6.5	Correction factors for p_T extrapolation and $b \rightarrow c \rightarrow e$ subtraction	101
6.6	Electron branching ratios of bottom hadrons	101
6.7	Correction factors for rapidity extrapolation	102
A.1	Invariant cross section of single non-photonic electrons from heavy flavor decays at $y=0$	110
A.2	The Data/FONLL ratios of single non-photonic electron yield at $y=0$	111
A.3	Result of $(b \rightarrow e)/(c \rightarrow e + b \rightarrow e)$ in RUN5 and RUN6	111
A.4	Invariant cross section of electrons from charm and bottom	112
D.1	Detail of charm and bottom decay for electron p_T 3-4 GeV/c	124
D.2	Detail of charm and bottom decay for electron p_T 4-5 GeV/c	125
D.3	Detail of charm and bottom decay for electron p_T 5-7 GeV/c	126

Chapter 1

Introduction

This analysis note describes the studies of charm/bottom ratio in non-photonic electron via partial reconstruction of $D^0 \rightarrow e^+ K^- \nu_e$ in p+p collisions at $\sqrt{s} = 200$ GeV at RUN5 and RUN6[1, 2]. Electrons with their transverse momentum $2.0 < p_T < 7.0$ GeV/ c were selected in this study, since the ratio of non-photonic electrons over photonic electrons is near 1[9].

Chapter 2

Run and Track selection

This chapter describes data sets and cut conditions.

2.1 Data files

CNT_ERT and CNT_MinBias nDST files of p+p collisions at $\sqrt{s} = 200$ GeV at RUN5 and RUN6 were analyzed.

pro.72 and pro.73 nDST files located at CCJ disk was analyzed for RUN5 analysis. Analysis code is located at

CCJ::/ccj/w/r02/ymorino/run5_ana/fin_ana/

pro.74 nDST files located at RCF was analyzed for RUN6 analysis by analysis train91. Analysis code is located at

https://www.phenix.bnl.gov/viewcvs/offline/AnalysisTrain/ehana_run6/

output files were located at

RCF::/phenix/hl/data67/phnxhl12/ehcorr_taxi_yuhei/taxi_2008/Run6pp200ERT/ ehana_run6_anatrain.ta (RUN6 ERT)

RCF::/phenix/hl/data67/phnxhl12/ehcorr_taxi_yuhei/taxi_2008/Run6pp200MinBias/ ehana_run6_anatrain.ta (RUN6 MinBias)

CCJ::/ccj/w/data53/eh-correlation/corr_data_run5_fin/ert (RUN5 ERT)

CCJ::/ccj/w/data53/eh-correlation/corr_data_run5_fin/mib (RUN5 MinBias)

2.2 Event and track cuts

2.2.1 Global cuts

Following cuts were applied for charged particle tracks at RUN5 and RUN6.

Zvtx cuts

$-25 < zvtx < 25$ (cm)

Track quality

quality >15 was required. Since this analysis is for p+p collisions, loose quality cut is applied.

Fiducial Cuts

Fiducial cuts for Drift chamber (DC) and Pad chamber1 (PC1) were applied for good agreement with simulation. Dead maps of DC and PC1 were described at Analysis note 615 for RUN5 and Analysis note 656 for RUN6.

2.2.2 hadron cuts

Following cuts are required for hadron tracks

p_T range

$$0.4 < p_T < 5.0 \text{ GeV}/c$$

electron veto

$$n_0 < 0$$

2.2.3 Normal electron cuts

MVD pipe Cuts

$(-1.37 < \phi_0 \ \&\& \ \phi_0 < 1) \ || \ (2.14 < \phi_0 \ \&\& \ \phi_0 < 4.51)$ is required for the removal of MVD service pipe region.

p_T range

$$p_T < 5.0 \text{ GeV}/c$$

Electrons with $p_T > 2.0 \text{ GeV}/c$ were selected for correlation analysis due to good ratio of non-photonics electrons over photonics electrons.

RICH variables

$$n_0 > 1$$

$$\text{disp} < 6$$

$$\text{chi}^2/n_{\text{pe}0} \leq 25$$

EMCal variables

$$|\text{emcsd}\phi_e| < 4 \ \&\& \ |\text{emcsd}z_e| < 4$$

$$1.4 > \text{ecore}/\text{mom} > 0.65 \ (p_T < 0.7 \text{ GeV}/c)$$

$$1.4 > \text{ecore}/\text{mom} > 0.7 \ (0.7 < p_T < 1 \text{ GeV}/c)$$

$$1.4 > \text{ecore}/\text{mom} > 0.75 \ (1 < p_T < 2 \text{ GeV}/c)$$

$$\text{prob} > 0.01$$

Matching parameters of EMC were recalibrated by private recalibrator.

2.2.4 Tight electron cuts

Tight electron cut was applied to identify high p_T ($> 5.0 \text{ GeV}/c$) electrons, since pion emitted Cerenkov light from $p_T > 4.7 \text{ GeV}/c$.

MVD pipe Cuts

$(-1.37 < \text{phi0} \ \&\& \ \text{phi0} < 1) \ || \ (2.14 < \text{phi0} \ \&\& \ \text{phi0} < 4.51)$ is required for the removal of MVD service pipe region.

 p_T range

$p_T < 9.0 \text{ GeV}/c$

RICH variables

$n0 > 1$

$n1 > 4$

$\text{disp} < 6$

$\text{chi2}/\text{npe0} \leq 25$

EMCal variables

$|\text{emcsdphi}_e| < 4 \ \&\& \ |\text{emcsdz}_e| < 4$

$1.4 > \text{ecore}/\text{mom} > 0.8$

$\text{prob} > 0.1$

2.3 Good Run Selection

2.3.1 Hadron good run at MB data set

RUN5 good runs

At first, good runs were selected for hadrons by studying the yields per MB event for each run.

Converter runs (run171595-172080) and high energy runs (run176417-176613) were removed from good runs.

Figure 2.1 show hadron yields in $0.4 < p_T < 5.0 \text{ GeV}/c$ per MB event ($N_{ch}(\text{run})$) as a function of runnumber at RUN5.

1. Mean of $N_{ch}(\text{run})$ in each good run ($\langle N_{ch} \rangle$) and RMS of $N_{ch}(\text{run})$ in good runs (σ) were obtained.
2. calculate the following ratio

$$\frac{|N_{ch}(\text{run}) - \langle N_{ch} \rangle|}{\sigma}$$

3. Remove runs which the ratio is above 2.5 from good runs.

The above procedure was continued, until no run was removed by the procedure.

In Fig.2.1, H and C represents high energy runs and converter runs respectively. In Fig 2.1, black points show good runs and blue points show bad runs. Red lines show $\langle N_{ch} \rangle$ and $\langle N_{ch} \rangle \pm 2.5 * \sigma$.

716 runs of 904 runs were selected as good runs by this procedure.

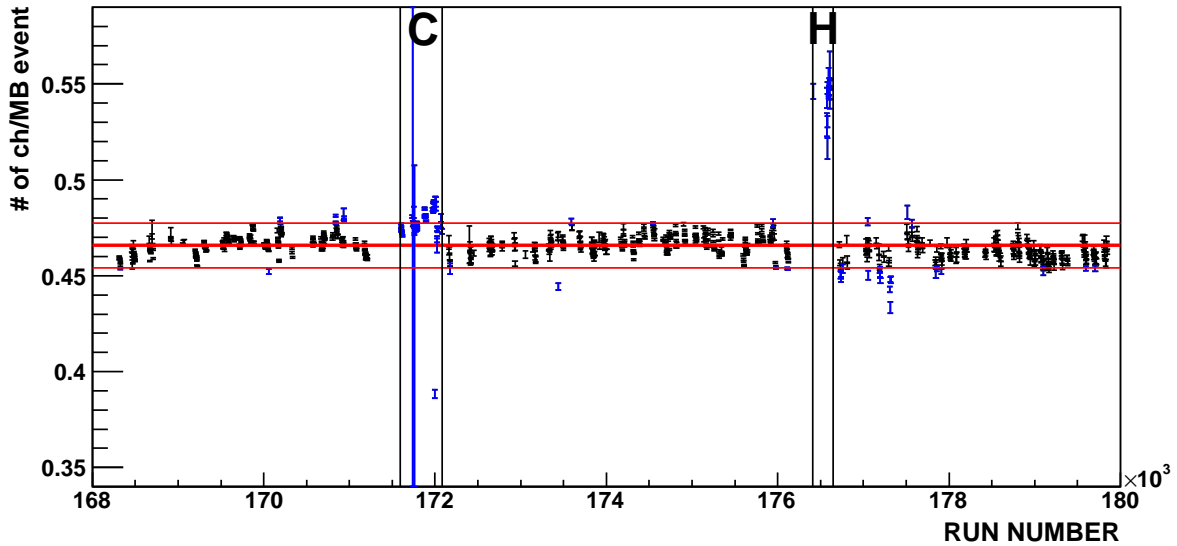


Figure 2.1: Hadron yield in 0.4-5.0 GeV/c per MB event at RUN5. black points show good runs and red points show bad runs.

RUN6 good runs

We apply the same procedure as RUN5 to select good runs in RUN6. Figure 2.2 show hadron yields in $0.4 < p_T < 5.0$ GeV/c per MB event ($N_{ch}(run)$) as a function of runnumber at RUN6. In Fig.2.2, H and C represents high energy runs and converter runs respectively. In Fig. 2.2, black points show good runs and blue points show bad runs. Red lines show $\langle N_{ch} \rangle$ and $\langle N_{ch} \rangle \pm 2.5 * \sigma$.

663 runs of 731 runs were selected as good runs by this procedure.

2.3.2 Electron good run at MB data set

RUN5 good runs

After good runs were selected by hadron yields, good runs were selected for electron by looking at electron yields per MB event. Figure 2.3 show electron yields in $0.5 < p_T < 5.0$ GeV/c per MB event ($N_{ele}(run)$) as a function of runnumber at RUN5. Electron yield in the MB after drops about 7% after run178937('L' region in Fig.2.3), since 2 RICH FEE modules became unstable. These runs are removed from good runs.

1. Mean of $N_{ele}(run)$ in each good run ($\langle N_{ele} \rangle$) and statistical errors of $N_{ele}(run)$ in good runs ($\sigma(run)$) were obtained.
2. calculate the following ratio

$$\frac{|N_{ele}(run) - \langle N_{ele} \rangle|}{\sigma(run)}$$

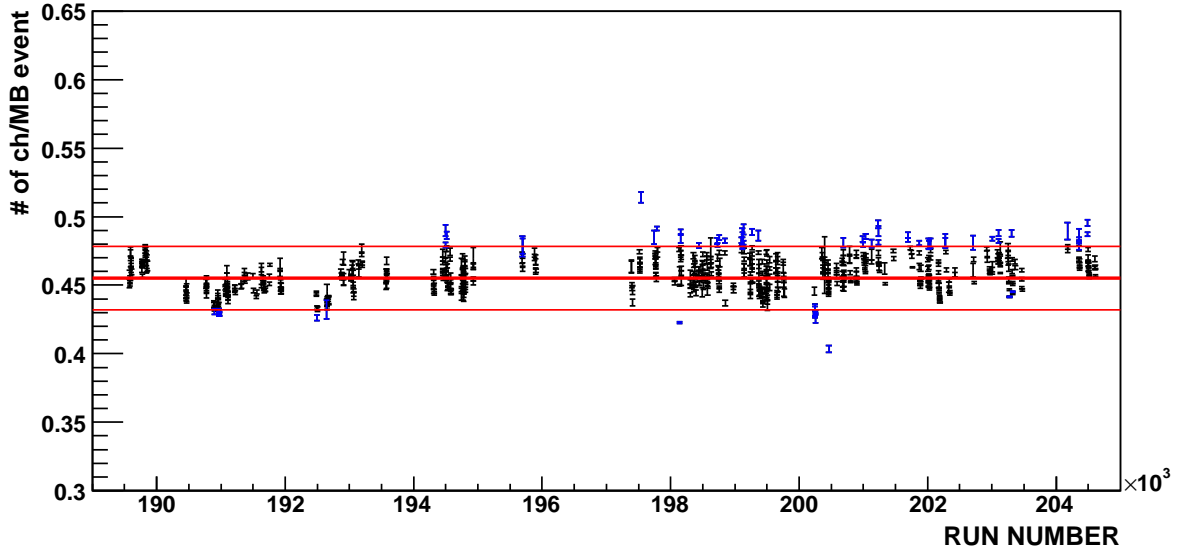


Figure 2.2: Hadron yield in 0.4-5.0 GeV/c per MB event at RUN6. black points show good runs and red points show bad runs.

3. Remove runs which the ratio is above 3 from good runs.

The above procedure was continued, until no run was removed by the procedure.

In Fig.2.3, black points show good runs and blue points show bad runs. Red lines show $\langle N_{ele} \rangle$. 613 runs were selected as good runs by this procedure. Electron yield in good runs is quite stable (χ^2/DOF is 697.4/613).

RUN6 good runs

Figure 2.4 show hadron yields in $0.5 < p_T < 5.0$ GeV/c per MB event as a function of runnumber at RUN6. In Fig.2.4, HBD represents HBD installed runs (run202500-end). These runs were removed from good runs at first. After that, we apply the same procedure as RUN5 to select good runs in RUN6.

In Fig.2.4, black points show good runs and blue points show bad runs. Red lines show $\langle N_{ele} \rangle$. 550 runs were selected as good runs by this procedure. Electron yield in good runs is quite stable (χ^2/DOF is 518.2/550).

2.3.3 Electron good run at PH trigger events

The procedure of selection of good runs similar to MB events were applied to the 4X4c triggered (PH trigger) events in the ERT data set.

To determine the electron yield per sampled event, we must know the number of sampled event in the data set. In this analysis, the number of sampled events was determined by PPG65 method[9].

The distribution of the ratio at RUN5 and RUN6, $Ratio_{PH_MB} = (\text{number of MB\&PH triggered})$

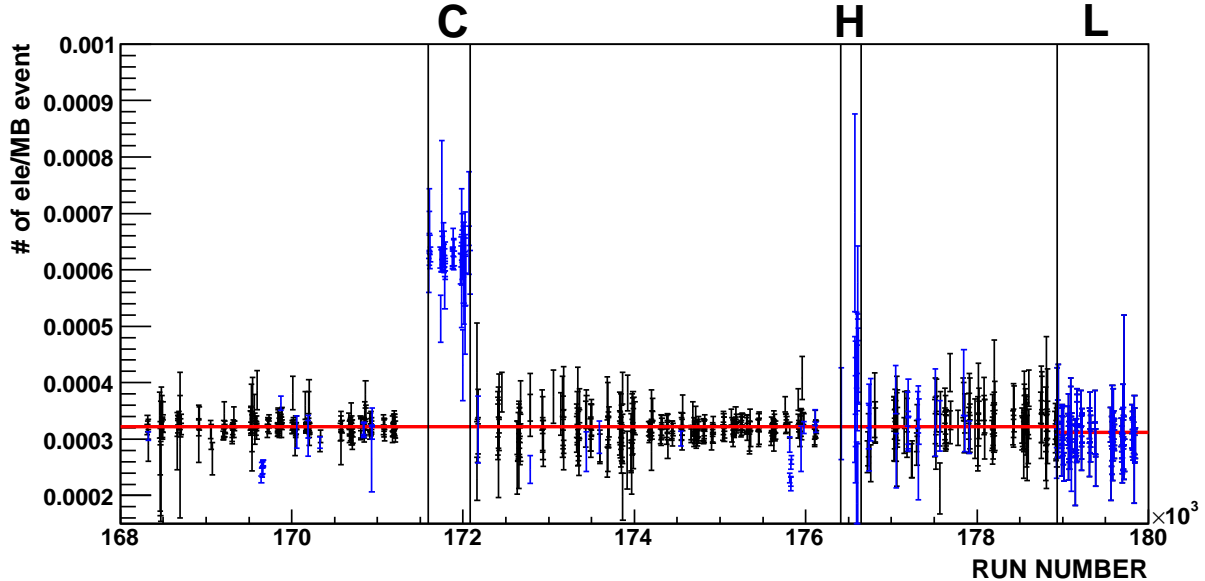


Figure 2.3: Electron yield in 0.5-5.0 GeV/c per MB event at RUN5. black points show good runs and red points show bad runs.

events in ERT data)/ (number of MB&PH triggered events in MB data) is shown at Figure 2.5 and Figure 2.6. The ratio should be 1 if the original data dataset is identical. However, when some of the run file segments are crashed during the data precessing, the ratio deviates from 1. We accept $0.5 < Ratio_{PH_{MB}} < 1.5$ runs.

RUN5 good runs

After good runs were selected by hadron and electron yields at MB data, good runs in ERT data set were selected by looking at electron yields which fire PH trigger per sample MB event. Figure 2.7 show PH triggered electron yields in $1.6 < p_T < 5.0$ GeV/c per sample MB event ($N_{ele}(run)$) as a function of runnumber at RUN5. The procedure to select good electron runs in MB data was applied for ERT data. In Fig.2.7, black points show good runs and blue points show bad runs. Red lines show $\langle N_{ele} \rangle$. 596 runs were selected as good runs by this procedure. These good runs were used in this analysis. Thus, 1.369880960×10^9 events in MB data set and $4.0809422848 \times 10^{10}$ sampled events in ERT data set were used for this analysis. Electron yield in good runs is quite stable (χ^2/DOF is 302.1/596). The ERT data set was divided into the following two run groups.

- **G1A** begin - 176573
- **G1B** 176574 - end

The PH trigger mask (4X4c) was slightly changed after RUN176754. We use G1A run group for converter analysis.

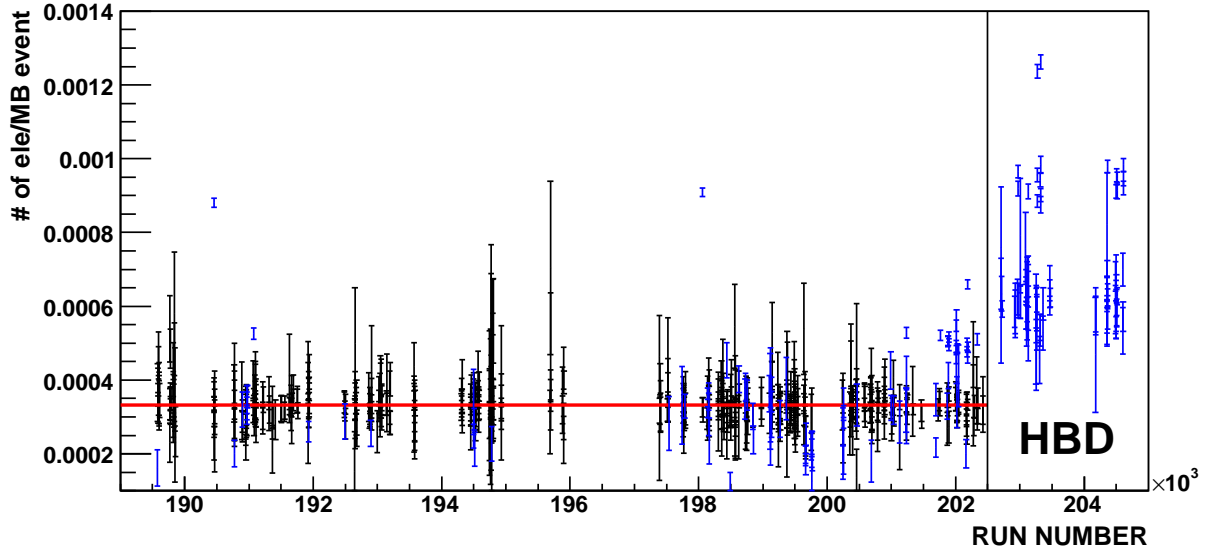


Figure 2.4: Electron yield in 0.5-5.0 GeV/ c per MB event at RUN6. black points show good runs and red points show bad runs.

RUN6 good runs

We apply the similar procedure to RUN5 to select good runs in RUN6. Since the PH trigger mask (4X4c) was changed at many times during RUN6, we apply offline mask for PH trigger instead of division several run groups to obtain stable trigger configuration.

Figure 2.8 and 2.9 show dead map of EMCAL east and west in PH triggered events with offline mask.

Figure 2.10 show PH triggered electron yields in $1.6 < p_T < 5.0$ GeV/ c per sample MB event ($N_{ele}(run)$) as a function of runnumber at RUN6. The procedure to select good electron runs in MB data was applied for ERT data. In Fig.2.10, black points show good runs and blue points show bad runs. Red lines show $\langle N_{ele} \rangle$. 501 runs were selected as good runs by this procedure. These good runs were used in this analysis. Thus, 1.38595083×10^8 events in MB data set and $9.7084454175 \times 10^{10}$ sampled events in ERT data set were used for this analysis. Electron yield in good runs is quite stable (χ^2/DOF is 311.6/511).

2.3.4 Electron good run in converter runs at RUN5

Electron good runs in converter runs at RUN5 in MB and ERT data set were selected by the above method.

Figure 2.11 show electron yields in $0.5 < p_T < 5.0$ GeV/ c per MB event ($N_{ele}(run)$) at RUN5 converter runs. Figure 2.12 show PH triggered electron yields in $1.6 < p_T < 5.0$ GeV/ c per sample MB event ($N_{ele}(run)$) at RUN5 converter runs. 51 runs in 58 runs were selected as good runs. This corresponds 8.6627032×10^7 events in MB data set and 3.544573696×10^9 sampled

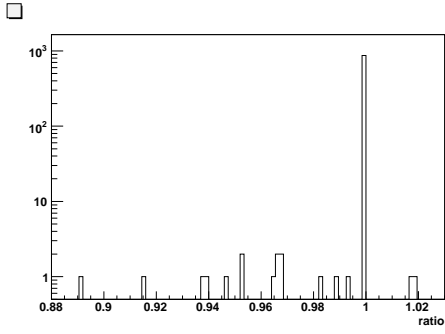


Figure 2.5: The distribution of the ratio at RUN5, $Ratio_{PHMB} = (\text{number of MB\&PH triggered events in ERT data}) / (\text{number of MB\&PH triggered events in MB data})$

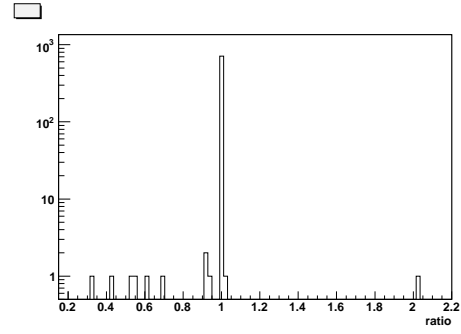


Figure 2.6: The distribution of the ratio at RUN6, $Ratio_{PHMB} = (\text{number of MB\&PH triggered events in ERT data}) / (\text{number of MB\&PH triggered events in MB data})$

events in ERT data set.

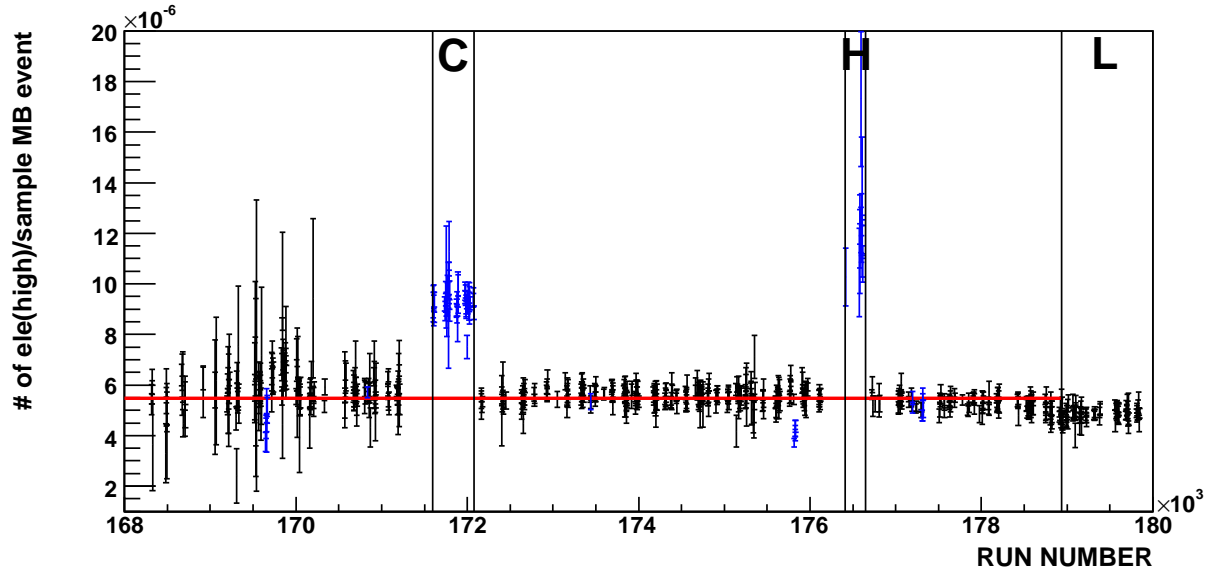


Figure 2.7: PH triggered electron yield in 1.6-5.0 GeV/c per sample MB event at RUN5. black points show good runs and red points show bad runs.

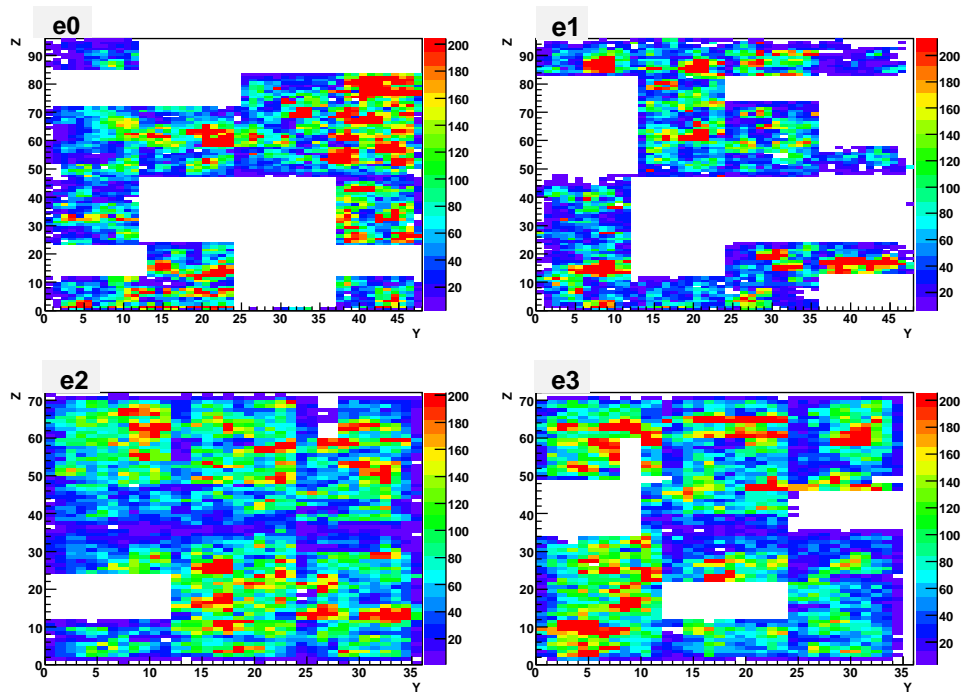


Figure 2.8: Dead map of EMCAL east in PH triggered events

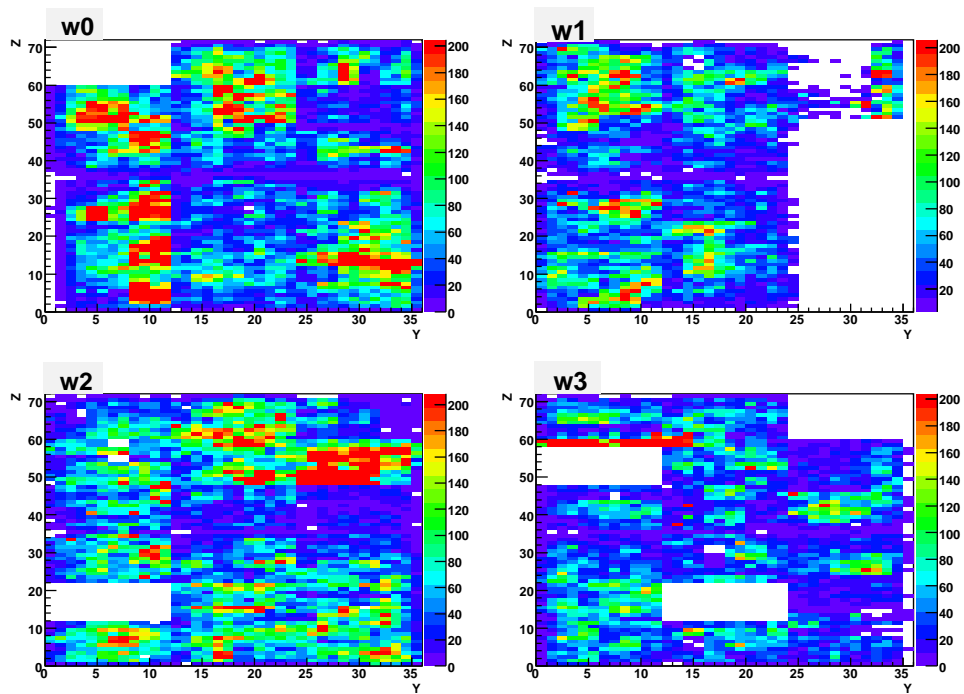


Figure 2.9: Dead map of EMCAL east in PH triggered events

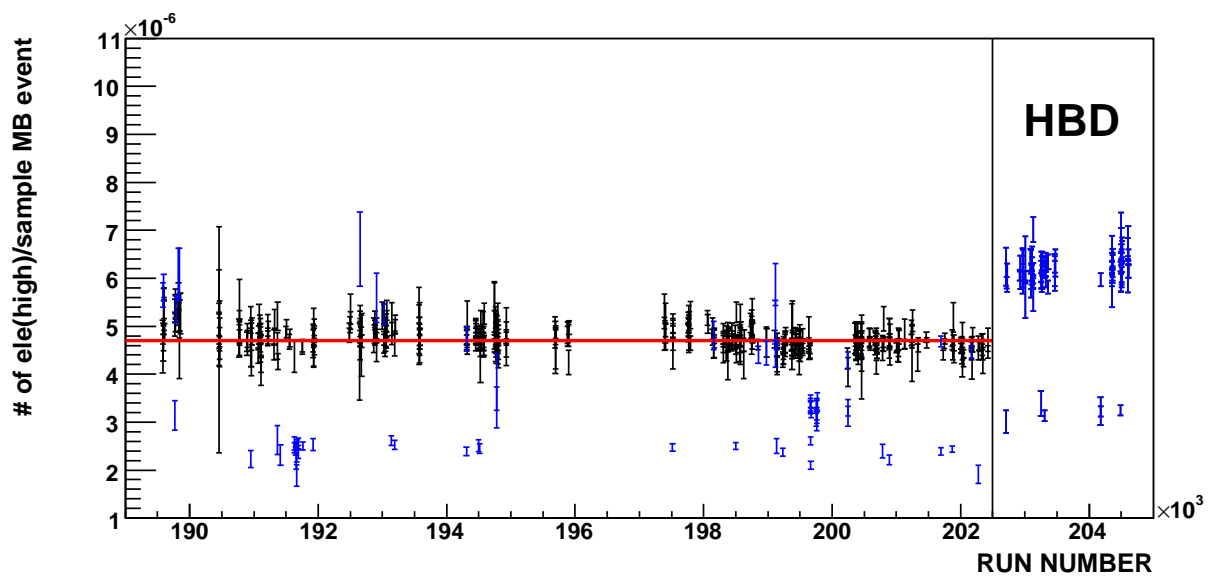


Figure 2.10: PH triggered electron yield in 1.6-5.0 GeV/c per sample MB event at RUN6. black points show good runs and red points show bad runs.

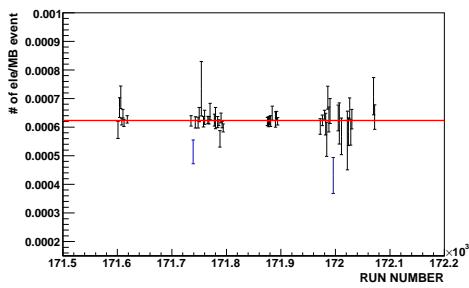


Figure 2.11: Electron yield in 0.5-5.0 GeV/ c per MB event at RUN5 converter runs. black points show good runs and red points show bad runs.

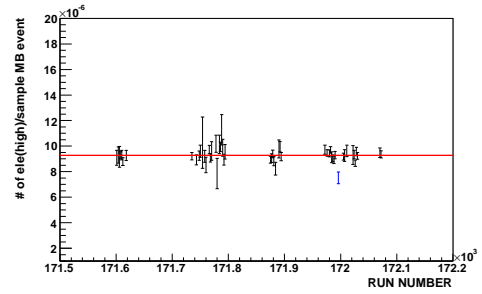


Figure 2.12: PH triggered electron yield in 1.6-5.0 GeV/ c per sample MB event at RUN5 converter runs. black points show good runs and red points show bad runs.

2.4 Momentum calibration for RUN6

The momentum recalibration including the beam offset correction and scale correction was applied by MasterRecalibrator for RUN6 p+p. The momentum scale factor is 0.97 at the current MasterRecalibrator for RUN6 p+p, which is estimated with TOF of protons[5]. However, the measured mass center of J/Ψ at RUN6 p+p was $3.061 \text{ GeV}/c^2$, which was 1% deviation from PDG value and the measured mass center of J/Ψ at RUN5 p+p. Thus, additional private momentum scaling correction of 1.013 was applied for RUN6 p+p analysis. Total momentum scaling factor was 0.982. This value is the same as the scaling factor used at χ_c analysis at RUN6 p+p[6].

Figure 2.13 shows the measured J/Ψ peak in RUN5 p+p. Figure 2.14 and Figure 2.15 shows the measured J/Ψ peak in RUN6 p+p without and with the private correction of 1.013. Red points show unlike charge sign electron pairs and blue points show unlike charge sign electron pairs at upper panels in Fig.2.13-2.15. Green points show net counts at lower panels in Fig.2.13-2.15. The measured mass and width, which was obtained from Gaussian fit, of J/Ψ at RUN5 and RUN6 are summarized at Table 2.1.

Table 2.1: The measured mass and width, which was obtained from Gaussian fit, of J/Ψ at RUN5 and 6.

RUN	Mass (GeV/c^2)	Width (GeV/c^2)
RUN5 p+p	3.100 ± 0.003	0.057 ± 0.003
RUN6 p+p without the private correction	3.061 ± 0.002	0.051 ± 0.002
RUN6 p+p with the private correction	3.100 ± 0.002	0.052 ± 0.002

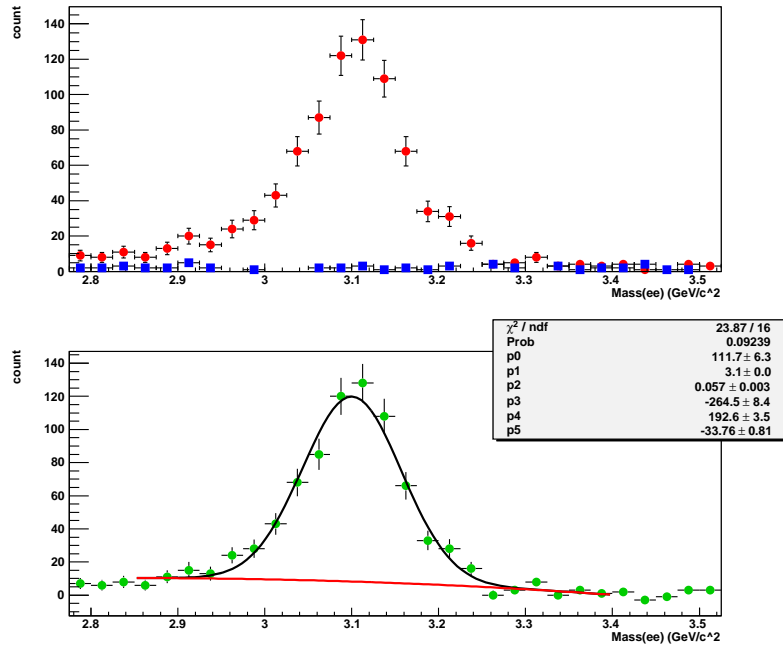


Figure 2.13: J/Ψ peak in RUN5 p+p

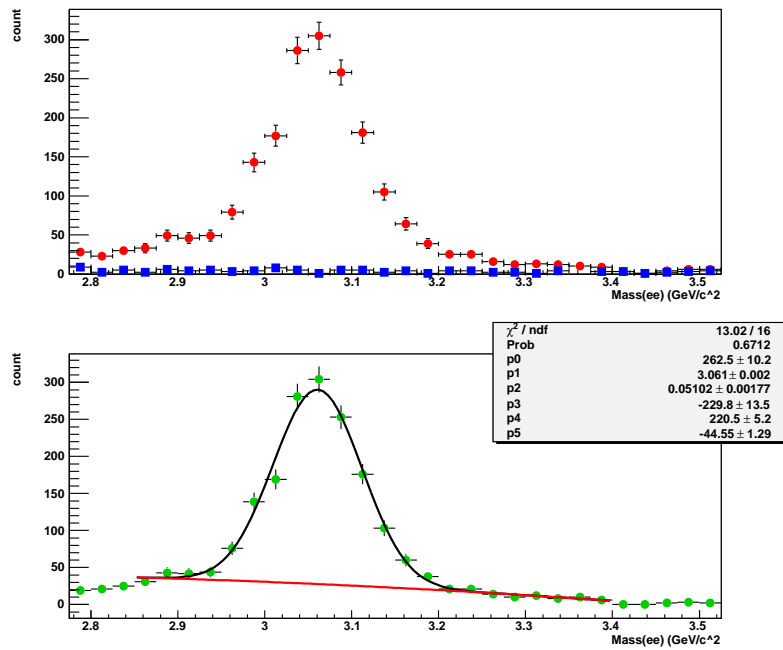


Figure 2.14: J/Ψ peak in RUN6 p+p without private correction

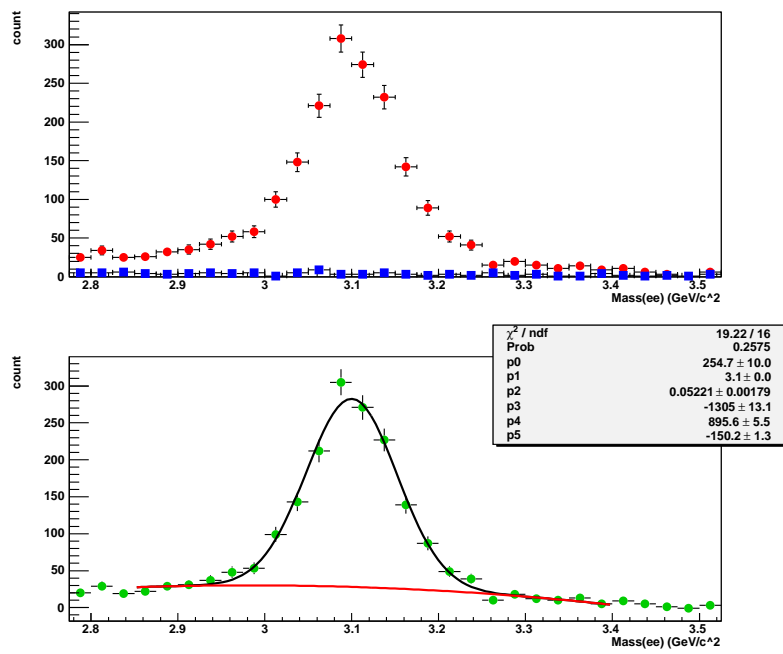


Figure 2.15: J/ψ peak in RUN6 p+p with private correction

Chapter 3

Measurement of Heavy Flavor Electron

This chapter describes measurement of inclusive electron in this analysis. Invariant cross section of inclusive electron in CNT_MinBias and CNT_ERT. 4X4c trigger is used for CNT_ERT analysis.

3.1 Invariant Yield

The invariant yield in Lorentz invariant form can be written as,

$$E \frac{d^3\sigma}{dp^3} = \frac{d^3\sigma}{p_T dy dp_T d\phi} = \frac{d^2\sigma}{2\pi p_T dp_T dy}, \quad (3.1)$$

where p is the momentum of the particle, y is the rapidity, $p_T = \sqrt{p_x^2 + p_y^2}$ is the transverse momentum, and ϕ is azimuthal angle.

The goal of this analysis is to obtain the invariant yield $d\sigma/dy$, differential cross section $d^2\sigma/dydp_T$ of the electrons from semi-leptonic decay of charm and bottom at mid-rapidity. Using the number of measured electrons, $d^2\sigma/dydp_T$ of the electrons can be extracted experimentally as follows.

$$\frac{1}{2\pi p_T} \frac{d^2\sigma}{dydp_T} = \frac{1}{2\pi p_T} \frac{N_e(p_T)}{\int L dt \epsilon(p_T) \epsilon_{bias} \Delta p_T \Delta y}, \quad (3.2)$$

where

- $N_e(p_T)$ is the number of reconstructed electrons in a p_T bin
- ϵ_{bias} is BBC trigger bias
- $\epsilon(p_T)$ is the overall efficiency including acceptance, reconstruction efficiency and trigger efficiency
- Δy is the rapidity bin width and is set to $\Delta y = 1$
- Δp_T is the p_T bin width
- $\int L dt$ is the integrated luminosity.

3.1.1 Integrated Luminosity

The integrated luminosity can be expressed using the number of minimum bias (MB) triggered events (N_{MB}).

$$\int Ldt = \frac{N_{MB}}{\sigma_{p+p}\epsilon_{BBC}^{p+p}}, \quad (3.3)$$

where σ_{p+p} is the cross section of inelastic p+p collisions at $\sqrt{s} = 200\text{GeV}$, and ϵ_{BBC}^{p+p} the BBC trigger (MB trigger) efficiency. The MB trigger cross section in p+p collisions, which is defined as $\sigma_{p+p}\epsilon_{BBC}^{p+p}$, is determined to be 21.8 ± 2.1 mb, by using a van der Meer scan measurement in Year-2002 RUN [30]. The MB trigger cross section in RUN5 and RUN6 is determined to be 23.0 ± 2.2 mb by making correction of BBC efficiency in RUN5 and RUN6 [9].

The equivalent number of sampled minimum bias events in the data taken with 4x4c ERT photon trigger (PH data), N_{MB}^{sample} instead of N_{MB} is used to obtain the integrated luminosity of PH data set. The *scale_down_factor* of 4x4c photon (PH) trigger, which represents the fraction of recorded MB events in triggered PH events, is determined and recorded at each run. N_{MB}^{sample} is determined as *scale_down_factor* \times N_{MB} .

3.1.2 BBC Trigger Bias

BBC trigger bias, ϵ_{bias} is PHENIX-specific term referring to the probability that the BBC counter makes MB trigger for an event containing specific particle of interest due to the acceptance of the BBCs. It is obvious that events with a hard parton scattering have higher probability of making BBC MB trigger because the track multiplicity in the BBC is higher for these events. This means that of all events that contain a hard scattering process, the apparent cross section of events which contain hard scattering will be higher than the BBC trigger cross section, $\sigma_{p+p}\epsilon_{BBC}^{p+p}$. The fact that the trigger cross section depends upon the physics process is what we term 'bias'.

ϵ_{bias} is determined to be 0.79 ± 0.02 as the p_T independent fraction for hard scattering process, from the yield ratio of high p_T π^0 with and without the BBC trigger [30]. This measured value of the constant BBC trigger bias is in good agreement with PYTHIA calculations of the BBC efficiency for hard pQCD partonic scattering processes.

3.2 Electron Identification

Electron identification is performed for the reconstructed particles by RICH and EMCal and is described in this section.

3.2.1 Detector Response

The variables used for the track reconstruction and the electron identification are studied in the real data and the simulation.

PISA Simulation

Detector simulation is performed PISA, using the GEANT3 simulator of the PHENIX detector. The PISA simulation is important in this analysis, since some of the correction factors are obtained from PISA simulation. To study the detector response with the PISA simulation, a single particle simulation for a sample of electrons is performed with the PISA simulation. CM- - magnetic field is used as the RUN5 configuration and CM++ magnetic field is used as the RUN6 configuration. Kinematic conditions of the generated single electron are as follows.

- Transverse momentum: $0. < p_T < 12.0$ GeV/ c (flat)
- Rapidity: $|y| < 0.5$ (flat)
- Azimuthal angle: $0 < \phi < 2\pi$ (flat)
- vertex z : $|\text{vertex } z| < 40$ cm

Distributions of each variable in simulation which characterizes detector response are weighted according to the input p_T , so that the distribution of the input p_T have a realistic p_T distribution of electrons.

Comparison Between Real Data and Simulation

Table 3.1: The eID cut used for the comparison of the variables.

Used cut	Compared variable					
	n0	disp	npe0/chi2	emcsdphi(z)_e	ecore/mom	prob
n0 >= 2	×(n1 >= 1)	○	○	○	○	○
disp < 6	○	×	○	○	○	○
npe0/chi2 < 25	○	○	×	○	○	○
emcsdphi(z)_e < 4	○	○	○	×	○	○
1.4 > ecore/mom > 0.65 ~ 0.8	○	○	○	○	×	○
prob > 0.01	○	○	○	○	○	×

The distributions of the variables for the electron identification in the PISA simulation are compared to those of the real data. The applied cuts for the comparison of each variable are summarized at Table 3.1. Electron sample with $0.5 < p_T < 5$ GeV/ c is selected for this comparison. Electron sample for the comparison is selected by the the 'standard eID' without the cut for the compared variable. $n1 \geq 1$ and $0.8 < \text{ecore/mom} < 1.4$ cut is used instead of $n0$ cut for the $n0$ comparison.

Figure 3.1, 3.2 and 3.3 show the distributions of RICH variables, $n0$, disp and chi2/npe0 at each RICH sector, respectively. In addition, Figure 3.4, 3.5 and 3.6 show the distributions of EMCal variables at each sector, emcsdphi_e , emcsdz_e and prob , respectively. Figure 3.7 and 3.8 show mean and sigma values of ecore/mom distributions as a function of electron p_T . In

Fig. 3.1-3.8, black squares show the results from the real data in RUN5 and red circles show these from the PISA simulation with RUN5 tuning parameters and CM- - field. The distribution in simulation is normalized by the number of entries at each sector. The distributions of the simulation and these of the real data match well. The difference of the efficiency of the cut for the each variable between the real data and the simulation is less than 1%, as described in Sec.3.3.5. The comparison between real data and simulation in RUN6 is described in Sec.B.1

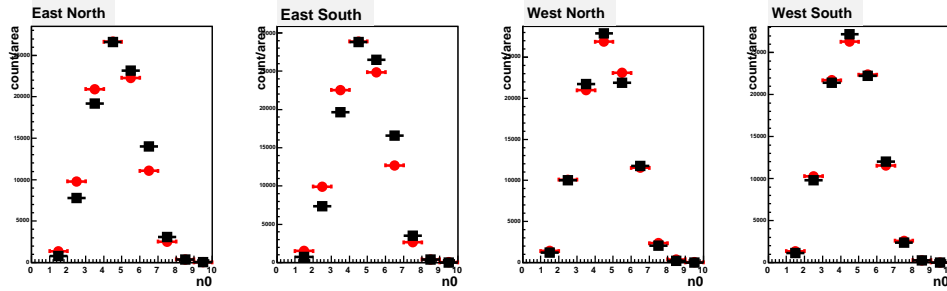


Figure 3.1: The distribution of n_0 with the standard eID cut without n_0 cut and the $0.5 < p_T < 5$ GeV/ c cut in the real data (square) and simulation (circle).

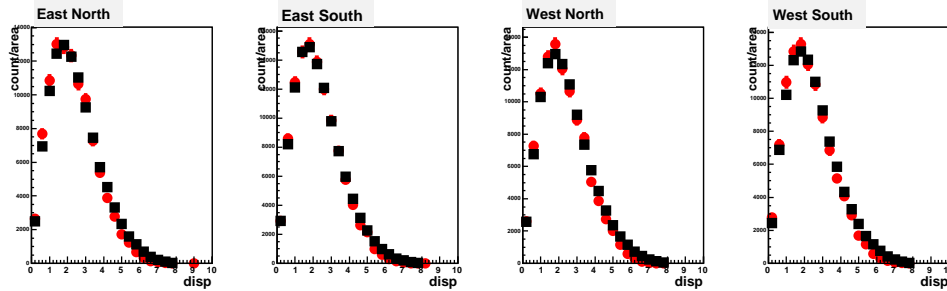


Figure 3.2: The distribution of $disp$ with the standard eID cut without $disp$ cut and the $0.5 < p_T < 5$ GeV/ c cut in the real data (square) and simulation (circle).

Acceptance Evaluation for eID

Detector area with low efficiency, dead or noisy is removed from the data analysis by fiducial cut. The same fiducial cut is also applied for the simulation to make the geometrical acceptance of the simulation identical as that of the real data, so that the reconstruction efficiency is evaluated from the simulation. The distributions of ϕ , zed of the simulation are compared with these of the real data for the electron samples selected by the standard eID and a transverse momentum with $0.5 < p_T < 5$ GeV/ c . Figure 3.9 shows the distributions of ϕ at North (top panel) and South (bottom panel) sector, and Figure 3.10 shows the distributions of zed at East (top panel) and West (bottom panel) sector. In Fig. 3.9 and 3.10, black squares show the real data in RUN5 and red circles show the PISA simulation with RUN5 tuning parameters and CM- - field. The

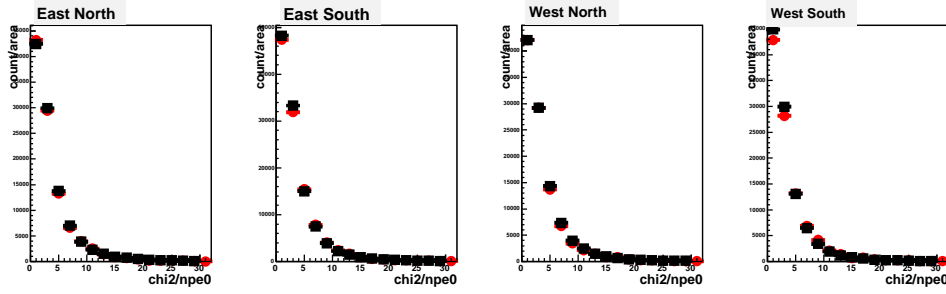


Figure 3.3: The distribution of $\chi^2/npe0$ with the standard eID cut without $\chi^2/npe0$ cut and the $0.5 < p_T < 5$ GeV/ c cut in the real data (square) and simulation (circle).

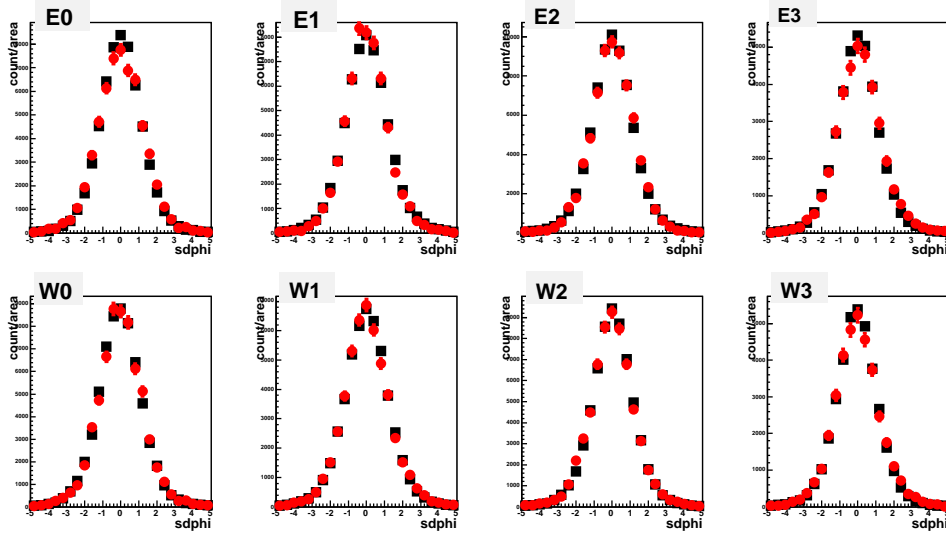


Figure 3.4: The distribution of $emcsdphi_e$ with the standard eID cut without $emcsdphi(z)_e$ cut and the $0.5 < p_T < 5$ GeV/ c cut in the real data (square) and simulation (circle).

distributions of simulation are normalized by number of entries in the reference regions, where are little low efficiency, dead or noisy area. In Fig 3.9 and 3.10, the used reference region to normalize is region 1. The ratio of the number of entries in the simulation over that in the real data except for the reference region used for the normalization is calculated for each reference region. The same procedure is done for the real data in RUN6 and the simulation with RUN6 tuning parameters and CM++ field. The distribution of ϕ , zed in RUN6 is described at Sec. B.2 The results of the ratios in RUN5 and RUN6 are summarized at Table 3.2. The geometrical acceptance of the PISA simulation agrees with the real data within 3%.

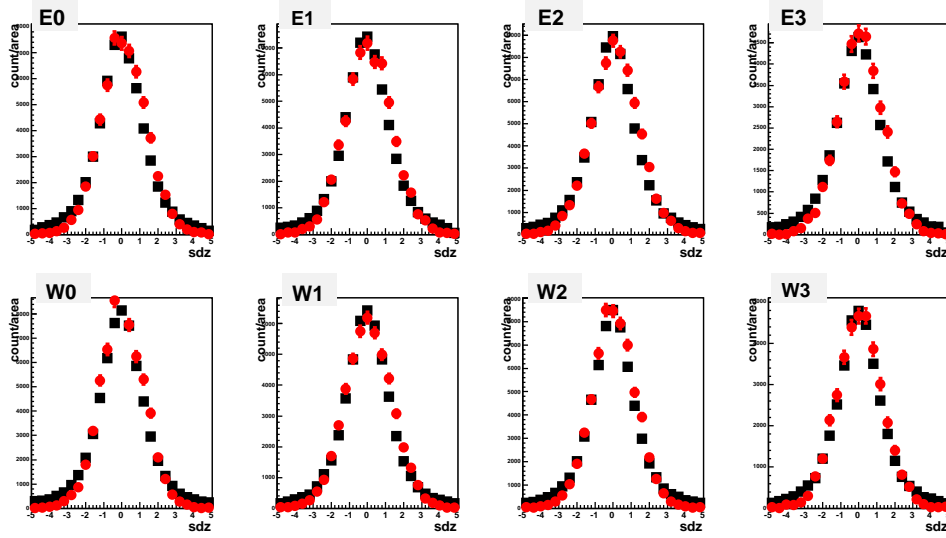


Figure 3.5: The distribution of $emcsdz_e$ with the standard eID cut without $emcsdphi(z)_e$ cut and the $0.5 < p_T < 5$ GeV/c cut in the real data (square) and simulation (circle).

Table 3.2: The ratio of the number of entries at the simulation over that at real data

reference region	the simulation/real (RUN5)	the simulation/real (RUN6)
region 1	0.98	1.01
region 2	0.97	0.97
region 3	0.98	1.01
region 4	0.99	0.98

3.3 Inclusive Electron Spectrum

Invariant yield of inclusive electron is obtained using Eq. 3.2 and this procedure is described in this section. In Eq 3.2, $\epsilon(p_T)$, which is the overall efficiency including acceptance, reconstruction efficiency and trigger efficiency, can be written as follows in MB and PH data.

$$\epsilon(p_T) = A \times \epsilon_{eff}(p_T) \quad (\text{MBdata}), \quad (3.4)$$

$$\epsilon(p_T) = A \times \epsilon_{eff}(p_T) \times \epsilon_{trig}(p_T) \quad (\text{PHdata}), \quad (3.5)$$

where $A \times \epsilon_{eff}(p_T)$ is the acceptance times the reconstruction efficiency for electrons and $\epsilon_{trig}(p_T)$ is the 4x4c (PH) trigger efficiency.

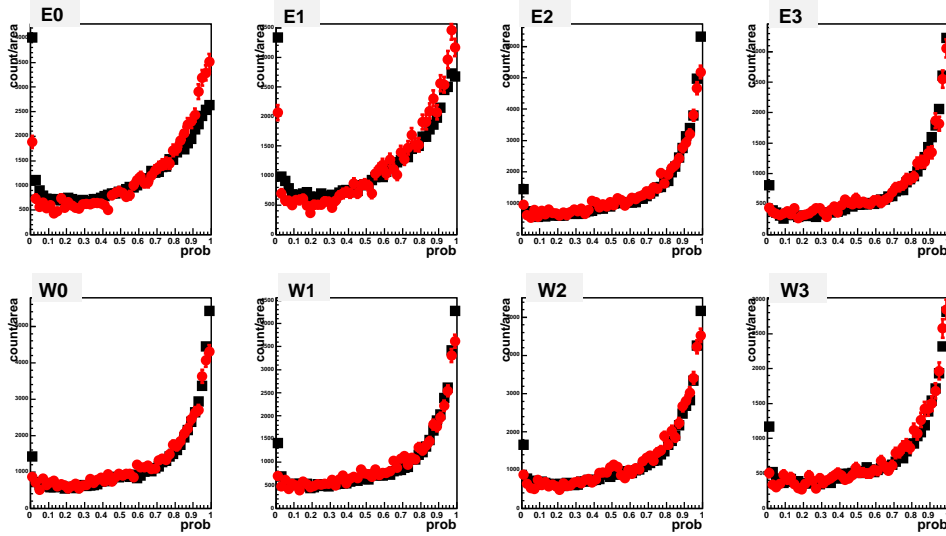


Figure 3.6: The distribution of prob with the standard eID cut without prob cut and the $0.5 < p_T < 5$ GeV/c cut in the real data (square) and simulation (circle).

3.3.1 Reconstruction Efficiency for Electron

Reconstruction Efficiency with Standard eID Cut

$A \times \epsilon_{eff}(p_T)$ with the standard eID cut is determined by the PISA simulation. The simulation sample described in Sec. 3.2.1 is used. $A \times \epsilon_{eff}(p_T)$ is determined as bellow.

$$A \times \epsilon_{eff}(p_T) = \frac{\text{output with standard eID cut}(p_T)}{\text{input}(p_T) \times w(p_T)}, \quad (3.6)$$

where $w(p_T)$ is the weighting factor which is used so that the input distribution of p_T in the simulation have the realistic form for inclusive electrons. Figure 3.11 shows the result of the geometrical acceptance times electron reconstruction efficiency as a function of electron p_T in RUN5. Figure 3.12 also shows the result of the geometrical acceptance times electron reconstruction efficiency in RUN6. Red points show electron efficiency and blue points show positron. Black points show efficiency of electron and positron. Green line is a fit function of efficiency of electron and positron. Fit function is

$$p_0 + \frac{p_1}{p_T} + \frac{p_2}{p_T^2} + p_3 \times p_T + p_4 \times p_T^2. \quad (3.7)$$

The fit function is used as the efficiency curve of electron and positron.

Reconstruction Efficiency with Tight eID

In p_T above 4.85 GeV/c, pions start emitting Cerenkov light in CO2 gas in the RICH detector. Since rejection power of RICH is reduced, the tight eID cut, as is defined at Sec 2.2.3 is applied above 5 GeV/c.

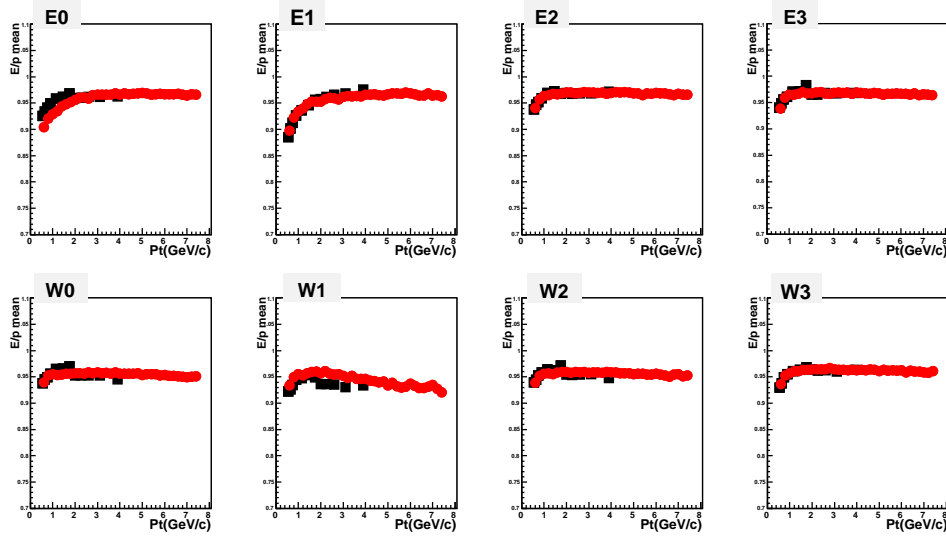


Figure 3.7: The mean value of $ecore/mom$ distribution with the standard eID cut as a function of electron p_T in the real data (square) and simulation (circle).

The tight eID cut requires $n1 > 4$ and $prob > 0.1$ in addition to the standard eID cut. Efficiency of tight eID cut is calculated as bellow.

$$\epsilon_{tight}(0.8 < ecore/mom < 1.4) = \epsilon_{standard}(0.8 < ecore/mom < 1.4) \times R_{tight}, \quad (3.8)$$

where R_{tight} is the efficiency corresponding to the additional cuts in the tight eID cut ($prob > 0.1$ and $n1 > 4$). R_{tight} is determined from the ratio of the number of electron in $0.8 < ecore/mom < 1.4$ with the tight eID cut over that with the standard eID cut in the real data. Figure 3.13 and Figure 3.14 show the ratios as a function of electron p_T in RUN5 and RUN6, respectively. These figures indicate the ratio is independent of the p_T in $2.0 < p_T < 5.0$ GeV/c and then it drops. The constant behavior below 5.0 GeV/c is due to independence of $n1$ and $prob$ cut on electron p_T . The drop is due to large hadron contamination in electron with standard eID cut. Therefore, R_{tight} itself is expected to be independent of p_T even above 5.0 GeV/c. In Fig.3.13 and Fig.3.14, black line is a constant value fit to the ratios in $2.0 < p_T < 5$ GeV/c. The fitted values are used as relative efficiency. The values are 0.587 ± 0.003 and 0.599 ± 0.002 for RUN5 and RUN6, respectively.

3.3.2 Trigger Efficiency

Figure 3.15 and 3.16 show raw spectra of electrons with the standard eID cut in RUN5 MB and RUN6 MB data, respectively. In Fig. 3.15 and 3.16, blue circles show all electron in MB data and red squares show 4x4c fired electrons. 4x4c trigger efficiency is determined as a ratio of PH fired electrons over measured electrons in MB data. Figure 3.17 and 3.18 shows the determined efficiency of PH trigger in RUN5 and RUN6.

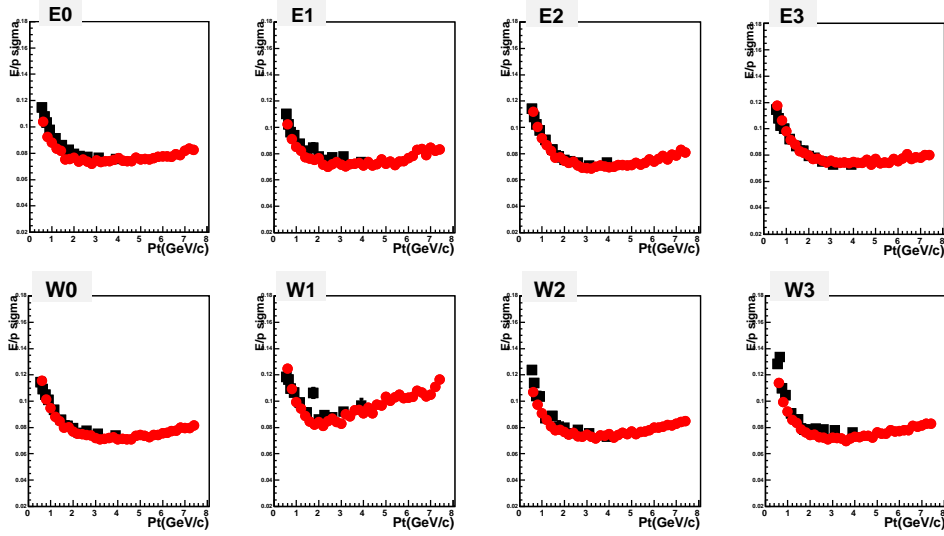


Figure 3.8: The sigma value of ecore/mom distribution with the standard eID cut as a function of electron p_T in the real data (square) and simulation (circle).

The solid curves in Fig. 3.17 and Fig. 3.18 are the fitted functions with the following parameterization:

$$\frac{p_0}{1 + p_3} \times (p_3 + \tanh(p_1 \times (p_T - p_2))). \quad (3.9)$$

These fitted functions are used for the efficiency of PH trigger in RUN5 and RUN6.

3.3.3 Hadron Contamination

Hadron contamination in the electrons selected with the standard eID cut using estimated via ecore/mom distribution. The distribution of ecore/mom has a peak around one in the case of the electron peak, while the hadron track has a small ecore/mom value.

Hadron Contamination below 5GeV/c

The idea is to use **prob** cut is to enrich the hadron contamination. The **prob** > 0.01 cut has about 50% hadron efficiency for $p_T > 1$ GeV/c and 99% efficiency to electrons. Therefore, the hadron contamination is increased by a factor of 100 if we reverse the **prob** cut (**prob** < 0.01). Then we can look at the ecore/mom distribution to see much enhanced hadron contamination.

The procedure we used is the following:

Two ecore/mom distributions of inclusive charged particles are prepared as the distributions of hadrons. (H_a) is the ecore/mom distribution of hadrons with **prob** < 0.01 (rejected sample) and (H_b) is the ecore/mom distribution of hadrons with **prob** > 0.01 (accepted sample).

We also make ecore/mom distribution of electron candidate with the reverse cut (**prob** < 0.01) and with normal cut (**prob** > 0.01). The former (E_a) contains large hadron contamination, and the latter (E_b) is the normal electron candidate sample. For both samples, the standard eID cuts except the **prob** cut is applied. The distribution of rejected hadron sample (H_a) is scaled

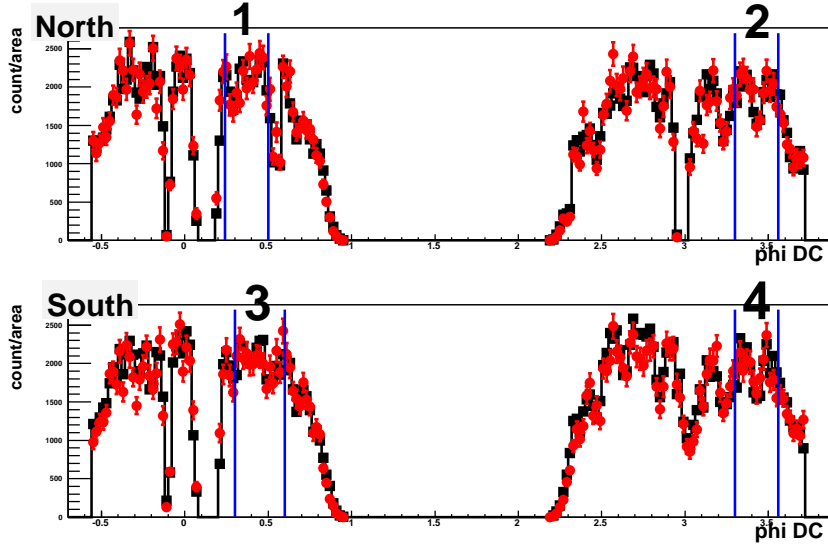


Figure 3.9: The distribution of phi with the standard eID cut and the $0.5 < p_T < 5 \text{ GeV}/c$ cut in the real data in RUN5 (square) and simulation (circle).

by a factor of f_h and the distribution of the accepted electron candidate (E_b) by a factor of f_e corresponding to the efficiency of the **prob** cut, so that sum of these two distribution reproduces the **ecore/mom** distribution of the rejected electron sample (E_a).

$$E_a \sim f_e \times E_b + f_h \times H_a, \quad (3.10)$$

When $f_e \times E_b + f_h \times H_a$ is roughly consistent with E_a , the $f_e \times E_b$ term corresponds to the real electron component in E_a , and the $f_h \times H_a$ term is the hadron component in E_a . Since $f_h \times H_a$ presents the hadron contamination in the rejected electron sample, the hadron contamination in accepted electron sample should be presented as the distribution $f_h \times H_b$ by using the fixed normalization factor f_h . In this way, the hadron contamination in the accepted electron sample can be determined as $(f_h \times H_b)/E_b$.

Figure 3.19 shows the comparison of the **ecore/mom** distribution in RUN5 MB data produced by this procedure. The four panels in the figure correspond to four different p_T bins. In each panel, the green histogram is the **ecore/mom** distribution of the rejected hadron (H_a), the black histogram is the distribution of the accepted electron sample (E_b) scaled by a factor of $f_e = 0.02$. The blue histogram is the sum of the two. The red histogram is the distribution of rejected electrons (E_a) and the magenta histogram is the distribution of accepted hadrons (H_b), which represents hadron contamination in the selected electrons with standard eID cut. The same rescaling factor f_h is used for all panels. The sum of the two distribution roughly reproduces the rejected electron distribution as described in Eq. 3.10.

The same comparison is done for ERT data to study the hadron contamination in the electrons with $2.0 < p_T < 5.0 \text{ GeV}/c$. The results of the estimation of hadron contamination in MB and ERT data are summarized at Table 3.3.

Hadron contamination is less than 1% for $0.7 \text{ GeV}/c < \text{electron } p_T < 4.5 \text{ GeV}/c$. In 4.5-5.0 GeV/c range, hadron contamination becomes about 2%, since pions start emitting Cerenkov

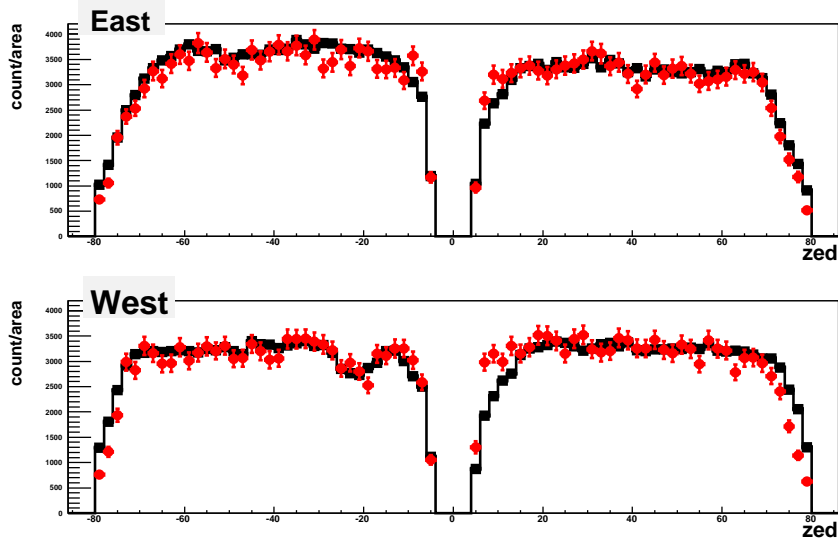


Figure 3.10: The distribution of zed with the standard eID cut and the $0.5 < p_T < 5$ GeV/ c cut in the real data in RUN5 (square) and simulation (circle).

light in CO₂ gas in RICH detector above 4.85 GeV/ c .

Table 3.3: Estimated hadron contamination

electron p_T range	hadron contamination(RUN5)	hadron contamination(RUN6)
0.5-0.7 GeV/ c	0.0123	0.0147
0.7-1.0 GeV/ c	0.0074	0.0089
1.0-2.0 GeV/ c	0.0042	0.0052
2.0-2.5 GeV/ c	0.0045	0.0044
2.5-3.0 GeV/ c	0.0036	0.0039
3.0-3.5 GeV/ c	0.0033	0.0039
3.5-4.0 GeV/ c	0.0035	0.0039
4.0-4.5 GeV/ c	0.0057	0.0061
4.5-5.0 GeV/ c	0.0155	0.0201

Hadron Contamination above 5GeV/ c

Hadron background is estimated by similar 'reverse prob method'. Hadron background is not negligible above $p_T > 5.0$ GeV/ c , even when the tight eID is applied.

R_{tight} shown at Fig. 3.13 drops into about half for electron $p_T > 5.0$ GeV/ c . This represents hadron contamination with the standard eID cut becomes $\sim 50\%$ above $p_T > 5.0$ GeV/ c . Therefore, when we apply the reverse **prob** cut (**prob** < 0.01), the selected particles are hadrons with $\sim 99\%$ purity since the reverse **prob** cut increases the hadron contamination by a factor of

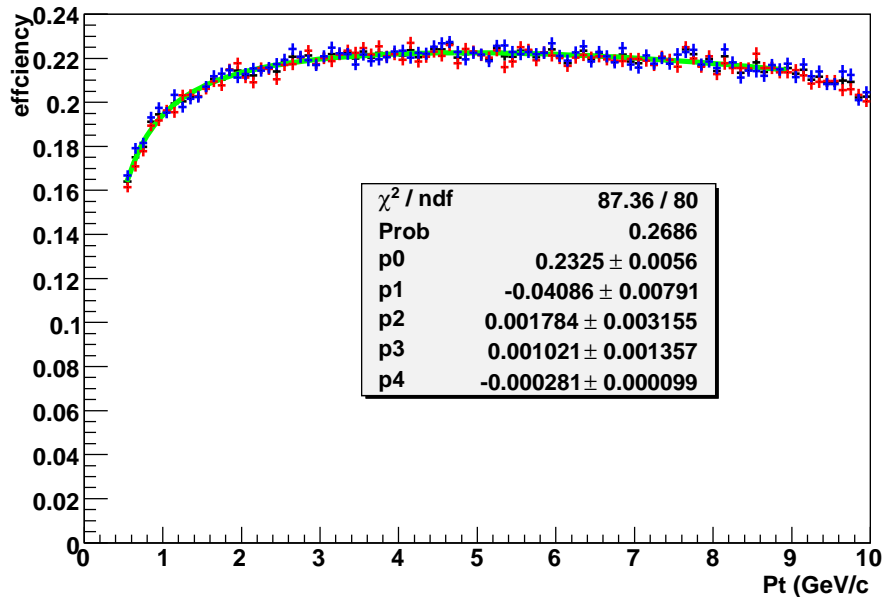


Figure 3.11: Electron efficiency as a function of electron p_T . Red points are electron efficiency and blue points are positron in RUN5. Black points are efficiency of electron and positron. Green line is a fit function of efficiency of electron and positron.

100. We use the $e\text{core}/\text{mom}$ distributions of the particles which is selected by the standard eID cut and the reverse prob cut to estimate hadron background in electron samples.

Figure 3.20 shows the $e\text{core}/\text{mom}$ distribution of electrons with tight eID cut and estimated that of hadron as described above from RUN5 data. Black points show the distribution of electron and blue points show estimated that of hadron. The estimated distribution of hadron is normalized by number of entries in $0.6 < e\text{core}/\text{mom} < 0.75$.

Blue lines are exponential fit to the $e\text{core}/\text{mom}$ distribution of hadron. Red lines are gauss + exponential fit to the distribution of electrons in the condition that exponential parts are fixed at blue lines.

Signals are counted as number of entries in $0.8 < e\text{core}/\text{mom} < 1.4$. Hadron background is estimated from fit functions. The fitting error is counted into the statistical error of the signals. The results for RUN5 and RUN6 are summarized in Table 3.4.

3.3.4 Invariant Cross Section of Inclusive Electron

The overall efficiency, $\epsilon(p_T)$ can be determined from the obtained electron reconstruction efficiency and trigger efficiency. Therefore, we are ready to determine invariant cross section of inclusive electron according to Eq 3.2

Figure 3.21 and 3.22 show invariant cross sections of inclusive electrons for MB and PH triggered events in RUN5 and RUN6, respectively. Blue circles show the spectrum of electrons in MB data and red squares show that of electrons in PH data with the standard eID cut.

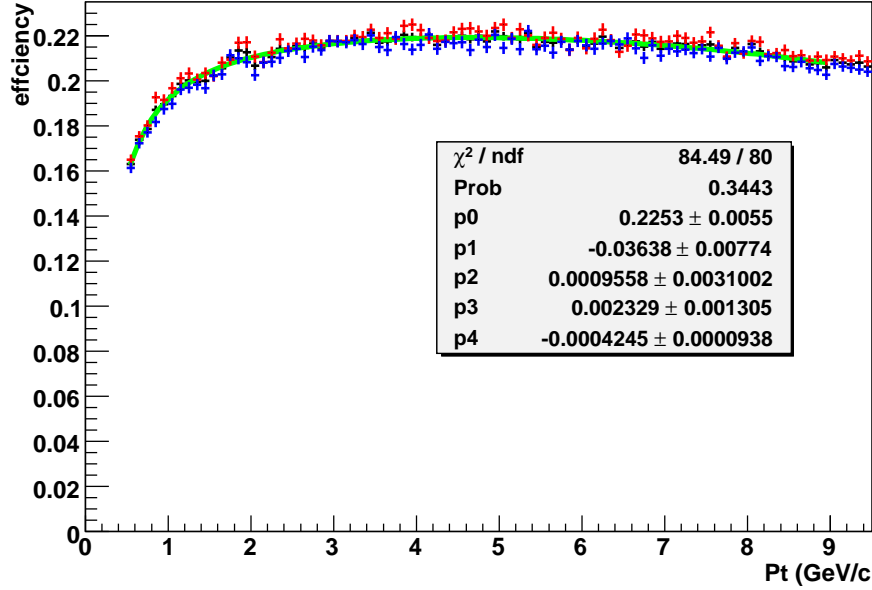


Figure 3.12: Electron efficiency as a function of electron p_T . Red points are electron efficiency and blue points are positron in RUN5. Black points are efficiency of electron and positron. Green line is a fit function of efficiency of electron and positron.

Green triangles show electrons for PH data with tight eID cut. These cross sections of inclusive electron are consistent with each other among three cases.

3.3.5 Systematic Errors

Geometrical Acceptance

Since the simulation reproduces the real data about the ϕ distribution within 3% as shown at Sec. 3.2.1, 3% systematic error is assigned for geometrical acceptance for RUN5 and RUN6.

Table 3.4: Estimated hadron background

electron p_T range	hadron background(RUN5)	hadron background(RUN6)
5.0-6.0 GeV/ c	0.033	0.038
6.0-7.0 GeV/ c	0.051	0.066
7.0-8.0 GeV/ c	0.137	0.146
8.0-9.0 GeV/ c	0.259	0.156
9.0-10.0 GeV/ c	0.257	0.250

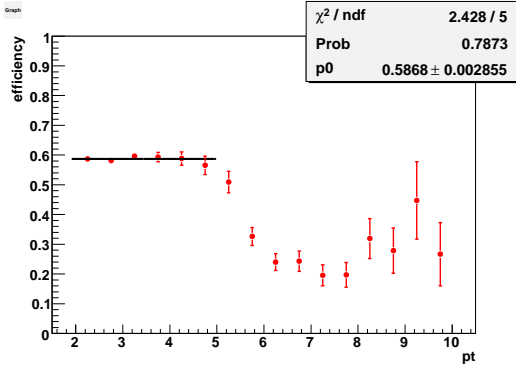


Figure 3.13: The ratios the number of electron in $0.8 < e_{core}/mom < 1.4$ with tight eID cut over that with standard eID cut as a function of electron p_T in RUN5.

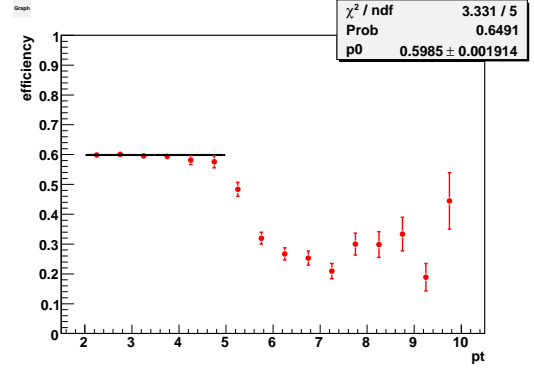


Figure 3.14: The ratios the number of electron in $0.8 < e_{core}/mom < 1.4$ with tight eID cut over that with standard eID cut as a function of electron p_T in RUN6.

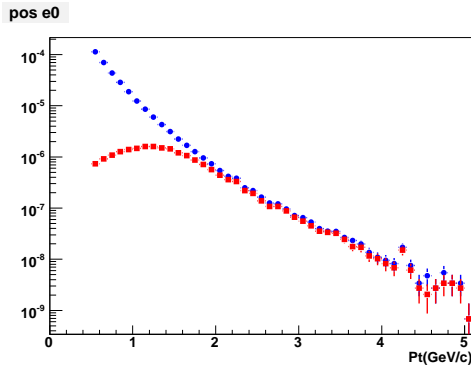


Figure 3.15: Raw spectra of electrons in RUN5 MB data. Blue circles show all electrons in MB data and red squares show 4X4c fired electrons.

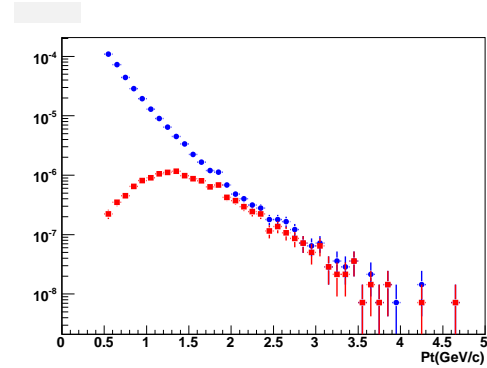


Figure 3.16: Raw spectra of electrons in RUN6 MB data. Blue points show all electrons in RUN6 MB data and red squares show 4X4c fired electrons.

eID Parameters

Systematic error for eID parameters is determined by the comparison of the efficiency of each eID parameter between the real data and the PISA simulation.

Efficiency of each eID parameter in the simulation is determined from the distribution of the parameter with other cuts being applied. For example, efficiency of n0 cut in the simulation is determined as follows.

$$\frac{\int_2 N(n0)dn0}{\int_0 N(n0)dn0}, \quad (3.11)$$

where N is the distribution of $n0$ with the standard cut except $n0$ being applied

The efficiency of each cut for eID parameter in the real data is determined by tagging the electrons from conversion and dalitz decay. The reconstructed invariant mass distribution of e^+e^- pair has the peaks at the low mass region as shown in Figure 3.23. It is a useful tool to tag

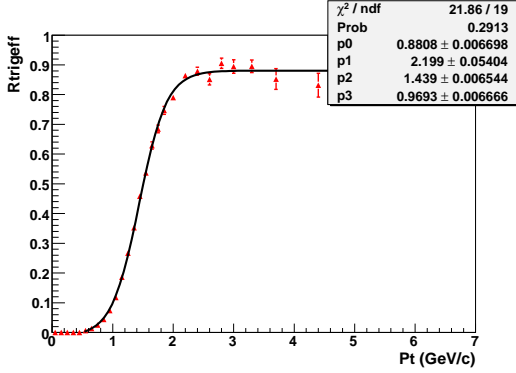


Figure 3.17: Trigger efficiency of 4x4c trigger in RUN5.

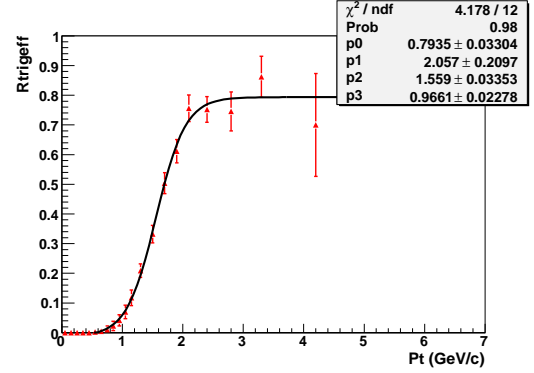


Figure 3.18: Trigger efficiency of 4x4c trigger in RUN6.

pure electrons. The sources of the peaks are π^0 Dalitz decay ($\pi^0 \rightarrow e^+e^-\gamma$) and γ conversion at the beam pipe. Since the track reconstruction algorithm assumes that all tracks come from the collision vertex, the electron pairs produced at the point with $R > 0$ are reconstructed to have incorrect momentum. This is schematically shown in Fig. 3.24. As a result, each of the conversion pairs acquires the fake p_T and the invariant mass is approximately proportional to $f Bdl$. Therefore, the reconstructed mass of conversion electron pairs is determined by the location of the conversion sources. The peak position of the pairs from γ conversion at the beam pipe is around $20 \text{ MeV}/c^2$.

Using these clearly tagged pairs of electrons, the efficiency of each eID cut in the real data could be evaluated. One electron is selected by the standard eID cut and the other electron is selected by the standard eID cut except the cut for the parameter whose efficiency will be evaluated. Figure 3.25 shows the invariant mass distribution of e^+e^- in RUN5 PH fired events. Black points show the mass distribution when both electrons are selected by the standard eID cut and red points show that when one electron is selected by the standard eID cut and the other is selected the cut without n0 (RICH fire ($n1 > 1$) is required) Efficiency of n0 cut in real data is determined as follows.

$$\frac{\int_0^{0.04} N(\text{mass}) d\text{mass} (n0 > 1)}{\int_0^{0.04} N(\text{mass}) d\text{mass}}, \quad (3.12)$$

where, N is the distribution of the invariant mass.

The efficiencies of other parameters are also determined in the same way. The results are summarized in Table 3.5. The efficiencies in the simulation agrees well with these in real data.

Systematic error of 1% is assigned for RICH parameters from Table 3.5, since the efficiencies of RICH parameter are expected not to depend on electron p_T . Systematic error of 2% is assigned for EMC parameters to be conservative, since the efficiencies of EMC parameters may have small p_T dependence.

Trigger Efficiency

The systematic error of the PH trigger efficiency is evaluated based on the error of the fit in Fig 3.17 and 3.18. We assign the systematic error of the PH trigger efficiency in RUN5 as 3%

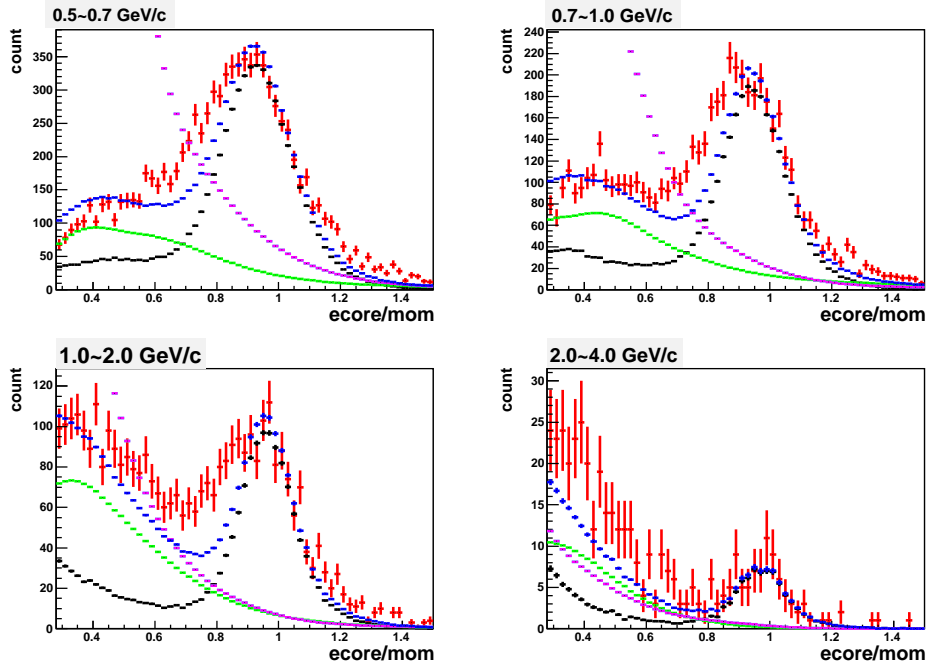


Figure 3.19: The distributions of $ecore/mom$ in RUN5 MB data were used to study hadron contamination in $0.5 < p_T < 4.0 \text{ GeV}/c$

$$\oplus 5\% \times \frac{1}{\epsilon_{trig}-1} \text{ and } 4\% \oplus 10\% \times \frac{1}{\epsilon_{trig}-1}.$$

Tight eID Efficiency

The relative efficiency (R_{tight}) is independent of p_T in $2 < p_T < 5 \text{ GeV}/c$ as shown in Fig. 3.13 and 3.14. The efficiency of the tighter RICH cut ($n1 > 4$) is $\sim 70\%$ and this part should be p_T independent. The efficiency of the **prob** cut is approximately 90%. The 10% loss due to the **prob** may have some small p_T dependence. We assign 20% of the 10% loss as possible p_T dependence of the **prob** cut. Therefore, the systematic error for the relative efficiency (R_{tight}) for high p_T extension is $10\% \times 20\% = 2\%$.

3.3.6 Absolute Normalization

Systematic error for absolute normalization is described in Sec. 3.1.1 and 3.1.2.

- We use $\sigma_{BBC} = 23.0 \pm 2.2 \text{ mb}$. Thus, systematic error is 9.6%
- We use $\epsilon_{bias} = 0.79 \pm 0.02$. Thus, systematic error is 2.5%

The systematic error for the absolute normalization is assigned to 9.9% from the quadratic sum of the two components.

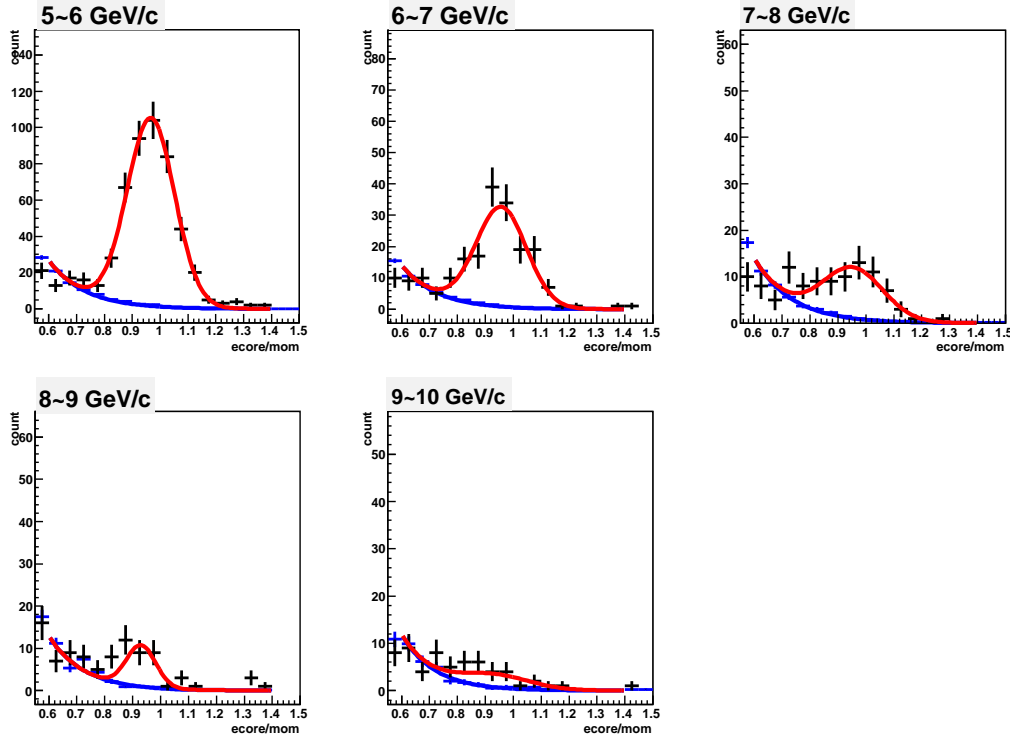


Figure 3.20: The $ecore/mom$ distribution of electrons with tight eID cut and estimated that of hadron as described above in RUN5. Black points show the distribution of electron and blue points show estimated that of hadron.

3.4 Comparison with PPG65

The invariant cross section of inclusive electrons in RUN5 at this analysis was compared with PPG65 result. Figure 3.26 show the ratio of invariant cross section of inclusive electrons in this analysis over PPG65 result. The discrepancy between PPG65 and this analysis was 8% around low electron p_T region.

One of the reason of this discrepancy was the difference between pro.72 CNT (this analysis) and pro.68 EWG (PPG65), while these two results were within systematic error. $n_0 > 1$ cut and $|\eta_{EMCSD}| < 4$ && $|\eta_{EMCSDZ}| < 4$ cut was applied implicitly, when EWG was made. A few % electrons were lost by implicit $|\eta_{EMCSD}| < 4$ && $|\eta_{EMCSDZ}| < 4$, since any correction was not applied for EMC matching parameters when pro.68 EWG was made. We made two raw spectra to study this effect.

- The PPG65 analysis cut was applied for pro.72 and pro.73 CNT files. (1)
- The PPG65 analysis cut was applied for pro.72 and pro.73 CNT files, after $|\eta_{EMCSD}| < 4$ && $|\eta_{EMCSDZ}| < 4$ cut was applied. (2)

Figure 3.27 show the ratio of raw spectra in (1) over that in (2). It was estimated from Fig.3.27 that 2.5% electron was lost by implicit $|\eta_{EMCSD}| < 4$ && $|\eta_{EMCSDZ}| < 4$ cut.

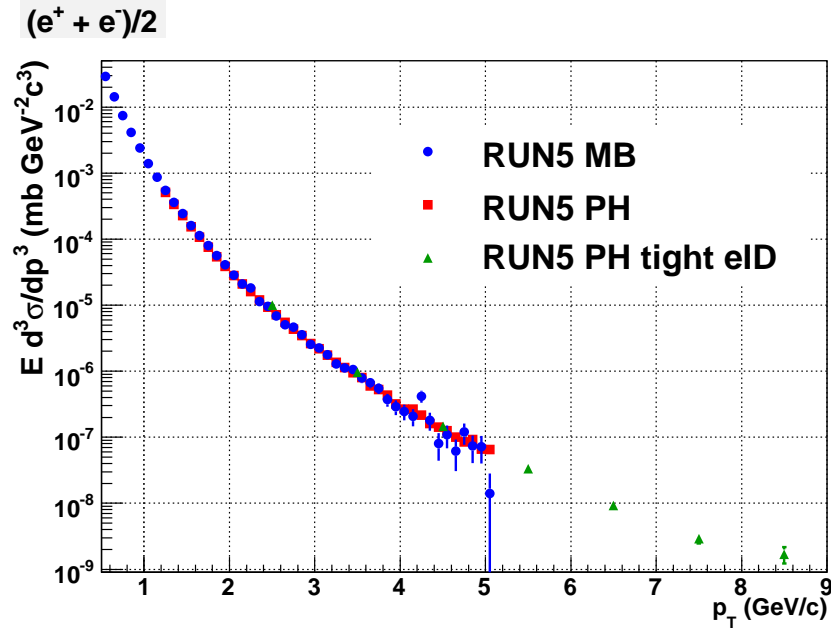


Figure 3.21: Invariant cross section of inclusive electrons in RUN5 MB and PH triggered events. Blue circles show electrons in MB events and red squares show electrons in PH triggered events with standard eID cut. Green triangles show electrons in PH triggered events with tight eID cut.

Figure 3.28 show the ratio of raw spectra in (1) over that in PPG65 analysis. The fraction of total lost electron in pro.68 EWG was found 3% from Fig.3.28. 0.5% electron was lost by RICH bug about n0 variable in pro.68 data set. Therefore, the result at PPG65 should be scaled by a factor of 1.03 for the precise comparison, while 3% was completely within systematic error at PPG65.

Figure 3.29 show the ratio of invariant cross section of inclusive electrons in this analysis over PPG65 result with 1.03 correction. The ratio was fitted by striate line for $0.5 \leq p_T < 5 \text{ GeV}/c$ and $1.8 \leq p_T < 5 \text{ GeV}/c$. The fitted values were 1.05 and 0.99 for for $0.5 \leq p_T < 5 \text{ GeV}/c$ and $1.8 \leq p_T < 5 \text{ GeV}/c$, respectively. Thus, this analysis and PPG65 were consistent, since this discrepancy was within systematic error. Slightly larger cross section around low electron p_T than PPG65 may be from increasing Ke3 electron due to low track quality cut in this analysis.

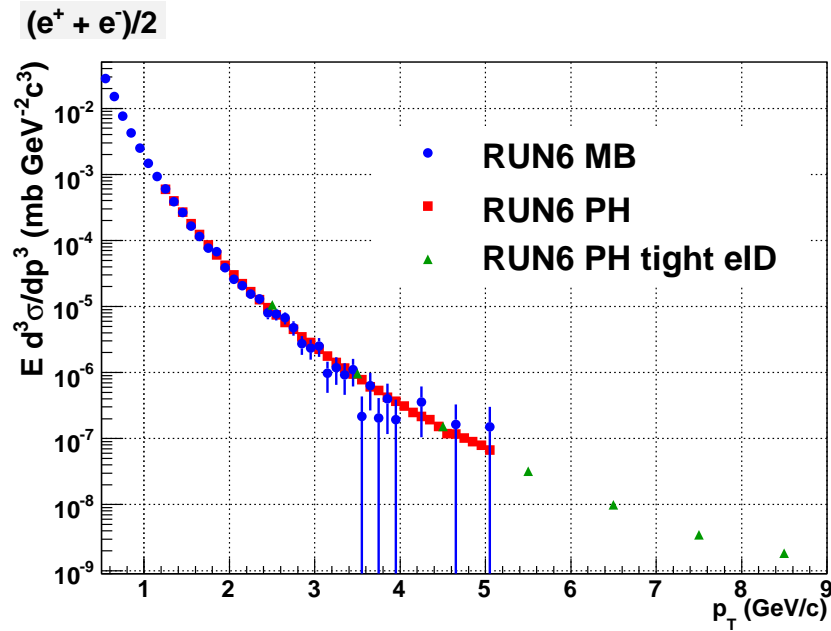


Figure 3.22: Invariant cross section of inclusive electrons in RUN6 MB and PH triggered events. Blue circles show electrons in MB events and red squares show electrons in PH triggered events with standard eID cut. Green triangles show electrons in PH triggered events with tight eID cut.

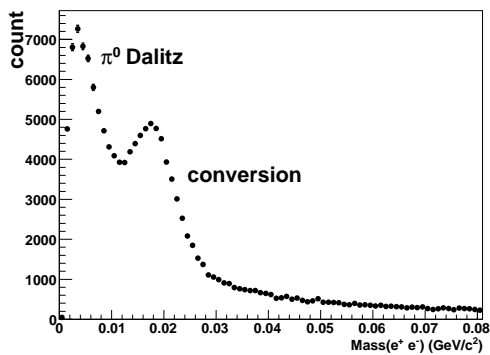


Figure 3.23: The invariant $e^+ e^-$ mass peak in data sample.

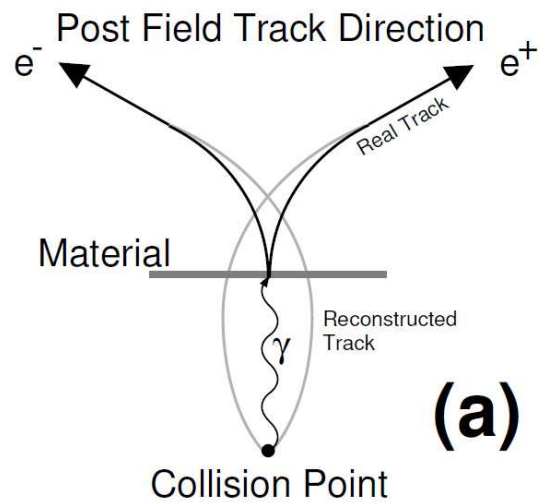


Figure 3.24: The production of conversion electrons.

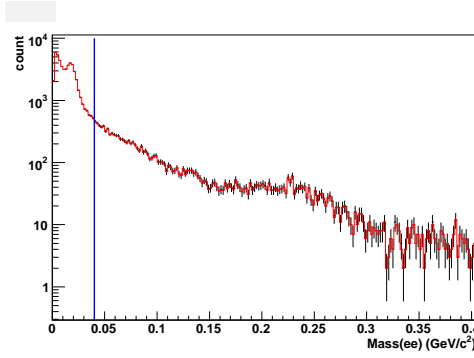


Figure 3.25: e^+e^- mass distribution in RUN5 PH fired events. Black points show the mass distribution when both electrons are applied all cuts and red points show the one when one electron is applied all cuts and the other is applied all cuts except n0 cut.

Table 3.5: The efficiency of eID parameter at real data and the simulation

eID parameter	real (RUN5)	simulation (RUN5)	real (RUN6)	simulation (RUN6)
RICH				
n0	99.4%	98.5%	99.3%	98.5 %
disp	99.0%	99.3%	99.2%	99.3 %
chi ²	99.7%	99.4%	99.6%	99.4 %
EMC				
e/p	97.7%	97.6%	96.1%	97.1 %
prob	98.8%	98.7%	98.4%	98.7 %
$\delta\phi_{EMC}$	99.3%	99.5%	99.1%	99.4 %
δZ_{EMC}	99.3%	99.5%	99.4%	99.5 %

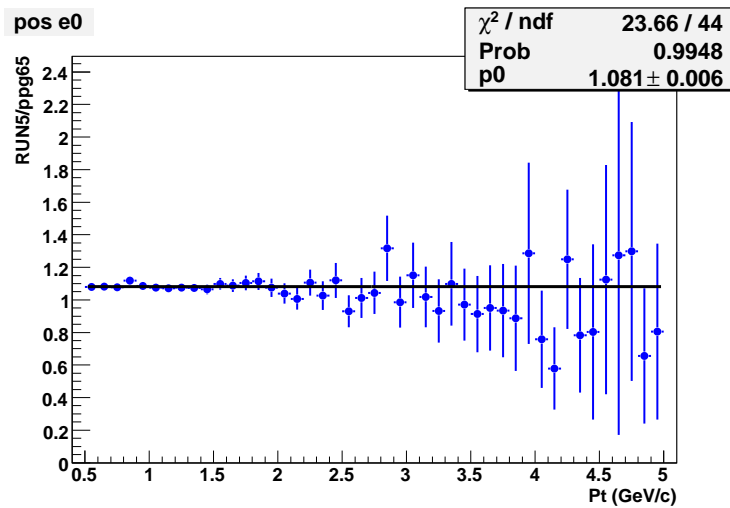


Figure 3.26: The ratio of invariant cross section of inclusive electrons in this analysis over PPG65 result.

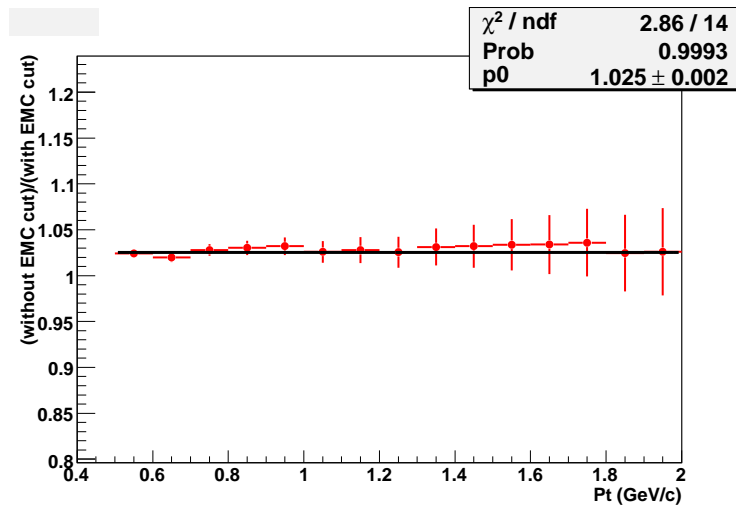


Figure 3.27: The ratio of raw spectra in (1) over that in (2). See the text for the detail.

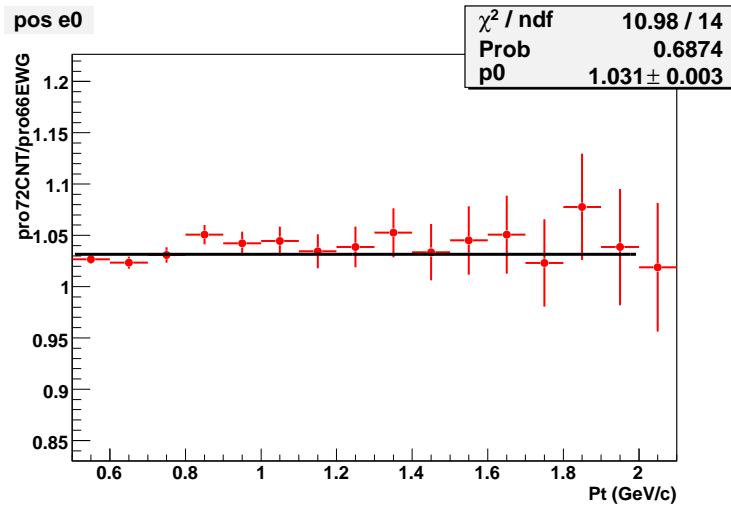


Figure 3.28: the ratio of raw spectra in (1) over that in PPG65 analysis. See the text for the detail.

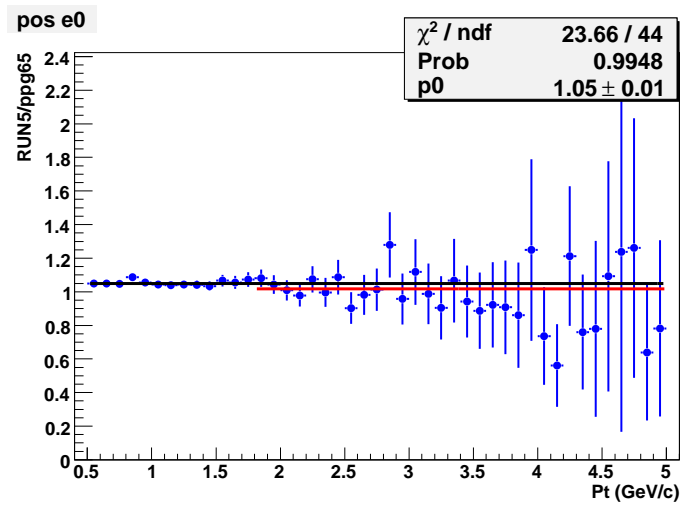


Figure 3.29: The ratio of invariant cross section of inclusive electrons in this analysis over PPG65 result with 1.03 correction.

Chapter 4

Measurement of electrons from heavy flavor decays

This chapter describes measurement of electrons from heavy flavor decays at RUN5 and RUN6. Cocktail method and converter method were used to subtract background.

1. 'non-photonic' electrons from semi-leptonic decay of heavy-flavor (single non-photonic electron).
2. 'photonic' background from Dalitz decays of light neutral mesons and external photon conversions (mainly in the beam pipe).
3. 'non-photonic' background from $K \rightarrow e\pi\nu$ (K_{e3}), dielectron decays of vector mesons and quarkonium (J/ψ and Υ) and Drell-Yan process.

The photonic background is much larger than the non-photonic background except at highest p_T ($>5\text{GeV}/c$). The signal of electrons from heavy-flavor decays is small compared to the background at low p_T ($S/B < 0.2$ for $p_T < 0.5 \text{ GeV}/c$) but rises with increasing p_T ($S/B > 1$ for $p_T > 2 \text{ GeV}/c$). In order to extract the heavy-flavor signal, the background has to be subtracted from the inclusive electron spectrum. 'cocktail method' and 'converter method' are used in this analysis to subtract the electron background [9, 11].

4.1 Cocktail Method

One technique to accomplish this task is the so-called 'cocktail subtraction' method. A cocktail of electron spectra from all background sources is calculated using EXODUS and then subtracted from the inclusive electron spectra. This technique relies on the fact that the p_T distributions of the relevant background sources are known well enough. It turns out that the PHENIX measurements of the relevant electron sources are precise enough to allow for cocktail calculations that constrain the background within a systematic uncertainty better than 15 % for all p_T . This uncertainty is in the same order with the signal to background ratio at the lowest p_T and, therefore, it is not sufficiently small to extract the heavy-flavor signal via the cocktail subtraction over the full p_T range. The cocktail method is useful at high p_T , *e.g.* for

$p_T > 2 \text{ GeV}/c$, where signal to background ratio is large and the cocktail input is known with small systematic uncertainties as discussed in the following.

4.1.1 Neutral Pions

The most important background source is the π^0 . π^0 decays contribute to the photonic background in two ways. First, the Dalitz decay of π^0 ($\pi^0 \rightarrow e^+e^-\gamma$) is a primary source of electrons from the collision vertex and, second, the conversion of photons from the decay $\pi^0 \rightarrow \gamma\gamma$ in material in the PHENIX central arm aperture (mainly the beam pipe) gives a source of electrons originating not from the original collision vertex. The contribution from photon conversions is small compared to the contribution from Dalitz decays, since material budget in the PHENIX central arms is well controlled.

The p_T distribution of π^0 is obtained via simultaneous fit to π^\pm (low p_T) and π^0 (high p_T) spectra at PHENIX [9]. This approach is only valid under the assumption that the invariant π^0 spectrum and the averaged charged pion spectrum $(\pi^+ + \pi^-)/2$ are the same. This assumption is justified with a few % precision at PHENIX, while at low p_T , *i.e.* for $p_T < 1 \text{ GeV}/c$, the decay of η mesons into three π^0 creates a tiny charge asymmetry.

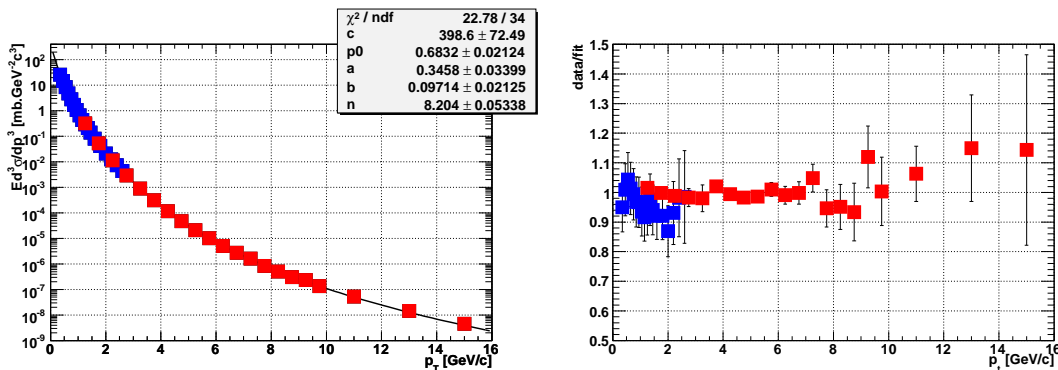


Figure 4.1: Invariant differential cross section of (blue symbols at low p_T) and π^0 s (red symbols) together with a fit according to π^\pm Eq. 4.1 (left panel). Ratio of the data to the fit (right panel).

Figure. 4.1 shows the comparison of the neutral and charged averaged invariant differential cross sections of pions in p+p collisions at $\sqrt{s} = 200 \text{ GeV}$ in comparison with a simultaneous fit to the data with a modified Hagedorn parameterization:

$$E \frac{d^3\sigma}{d^3p} = \frac{c}{(\exp(-ap_T - bp_T^2) + p_T/p_0)^n}. \quad (4.1)$$

Both an absolute comparison as well as the ratio of the data to the fit are shown to demonstrate the good quality of the parameterization.

4.1.2 Other Light Mesons

Other light mesons contributing to the electron cocktail are the η , ρ , ω , η' , and ϕ mesons. The η meson has the largest contribution among these mesons.

For the cocktail calculation, the shape of the invariant p_T distributions, and the relative yield to the π^0 yield are required as input parameter. The p_T spectra are derived from the pion spectrum assuming the m_T scaling, *i.e.* the same modified Hagedorn parameterizations are used (Eq. 4.1), only p_T is replaced by $\sqrt{p_T^2 + m_{meson}^2 - m_{\pi^0}^2}$.

Since this approach of m_T scaling ensures that at high p_T the spectral shapes of all meson distributions are the same, the normalization of the meson spectra relative to the pion spectrum can be given by the ratios meson-to-pion at high p_T (5 GeV/ c is used). The following values are used.

- $\eta/\pi^0 = 0.48 \pm 0.03$ [31]
- $\rho/\pi^0 = 1.00 \pm 0.30$ [32]
- $\omega/\pi^0 = 0.90 \pm 0.06$ [33]
- $\eta'/\pi^0 = 0.25 \pm 0.075$ [32]
- $\phi/\pi^0 = 0.40 \pm 0.12$ [32]

The resulting η/π^0 ratio agrees within experimental uncertainties for $p_T > 2$ GeV/ c with the corresponding PHENIX data for p+p collisions [31].

4.1.3 K_{e3} Decay

The contribution from the K_{e3} decay of Kaons in flight is evaluated via the PISA simulation to take into account the effect of the exact analysis cuts (specially `ecore/mom` cut). The measured yield of electrons originating not from the collisions vertex depends on the analysis cut. The input kaon spectra is parameterized based on the measured charged kaon spectrum in p+p collisions at PHENIX [34]. The contribution from kaon decays is only relevant (*i.e.* larger than 5 %) for electrons with $p_T < 1$ GeV/ c . The contribution becomes negligible for electrons with $p_T > 2$ GeV/ c .

4.1.4 Photon Conversions

The contribution from γ conversions depends almost entirely on the material present in the detector aperture. Apart from the beam pipe, which is made of Beryllium and contributes less than 0.3 % of a radiation length to the material budget, Helium bags constitute the only material between the beam pipe and the tracking and electron identification detectors in RUN5 setup. As is verified by the PISA simulation of π^0 decays, the ratio of electrons from the conversion of photons from $\pi^0 \rightarrow \gamma\gamma$ decays to electrons from π^0 Dalitz decays is 0.403 with a systematic uncertainty of about 10 %, independent of p_T in the relevant range. For heavier mesons, this ratio is rescaled in the cocktail to properly account for the fact that the branching

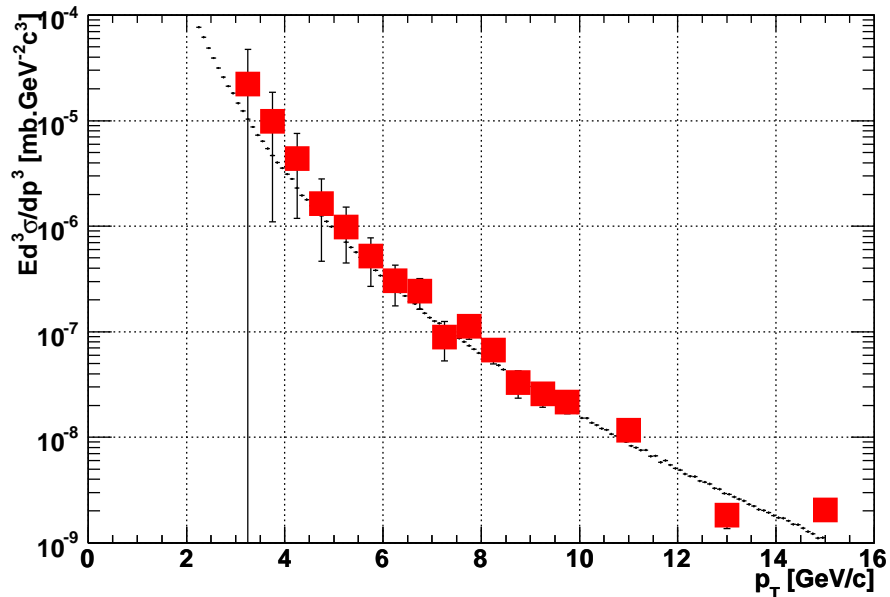


Figure 4.2: Measured direct photon spectrum (large symbols shown in red) compared with the cocktail parameterization (histogram indicated by small 'datapoints') for p+p collisions.

ratio of the Dalitz decay relative to the $\gamma\gamma$ decay increases slightly with increasing parent meson mass.

The material budget between the beam pipe and the tracking detector in RUN6 setup increase slightly, since there are not Helium bags at RUN6 to install HBD. The effect is also estimated by the PISA simulation. It is found that the ratio of the electrons from air conversion due to the absence of He bag to the electrons from π^0 Dalitz decays is $7\pm 1\%$. The detail is described in Appendix. E

It is crucial to note that the contribution from photon conversion to the background electron spectra is less than half of the contribution from direct Dalitz decays. For a reliable measurement of single non-photonic electrons, this is essential.

4.1.5 Direct Photon

Contributions to the background electrons from direct radiation have two process. First, real photons produced in initial hard scattering processes, *i.e.* direct photons convert to electron pairs in material in the PHENIX detector as photons from light neutral meson decays. Second, every source of real photons also presents a source of virtual photons. In the case of the π^0 these two sources are the the $\gamma\gamma$ decay of π^0 and the corresponding Dalitz decays, which is also called an internal conversion. Similarly, direct real photon production is accompanied by direct virtual photon production, *i.e.* the emission of e^+e^- pairs.

The measured real direct photon spectrum is parameterized. The corresponding conversion

electron spectrum of these is added to the electron cocktail. Figure 4.2 shows the measured direct photon spectrum with the cocktail parameterization [32].

The ratio of virtual direct photons to real direct photons depends on p_T because the phase space for dielectron emission increases with increasing p_T . The very same effect is seen in the Dalitz decays of light neutral mesons, *i.e.* the Dalitz decay branching ratio relative to the two photon decay branching ratio is larger for the η meson than for the π^0 . Consequently, the ratio of virtual and real direct photon emission increases with p_T or, to be more precise, a logarithmic dependence. Such dependence is implemented for internal conversion of virtual photons based on the theory.

4.1.6 Quarkonium and Drell-Yan

The contribution from di-electron decay of J/ψ and Υ becomes significant above ~ 2 GeV/ c due to their large mass, while the contribution is negligible at low p_T . The p_T spectrum of J/ψ is measured up to 9 GeV/ c via di-electron decay at mid-rapidity in p+p collisions at PHENIX. The p_T spectrum of J/ψ is fitted with a power-law function and mt scaling. The difference due to the parametrization is taken into account systematic errors.

Unlike the case of J/ψ , there is not a measured p_T spectrum of Υ at mid-rapidity in p+p collisions at $\sqrt{s} = 200$ GeV. Therefore, p_T spectrum of Υ is taken from NLO pQCD calculation [35]. The total cross section at mid-rapidity ($d\sigma/dy|_{y=0}$) in NLO pQCD is 6.89×10^{-6} mb. This value is compatible with the measured cross section at PHENIX and STAR and it is found the contribution of Υ is not significant [36, 37].

LO pQCD calculation is used for the estimation of the contribution of Drell-Yan process. The result from LO pQCD calculation is scaled by a factor of 1.5 to take into account the higher order effect. The contribution of Drell-Yan process becomes important as electron p_T increases. However, the contribution from Drell-Yan process is found not to be significant for the measured p_T range (up to 9 GeV/ c) compared to other background sources.

The implementation of these contribution is described in PPG77 analysis note.

4.1.7 Implemented Cocktail in RUN5 and RUN6

Figure 4.3 and 4.4 show the invariant cross section for background electrons calculated by cocktail method in the p+p collisions in RUN5 and RUN6, respectively.

4.1.8 Systematic Errors

Systematic errors are estimated for all cocktail ingredients, propagated to the corresponding electron spectra, and then added in quadrature to determine the total cocktail systematic error.

The following systematic errors are evaluated and listed up as follows.

- pion spectra: To evaluate this uncertainty the full cocktail calculation is repeated in $\pm 1\sigma$ uncertainty bands for the pion input, propagating the uncertainty in the pion spectra to the electron cocktail. With systematic uncertainty of 10 % almost independent on p_T ,

the pion input represents the largest contributor to the electron cocktail uncertainty up to $\sim 5 \text{ GeV}/c$.

- light mesons: Since the contributions from all other mesons are much smaller than the contribution from η decay only η is of practical relevance. The systematic uncertainties are calculated from particle ratios listed above. This contribution is small compared to the uncertainty in the pion spectra and it depends on p_T only slightly.
- conversion material: The contribution from photon conversions obviously depends on the material present in the aperture. An analysis of fully reconstructed dielectrons from photon conversions suggests that this uncertainty is not larger than 10 %. Therefore, 10% systematic error is assigned.
- K_{e3} decay: This contribution is estimated via the PISA simulation. Given the limited statistics of this calculation a 50 % systematic error is assigned, which is only relevant at low p_T , *i.e.* below $1 \text{ GeV}/c$.
- direct radiation: This contribution is directly propagated from the systematic error quoted for the direct photon measurement. It is relevant only at high p_T .
- quarkonium and Drell-Yan: The contribution from J/ψ di-electron decay among dominant in these contributions and becomes significant above $2 \text{ GeV}/c$. The p_T distribution of J/ψ is well measured at PHENIX and 10% error for two parametrization and these deviation is assigned for J/ψ contribution. 40% systematic error is assigned for the contribution from Υ based on the comparison of the total cross section between NLO pQCD and the result from PHENIX and STAR. The uncertainty of the contribution from Drell-Yan process is unclear. Therefore, 100% systematic error is assigned for the contribution from Drell-Yan process to be conservative.

Figure 4.5 shows individual contributions to the cocktail systematic error and the resulting total systematic error. A fit of the total systematic error is shown in Fig. 4.5, where the fitting function is parameterized as follows:

$$SE[\%] = p_0 \times \exp(p_1 \times p_T) + p_2 + p_3 \times p_T + p_4 \times p_T^2 + p_5 \times p_T^3. \quad (4.2)$$

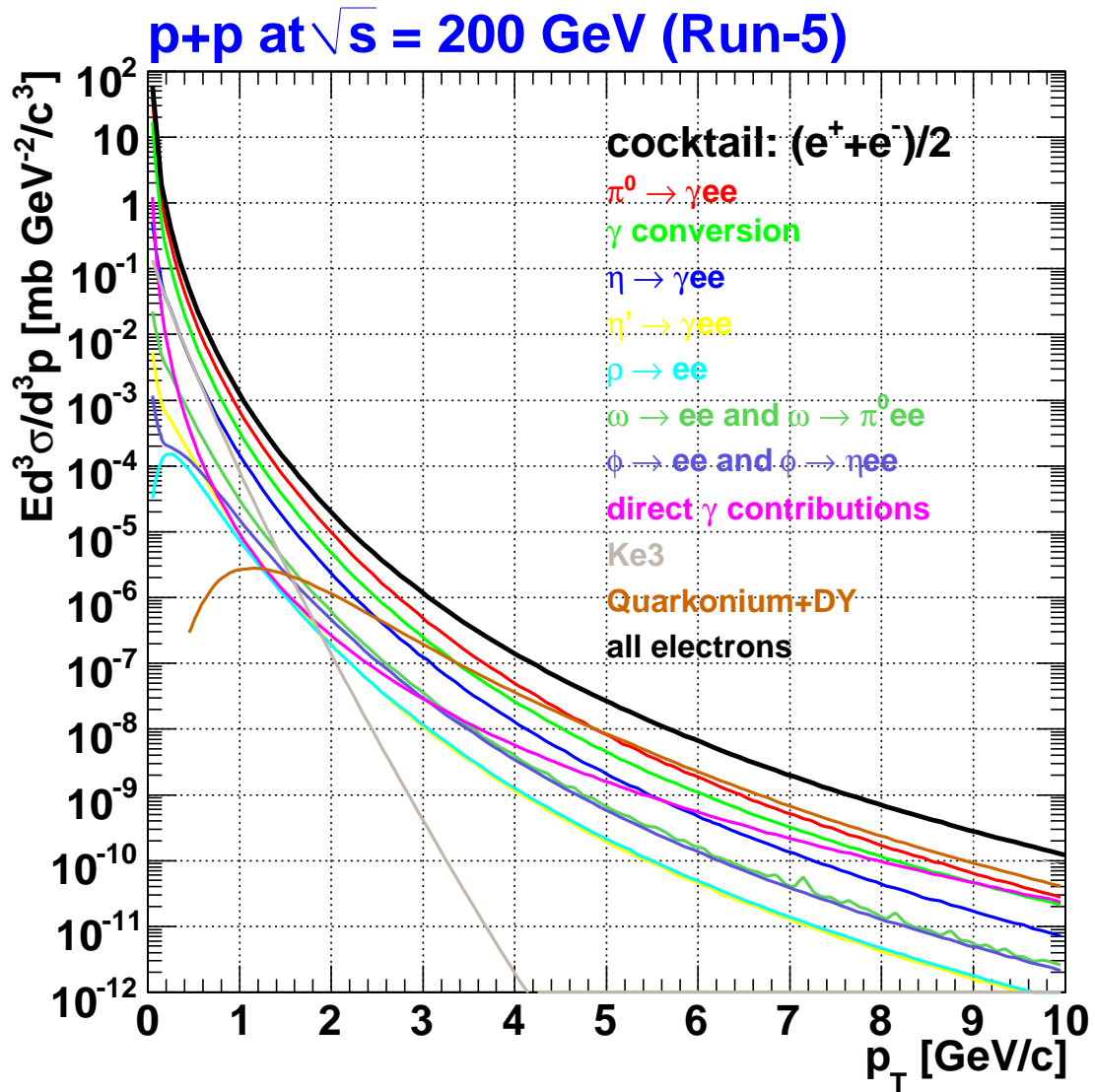


Figure 4.3: Invariant cross section of electrons from all sources considered in the RUN5 p+p cocktail

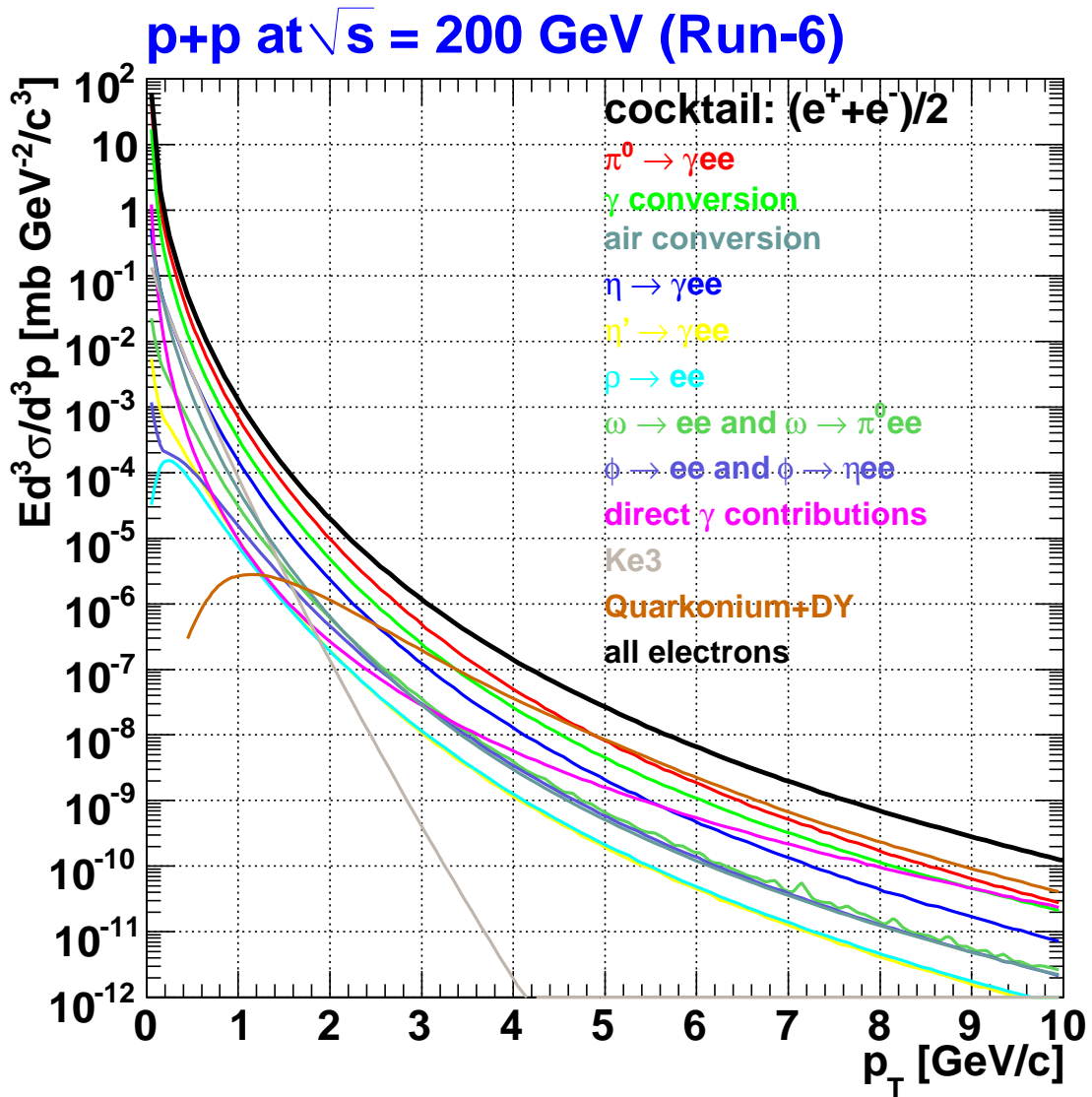


Figure 4.4: Invariant cross section of electrons from all sources considered in the RUN6 p+p cocktail

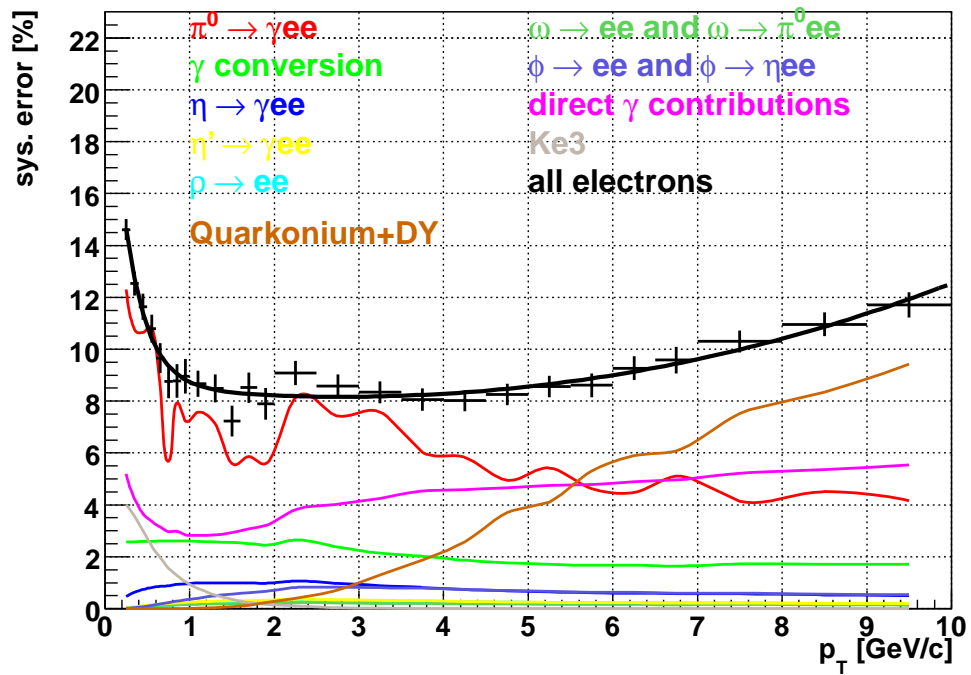


Figure 4.5: Individual contributions to the cocktail systematic error. The total error is depicted by the data points which are shown together with a fit.

4.2 Converter Method

The 'converter subtraction' method is used, which directly measures the photonic background and, thus, allows to extend the heavy-flavor measurement to the low p_T with good precision. Photonic and non-photonic electrons are obtained by measuring the difference of inclusive electron yields with and without a photon converter with precise and well known thickness: a brass sheet of 1.680 % radiation length (X_0).

The C run group in RUN5 is the physics run with the converter. The G5A run group in RUN5 is used to compare with the electron yield with that in C run group. Figure 4.6 shows the corresponding inclusive electron spectra. In Fig. 4.6, open symbols show the spectra in the converter run and closed symbols show the spectra in the non-converter run. Red squares show the results in the PH data set and blue circles show the results in the MB data set.

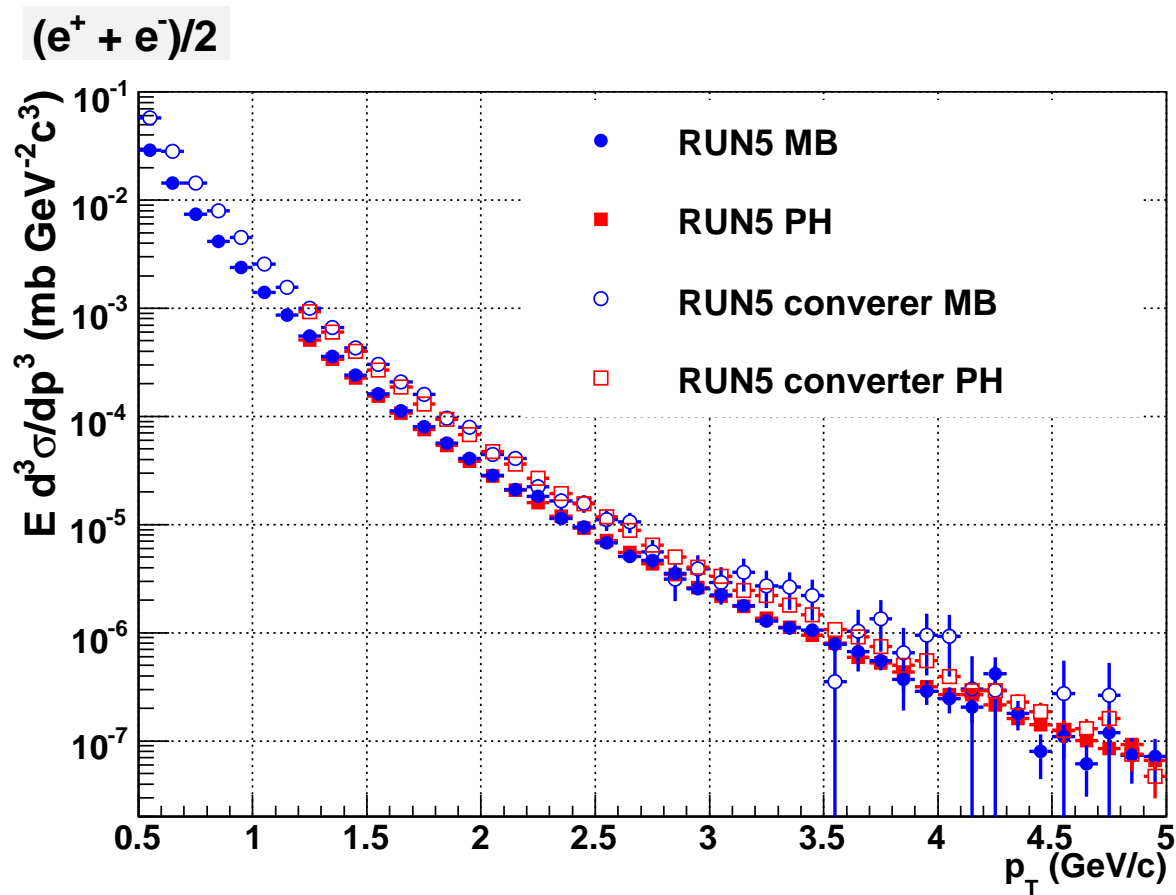


Figure 4.6: Invariant yields of inclusive electrons in coveter and non-converter runs. Open symbols show the spectra in the converter run and closed symbols show the spectra in the non-converter run. Red squares show the results in PH data set and blue circles show the results in MB data set.

4.2.1 Method to Subtract Photonic Electrons

Raw yields in coveter and non-converter runs can be expressed as the following relations:

$$N_e^{\text{Conv-out}} = N_e^\gamma + N_e^{\text{Non-}\gamma}, \quad (4.3)$$

$$N_e^{\text{Conv-in}} = R_\gamma N_e^\gamma + (1 - \epsilon) N_e^{\text{Non-}\gamma}. \quad (4.4)$$

Here, $N_e^{\text{Conv-in}}$ ($N_e^{\text{Conv-out}}$) is the measured electron raw yield with (without) the converter. N_e^γ ($N_e^{\text{Non-}\gamma}$) is the photonic (non-photonic) electron yields. ϵ represents the blocking factor of the converter which is a small loss of $N_e^{\text{Non-}\gamma}$ due to the converter. R_γ is the multiplication factor of the photonic electron due to the existence of the converter. Then, N_e^γ and $N_e^{\text{Non-}\gamma}$ are determined as follows.

$$N_e^\gamma = \frac{N_e^{\text{Conv-in}} - N_e^{\text{Conv-out}}}{R_\gamma - 1 + \epsilon}, \quad (4.5)$$

$$N_e^{\text{Non-}\gamma} = \frac{R_\gamma N_e^{\text{Conv-out}} - N_e^{\text{Conv-in}}}{R_\gamma - 1 + \epsilon}. \quad (4.6)$$

Non-photonic electrons still include a small background which needs to be subtracted to obtain the electrons from semi-leptonic decay of heavy flavor. These are K_{e3} electrons ($E \frac{d^3\sigma^{K_{e3}}}{dp^3}$), $\rho \rightarrow e^+e^- E \frac{d^3\sigma^{\rho \rightarrow e^+e^-}}{dp^3}$, $\omega \rightarrow e^+e^- E \frac{d^3\sigma^{\omega \rightarrow e^+e^-}}{dp^3}$, $J/\psi, \Upsilon \rightarrow e^+e^- E \frac{d^3\sigma^{J/\psi, \Upsilon \rightarrow e^+e^-}}{dp^3}$ and Drell-Yan process. The spectrum of the electrons from semi-leptonic decay of heavy flavor (single non-photonic electrons) is determined as follows.

$$\begin{aligned} E \frac{d^3\sigma^{HQ}}{dp^3} &= E \frac{d^3\sigma^{\text{non-}\gamma}}{dp^3} - E \frac{d^3\sigma^{K_{e3}}}{dp^3} - E \frac{d^3\sigma^{\rho \rightarrow e^+e^-}}{dp^3} - E \frac{d^3\sigma^{\omega \rightarrow e^+e^-}}{dp^3} \\ &- E \frac{d^3\sigma^{J/\psi, \Upsilon \rightarrow e^+e^-}}{dp^3} - E \frac{d^3\sigma^{DY}}{dp^3}. \end{aligned} \quad (4.7)$$

The yield of K_{e3} electrons, $\rho \rightarrow e^+e^-$, $\omega \rightarrow e^+e^-$, J/ψ $\Upsilon \rightarrow e^+e^-$ and Drell-Yan process are determined at the cocktail calculation. Obtained $E \frac{d^3\sigma^{HQ}}{dp^3}$ still have little background, di-electron decay of light mesons. Such background is negligible.

4.2.2 R_γ and the Blocking Factor

The blocking factor is determined to be $2.1\% \pm 1\%$ from the comparison of the conversion peak at the beam pipe between the simulation and real data [9, 11].

R_γ is the crucial parameter in the converter subtraction method. The source of photonic electron is a mixture of mesons (π^0 , η , η' , ω , and ϕ) decaying into real or virtual photons with their different p_T slopes. However, the photonic electron contributions from π^0 decays occupies almost of all photonic electrons and determine R_γ .

To calculate R_γ , it is necessary to know exactly the amount of material amounts near the interaction point. Table 4.1 shows the list of each material thickness. The converter sheet is rolled just around beam pipe in converter runs. Conversion probability (P^{Conv}) in Tab. 4.1 is calculated for the case of electrons emitted from photon with $p_T = 1.0 \text{ GeV}/c$ [7]. The

Table 4.1: Radiation length (L) of each material near the interaction point. Conversion probability (P^{Conv}) is calculated for the case of electrons emitted from photon with $p_T = 1.0 \text{ GeV}/c$.

Material	L (X_0 [g/cm ²])	P^{Conv}
Beam pipe (Be)	0.288 %	0.201 %
Air ($r < 30 \text{ cm}$)	0.099 %	0.069 %
Total	0.387 %	0.270 %
Converter (brass)	1.680 %	1.226 %

equivalent conversion probability of a virtual photon in π^0 Dalitz decay (P^{Dalitz}) is 0.598% [7]. R_γ can be estimated with these values for the photon with $p_T = 1.0 \text{ GeV}/c$.

$$R_\gamma = \frac{P^{\text{Conv}} + P^{\text{Dalitz}} \text{ (with converter)}}{P^{\text{Conv}} + P^{\text{Dalitz}} \text{ (without converter)}} \sim 2.41. \quad (4.8)$$

To obtain more realistic R_γ for considering geometrical effects and p_T dependence of the conversion probability, the PISA simulations for photon conversions from π^0 are performed with (without) the converter. We use the spectra of the light mesons which are used cocktail calculation. The R_γ for π^0 ($R_\gamma^{\pi^0}$) is determined from the the simulation as bellow.

$$R_\gamma^{\pi^0} = 2.37 + 0.07 \tanh(0.6p_T). \quad (4.9)$$

The η meson is the second dominant source of the photonic electrons. Since η mass is larger than π^0 mass, the phase space of η Dalitz decay is slightly than π^0 . The relative branching ratio (Dalitz decay)/(two γ decay) is 1.2% for π^0 and 1.5 % for η [17]. This difference makes R_γ^η smaller than $R_\gamma^{\pi^0}$. R_γ for η (R_γ^η) is determined as bellow.

$$R_\gamma^\eta = \frac{P_{\text{bp}} + P_{\text{air}} + P_{\text{Dalitz}}^\eta + P_{\text{conv}}}{P_{\text{bp}} + P_{\text{air}} + P_{\text{Dalitz}}^\eta} \sim 1 + (R_\gamma^{\pi^0} - 1) \times \frac{0.87\%}{1.1\%}. \quad (4.10)$$

Contributions from other mesons which undergo Dalitz decay (η' , ρ , ω , and ϕ) are small (6 % at $p_T = 3 \text{ GeV}/c$, and smaller at lower p_T). The particle ratios used in the cocktail calculation are used to calculate total R_γ . The uncertainties in the particle ratios are included in the systematic uncertainties of R_γ .

In this method, it is essential that the amount of material is accurately modeled in the simulation. We compare the yield of identified photon conversion pairs in the data and in the simulation, and conclude that the simulation reproduces R_γ within $\pm 2.7\%$. Figure. 4.7 and 4.8 show R_γ as a solid curve, which is compared with the ratio of inclusive electron yield with/without photon converter (R_{CN})

4.2.3 R_{CN}

R_{CN} is defined as the ratio of inclusive electron yield with/without photon converter. Figure. 4.7 and 4.8 show R_{CN} measured in RUN5 MB and PH data, respectively.

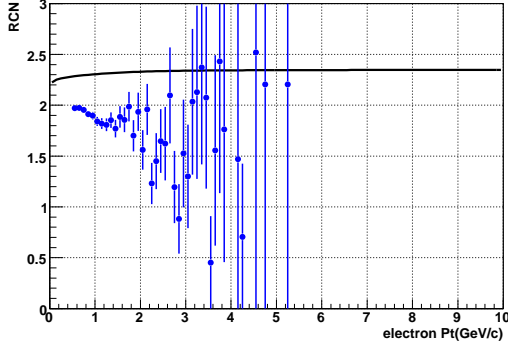


Figure 4.7: The ratios of the electron yield in the converter run over the non-converter run (R_{CN}) as a function of electron p_T in RUN5 MB data. The black line is $R_\gamma(p_T)$

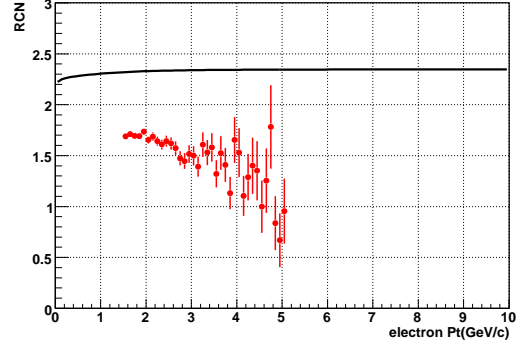


Figure 4.8: The ratios of the electron yield in the converter run over the non-converter run (R_{CN}) as a function of electron p_T in RUN5 PH data. The black line is $R_\gamma(p_T)$

If there are no non-photon contribution, then $R_{CN} = R_\gamma$. Figure 4.7 and 4.8 show that R_{CN} gradually decreases with increasing p_{Te} , while R_γ slightly increases with p_T . The difference between R_{CN} and R_γ proves the existence of non-photon electrons. The systematic error of R_{CN} is originated from the instability of the efficiency of electron reconstruction during the C run group and the G5A run group. We assign 1% systematic error for R_{CN} .

4.2.4 Converter Method for RUN6

Since there are no converter run during RUN6, we use R_{CN} measured in RUN5 for RUN6 converter analysis. Statistics is improved in RUN6 and this is the great advance in RUN6 data analysis. However, the statistical error of non-photon electron yield in the converter method is not improved in RUN6, since the statistics in the converter method is determined by the RUN5 converter run. Thus, we obtain only photon electron spectrum to compare with cocktail. The comparison with photon electrons in the cocktail between the measured photon electrons is used to determine the normalization factor of cocktail. The difference of the photon electron between RUN5 and RUN6 due to the absence of the Helium bags is taken into account as follows.

$$E \frac{d^3\sigma^\gamma}{dp^3} = \left(E \frac{d^3\sigma^{incl}}{dp^3} - E \frac{d^3\sigma^{air}}{dp^3} \right) \times \frac{R_{CN}(RUN5)-1+\epsilon}{R_\gamma(p_T)-1+\epsilon}, \quad (4.11)$$

$$E \frac{d^3\sigma^{non-\gamma}}{dp^3} = \left(E \frac{d^3\sigma^{incl}}{dp^3} - E \frac{d^3\sigma^{air}}{dp^3} \right) \times \frac{R_\gamma(p_T)-R_{CN}(RUN5)}{R_\gamma(p_T)-1+\epsilon}. \quad (4.12)$$

Here,

- $E \frac{d^3\sigma^{incl}}{dp^3}$ is the spectrum of inclusive electrons in RUN6.
- $E \frac{d^3\sigma^{air}}{dp^3}$ is the spectrum of electrons from air conversion, which is determined by the cocktail calculation without He bag.
- $R_{CN}(RUN5)$ is the R_{CN} which is measured in RUN5.

4.2.5 Systematic Errors

The systematic error of converter analysis is determined as follows. The details of each systematic error are already described.

- $R_\gamma(p_T)$: The systematic error of $R_\gamma(p_T)$ is assigned 0.062.
- R_{CN} : 1% systematic error is assigned to R_{CN} .
- ϵ : 0.01 is assigned as systematic error.

The systematic error is defined as the quadratic sum of the deviation from the above change of each parameters.

4.3 Comparison of the Results from Two Methods

The spectra of photonic and non-photonic electrons are obtained from the two methods, cocktail method and converter method. The results from these methods should be consistent with each other. This comparison can be used to reduce the uncertainty of the cocktail. The spectrum shape of the cocktail is determined by the spectrum shape of the parent mesons, dominated by π^0 . At high p_T , the acceptance curve for parent mesons becomes almost constant in p_T . The shape and slope of the spectrum is well determined, while it is more difficult to determine the absolute normalization of the data. Therefore in the cocktail calculation, the shape of the spectrum can well be determined. It is useful to tune the absolute normalization of the cocktail from the comparison between the measure photonic electrons and the cocktail at high p_T .

4.3.1 Photonic Electrons

The photonic electrons are obtained according to Eq. 4.5 and Eq. 4.11. The spectra of the measured photonic electrons are compared with the photonic component in the cocktail. Figure 4.9 and 4.10 show the ratio of measured/cocktail photonic electron spectra in RUN5 and RUN6, respectively. In Fig. 4.9 and 4.10, blue circles show the ratios in MB data and red squares show the ratios in PH data. Systematic error of the cocktail is also shown as the dotted line in these figures. The spectra of the cocktail are consistent with those of the measure photonic electrons within the systematic error of the cocktail.

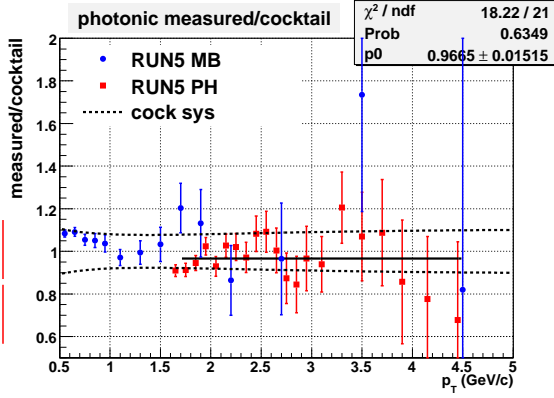


Figure 4.9: The ratio of measured/cocktail photonic electron spectra in RUN5. Blue circles show the ratios at MB data and red squares show the ratios in PH data. Dotted line show systematic error of the cocktail.

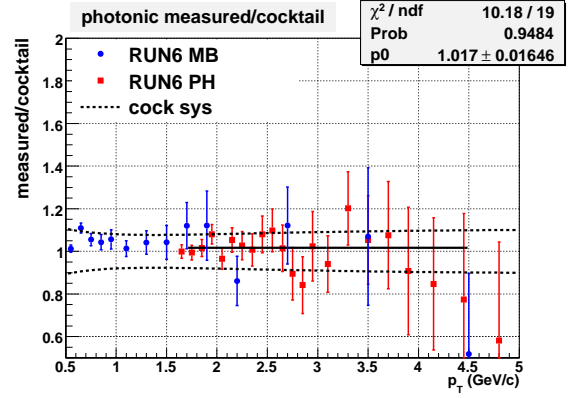


Figure 4.10: The ratio of measured/cocktail photonic electron spectra in RUN6. Blue circles show the ratios at MB data and red squares show the ratios in PH data. Dotted line show systematic error of the cocktail.

4.3.2 Normalization of Cocktail

We tune the absolute normalization of the photonic component in the cocktail from the comparison with the measured photonic electrons and the photonic electrons in the cocktail. The shape and slope of the meson spectra, which is used as the input of cocktail, is determined with the best precision for high p_T at PHENIX.

The ratios of measured/cocktail photonic electron spectra above 1.7 GeV/ c are fitted with a constant, which is expected behavior. The fitted lines are shown as striate lines in Fig. 4.9 and Fig. 4.10. The fitted values are 0.97 ± 0.02 and 1.017 ± 0.02 in RUN5 and RUN6, respectively. We calculate the re-normalization factor of the cocktail as 0.992 ± 0.025 for RUN5 and RUN6, since the normalization factor should be common within RUN5 and RUN6.

After the rescaling, systematic error of the photonic component in the cocktail is determined as follows.

$$SE_R^{photo}(p_T) = \sqrt{(SE^{photo}(p_T) - SE^{photo}(1.9\text{GeV}/c))^2 + \left(\frac{0.025}{0.992}\right)^2}, \quad (4.13)$$

where $SE^{photo}(p_T)$ is the systematic error of the photonic component before the normalization and $SE_R^{photo}(p_T)$ is the systematic error of the photonic component after the normalization. Since the normalization point is 1.9GeV/ c , the deviation from 1.9GeV/ c is taken into account as the systematic error. Total systematic error is defined as the quadratic sum of $SE_R^{photo}(p_T)$ and the systematic error of non-photonic background that is dominated by J/ψ . Figure 4.11 show the systematic error of the cocktail. Black line shows the systematic error of the photonic component in the cocktail before the normalization. Red line shows the systematic error of the photonic component after the normalization. Orange line shows the systematic error of non-photonic background and blue line shows the calculated total systematic error.

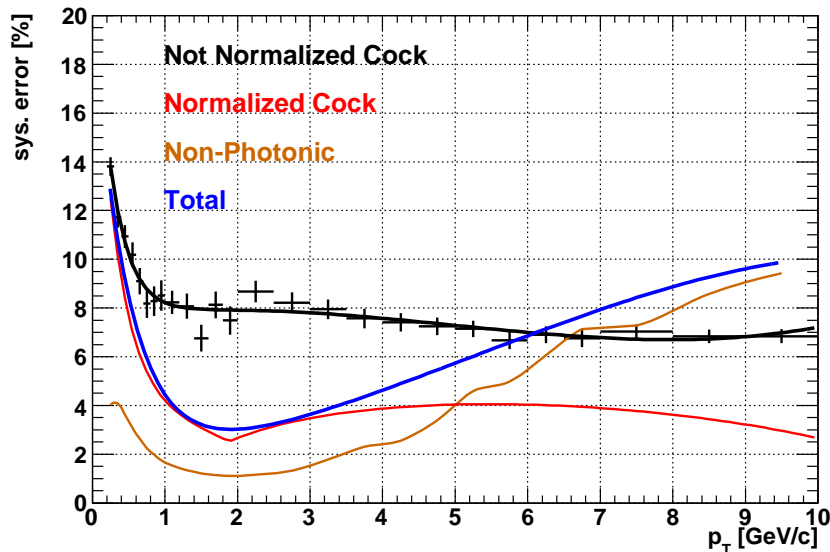


Figure 4.11: The systematic error of the cocktail. Black line show the total systematic error of the cocktail before the normalization of the cocktail. Red line shows the systematic error after the normalization.

4.4 Results

The spectra of the single non-photonic electron are determined via two independent method, cocktail method and converter method in RUN5 and RUN6. Converter method could determine the spectrum of the single non-photonic electrons at low p_T with good precision as already described. On the other hand, cocktail method provides better precision than converter method towards high p_T , *e.g.* for $p_T \sim 1.5$ GeV/ c , since the converter method starts to suffer from a lack of statistical precision and the cocktail input is known with small systematic uncertainties at high p_T . Therefore, we use cocktail method at high p_T and converter method at low p_T .

4.4.1 RUN5 and RUN6 Results

Figure 4.12 and 4.13 show the obtained invariant cross section of the single non-photonic electrons with systematic errors in RUN 5 and RUN6, respectively. 9.9% systematic error for the absolute normalization is **NOT** included in Fig.4.12 and 4.13. Circle points show the result from converter method and triangle points show the result from cocktail method. Open symbols show the result from MB data and closed symbols show the result from PH data. Closed squares show the result from PH data with tight eID cut.

4.4.2 Combined Result

The result from converter method in RUN5 is used for low p_T and the combined result in RUN5 and RUN6 from cocktail method is used for high p_T . Since the precision of the converter

analysis is determined by the statistics at the converter runs in RUN5, we use only the result from converter method at RUN5 MB data for low p_T . When the results from RUN5 and RUN6 with cocktail method are combined, the results from PH data are used to improve the statistics for high p_T . BLUE (Best Linear Unbiased Estimate) method is applied to combine the results of RUN5 and RUN6 [2], since a part of systematic errors of RUN5 and RUN6 are correlated. Error sources are summarized at Table 4.2. Error sources are divided into three types in this thesis as follows according to the nature of the error.

- **TYPE A** Point-to-point errors.
- **TYPE B** momentum-correlated errors.
- **TYPE C** Absolute normalization errors.

The averages and errors were determined according to BLUE as bellow.

$$\langle r \rangle = \frac{r_{run5}(\sigma_{run6}^2 - \rho\sigma_{run5}\sigma_{run6}) + r_{run6}(\sigma_{run5}^2 - \rho\sigma_{run5}\sigma_{run6})}{\sigma_{run5}^2 + \sigma_{run6}^2 - 2\rho\sigma_{run5}\sigma_{run6}}, \quad (4.14)$$

$$\sigma = \sqrt{\frac{\sigma_{run5}^2\sigma_{run6}^2(1 - \rho^2)}{\sigma_{run5}^2 + \sigma_{run6}^2 - 2\rho\sigma_{run5}\sigma_{run6}}}. \quad (4.15)$$

Here, r_{runi} and σ_{runi} are respectively the average of the yield of the single non-photonic electrons and total error in RUNi (i=5 or 6). ρ is the correlation coefficient between RUN5 and RUN6. ρ is defined as

$$\rho = \frac{\sum_{\alpha} \rho^{\alpha} \sigma_{run5}^{\alpha} \sigma_{run6}^{\alpha}}{\sigma_{run5} \sigma_{run6}}, \quad (4.16)$$

where α is the type of error. $\alpha = A, B$ or C . Total errors were determined as below.

$$\sigma_{runi} = \sqrt{(\sigma_{runi}^{stat})^2 + (\sigma_{runi}^{sys})^2}. \quad (4.17)$$

Table 4.2: Summary of error source

error source	correlation run5/6 (Type)
statistics	0 % (A)
PISA geometries	0%(B)
eID cut	0%(B)
cocktail calculation	100%(B)
trigger efficiency	0% (B)

The combined results from cocktail method are shown in Figure 4.14 and 4.15. χ^2/ndf is 18.7/33 with the standard eID cuts from 1.7GeV/c to 5GeV/c and is 1.4/7 with the tight

eID cut from $1.7\text{GeV}/c$ to $9\text{GeV}/c$. The values indicate the results in RUN5 and RUN6 are consistent.

The spectrum of the single non-photonic electron is shown in Figure 4.16. FONLL calculation, which is Fixed-Order plus Next-to-Leading-Log perturbative QCD calculation [38], is also shown in Fig 4.16.

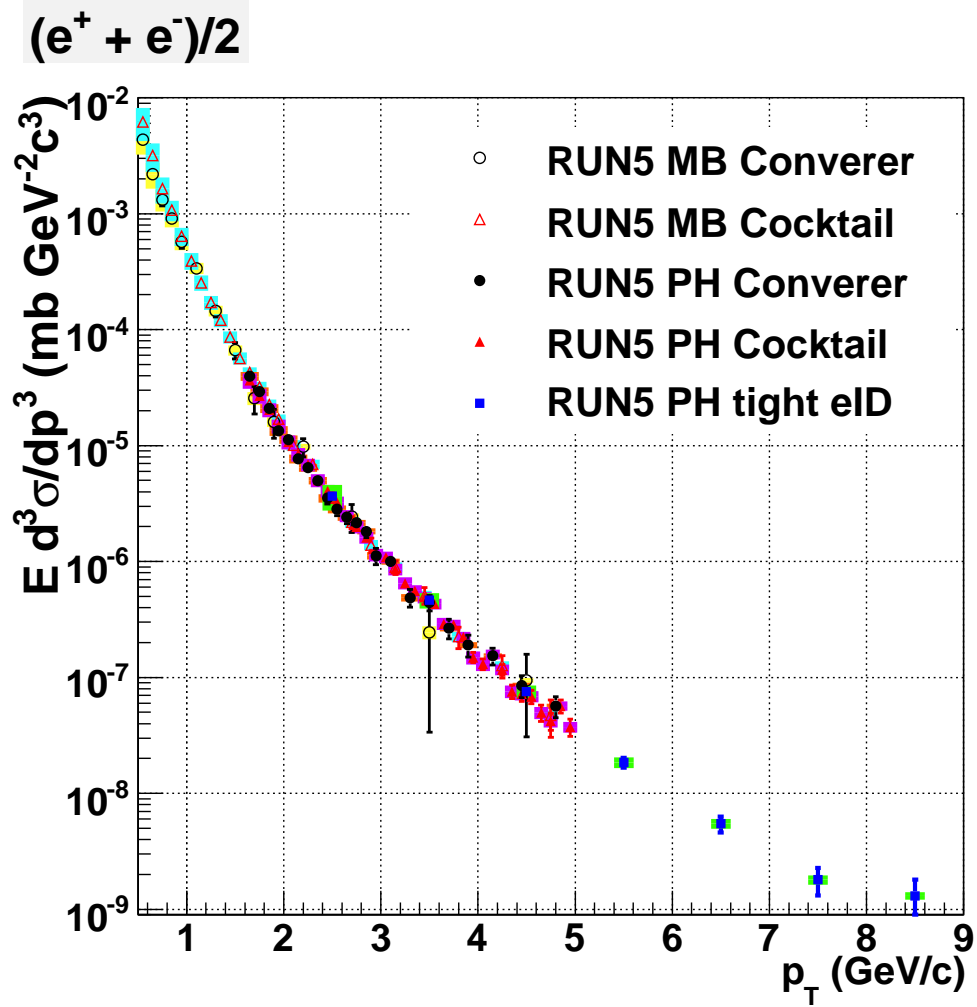


Figure 4.12: The invariant cross section of electrons from heavy flavor decay in RUN5 MB and PH data. Circle points show the result from converter method and triangle points show the result from cocktail method. Open symbols show the result at MB data and closed symbols show the result at PH data. Closed squares show the result at PH data with tight eID cut.

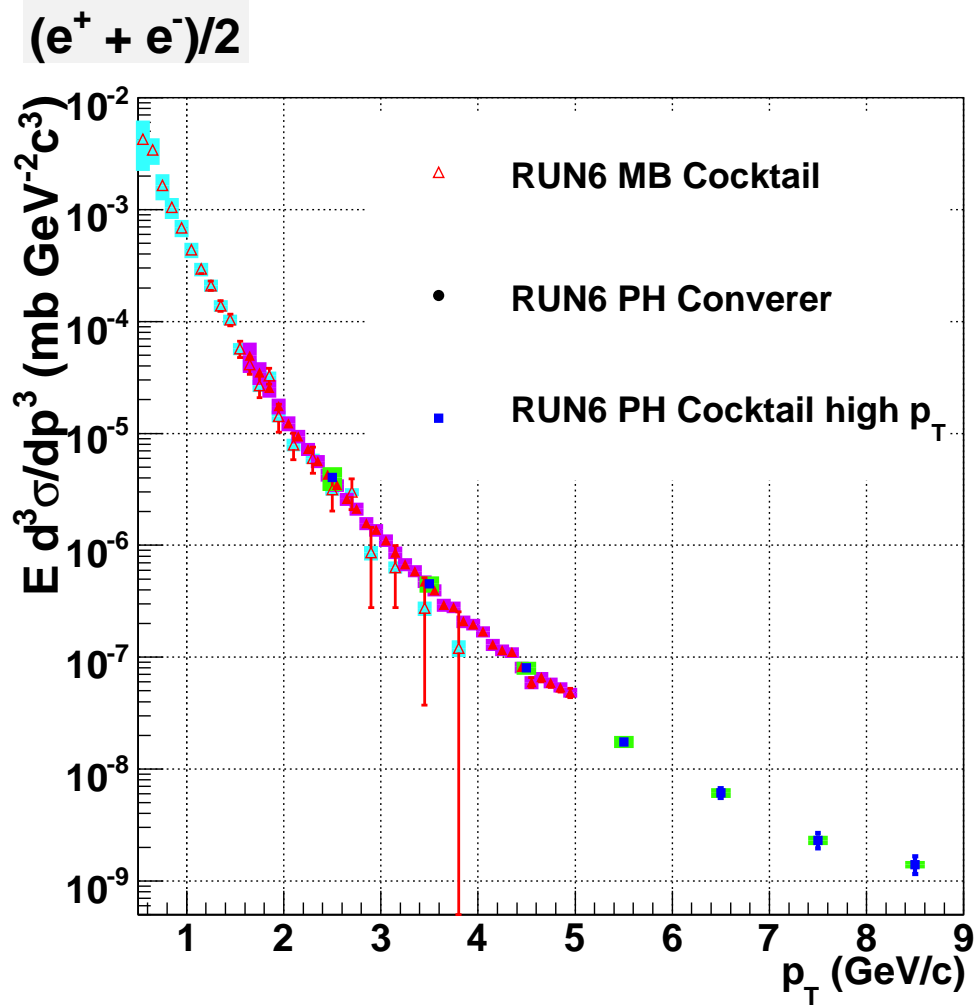


Figure 4.13: The invariant cross section of electrons from heavy flavor decay in RUN6 MB and PH data. Circle points show the result from converter method and triangle points show the result from cocktail method. Open symbols show the result at MB data and closed symbols show the result at PH data. Closed squares show the result at PH data with tight eID cut.

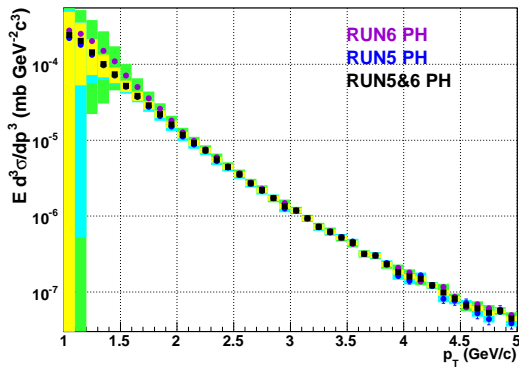


Figure 4.14: The invariant cross section of electrons from heavy flavor decay in RUN6 PH data. Red points show the results from cocktail method and black points show the result at high p_T extension.

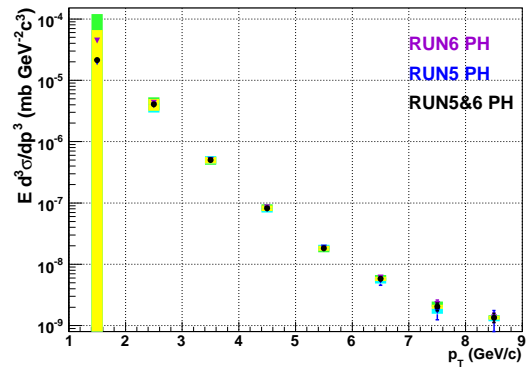


Figure 4.15: The invariant cross section of electrons from heavy flavor decay in RUN6 PH data. Red points show the results from cocktail method and black points show the result at high p_T extension.

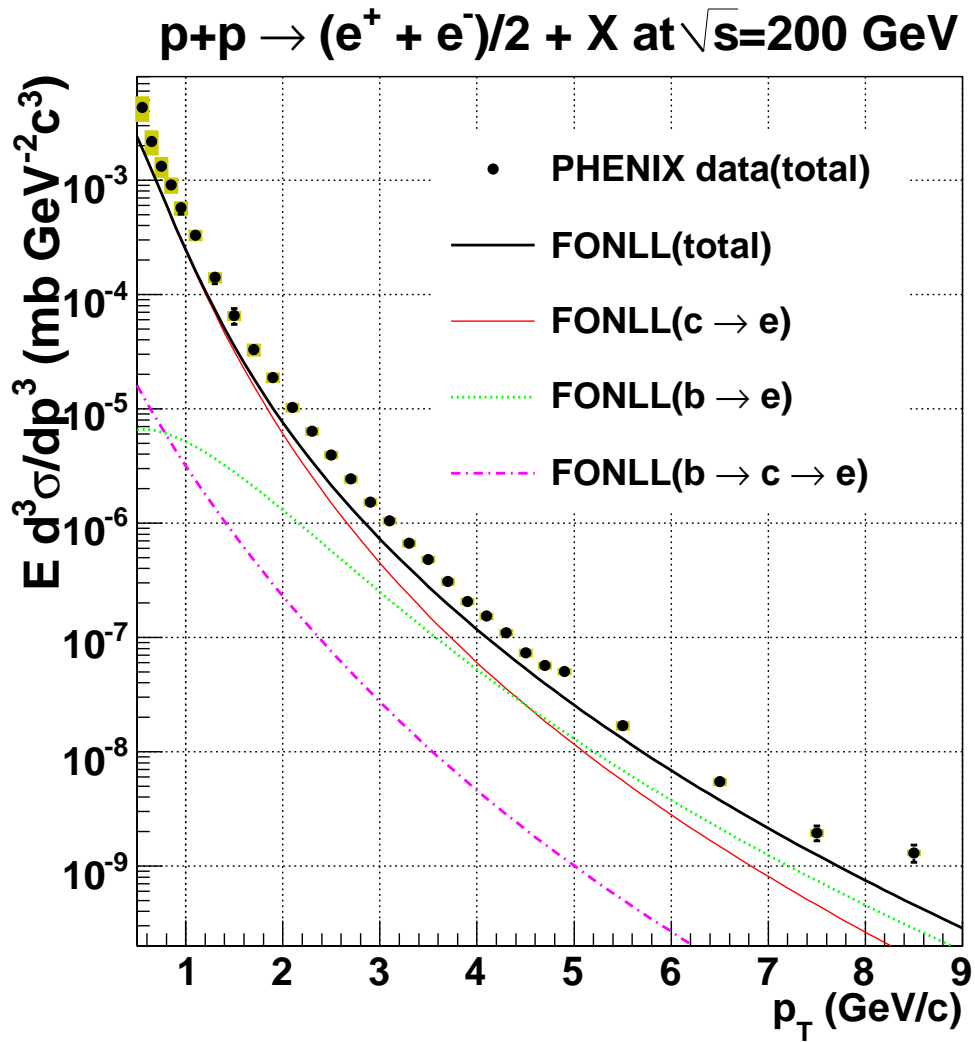


Figure 4.16: The spectrum of the single non-photonic electrons in RUN5 and RUN6 with FONLL calculation [38].

Chapter 5

Correlation analysis

This chapter describes real data analysis. Calculation of ϵ_{data} is described at this chapter. All trigger electrons and associated charged particles in CNT_ERT data set at RUN5 and RUN6 was used for this analysis. Trigger electrons are required $2.0 < p_T$ GeV/ c The analysis process is also described at [1, 2].

5.1 Extraction Method

The extraction of $(b \rightarrow e)/(c \rightarrow e + b \rightarrow e)$ by utilizing the correlation of the single non-photonic electrons and the associated hadrons is based on partial reconstruction of $D^0 \rightarrow e^+ K^- \nu_e$ decay. Unlike charge sign pairs of trigger electrons for $2.0 < p_T < 7.0$ GeV/ c and associated hadrons for $0.4 < p_T < 5.0$ GeV/ c are reconstructed as partial reconstruction of $D^0 \rightarrow e^+ K^- \nu_e$ decay. Since most of charged kaon do not reach the hadron identification detector (TOF and EMCal) due to their short life time, the reconstruction efficiency of identified charged kaon is rather small. Therefore, kaon identification is not performed in the analysis and inclusive hadrons are assigned to be kaons. As a result, this analysis is NO Particle IDentified (NO PID) partial reconstruction of D^0 .

Determination of the background is crucial for this analysis, since the signal to background ratio is not good ($\sim 1/10$). There are two main sources in the background. The one is the combinatorial background from electrons and hadrons, where the selected trigger electron is not from semi-leptonic decay of heavy flavor. The other is the combinatorial background, where the trigger electron is the single non-photonic electron and the associated hadron is not from heavy flavor decay. The best way to subtract these backgrounds is to use like sign charge pairs of electrons and hadrons. This subtraction method is essential in this analysis. Since electron hadron pairs with opposite charge signs are produced only by weak decay, the background subtraction using like sign pairs cancel out the combinatorial background completely for the contribution of the trigger electron from e^+e^- pair creation. The electrons from e^+e^- pair creation are most in all background of the trigger electrons. Moreover, most of the associated hadrons not from heavy flavor decay are from jet fragmentation. The background subtraction using like sign pair cancel out most of contribution from the combination of the single non-photonic electrons and the hadrons from jet fragmentation, since jet is basically charge independent.

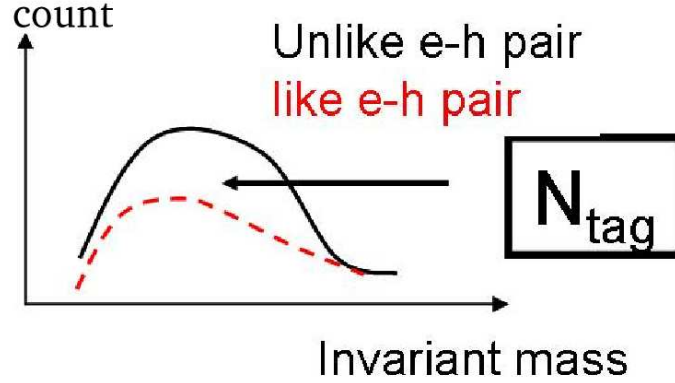


Figure 5.1: A conceptual view of invariant mass distributions of unlike sign pairs and like sign pairs.

Figure 5.1 shows a conceptual view of invariant mass distributions of unlike sign pairs and like sign pairs. N_{tag} is defined as the number of unlike sign electron-hadron pair entries (N_{unlike}) minus number of like sign electron-hadron pair entries (N_{like}). As already described, extracted signals N_{tag} are interpreted as the electron-hadron pairs mostly from heavy flavor decays, which are reconstructed partially such as $D^0 \rightarrow e^+ K^- \nu_e$ decay. N_{tag} contains inclusive signals from other heavy flavored hadrons (D^+, B^+, B^0 etc) and the remaining contribution from the associated hadron which is not from heavy flavor decay. These effects are evaluated by using the Monte-Carlo event generators.

The analysis procedure is as follows.

Tagging efficiency (ϵ_{data}), which is a similar variable as a conditional probability of the detection of an associated hadron in PHENIX detector when the electron from semi-leptonic decay of heavy flavored hadron is detected, is defined as below.

$$\epsilon_{data} \equiv \frac{N_{tag}}{N_{e(HF)}} = \frac{N_{c \rightarrow tag} + N_{b \rightarrow tag}}{N_{c \rightarrow e} + N_{b \rightarrow e}}, \quad (5.1)$$

where $N_{e(HF)}$ is the number of electrons from semi-leptonic decay of heavy flavor. $N_{c(b) \rightarrow e}$ is the number of electrons from semi-leptonic decay of charmed (bottomed) hadrons. $N_{c(b) \rightarrow tag}$ is the number of reconstructed signals (N_{tag}) for charm (bottom) production. Since N_{tag} include the contribution only from the single electrons from heavy flavor, ϵ_{data} could be written by only charm and bottom terms. ϵ_{data} is determined from real data analysis. The analysis detail to obtain ϵ_{data} is written at Sec. 5.3.

As a next step, tagging efficiency in the case of charm production ϵ_c and tagging efficiency in the case of bottom production ϵ_b are defined as below.

$$\epsilon_c \equiv \frac{N_{c \rightarrow tag}}{N_{c \rightarrow e}}, \quad \epsilon_b \equiv \frac{N_{b \rightarrow tag}}{N_{b \rightarrow e}}. \quad (5.2)$$

$\epsilon_{c(b)}$ is determined from the Monte-Carlo event generators. Since the extracted signal N_{tag} is dominated by decay products of heavy flavored hadrons, tagging efficiency is determined by

decay kinematics in the first order. Therefore, we can determine $\epsilon_{c(b)}$ with good precision using the simulation. The analysis detail to obtain $\epsilon_{c(b)}$ is written at Sec. 5.8.

Then, the fraction of bottom contribution to the electrons from heavy flavor is determined as,

$$\frac{N_{b \rightarrow e}}{N_{c \rightarrow e} + N_{b \rightarrow e}} = \frac{\epsilon_c - \epsilon_{data}}{\epsilon_c - \epsilon_b}, \quad (5.3)$$

5.2 Electrons from e^+e^- Creation

The contribution of the trigger electrons from e^+e^- creation must be canceled out in the subtraction of like sign electron-hadron pairs. This is the most important issue in this analysis. This fact is confirmed by PYTHIA event generator. Figure 5.2 shows invariant mass distributions of unlike sign electron-hadron pairs (black) and like sign electron-hadron pairs (red) in $|y| < 0.4$, where the trigger electron is from e^+e^- creation in PYTHIA events. Subtracted invariant mass distribution of electron-hadron pairs is shown in the right panels. Tagging effi-

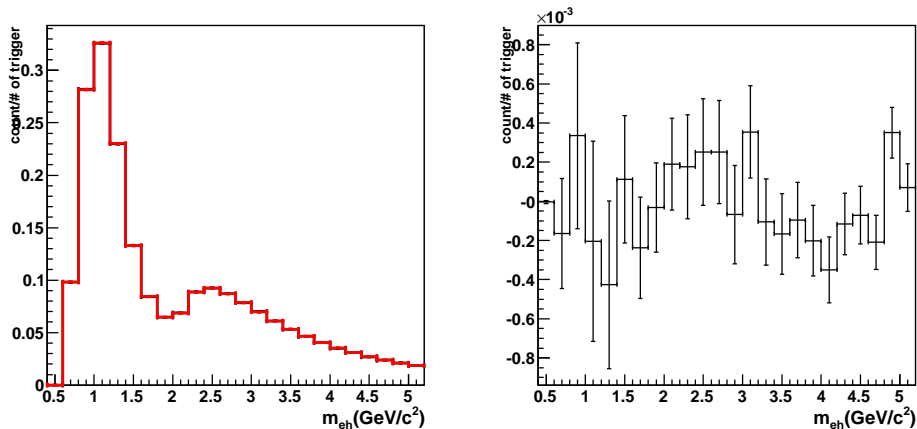


Figure 5.2: The invariant mass distribution of electron-hadron pairs in $|y| < 0.4$, when the trigger electron is photonic electron. In left panels, black lines are unlike charge sign pairs and red lines are like charge sign pairs. Subtracted invariant mass distribution of electron-hadron pairs was shown in the right panels.

ciency for the electrons from e^+e^- creation, ϵ_{photo} is -0.00051 ± 0.00097 in $|y| < 0.4$. This result confirms the issue that the contribution of the electrons from e^+e^- creation is canceled out completely.

5.3 Correlation Analysis at Real Data

In this section, tagging efficiency in the real data analysis, ϵ_{data} , is obtained. ERT triggered data in RUN5 and RUN6 is used in this correlation analysis.

5.4 Used Cut for the Correlation Analysis

The following cuts are used to select the trigger electrons and the associated hadrons in real data and the simulation.

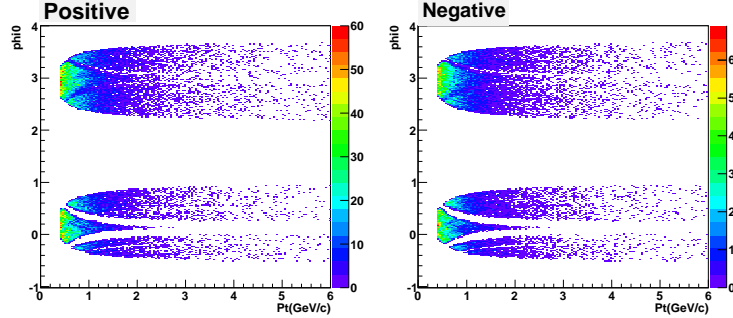


Figure 5.3: Phase spaces of positive charged hadron with the geometrical cut in RUN5.

- **Event Cut:** $-25 < \text{bbcz} < 25$ (cm)
- **Electron Cut:** The standard electron cut is applied for the tracks with $2 < p_T < 5$ GeV/ c and the tight electron cut is applied above 5 GeV/ c . The details of this cut are described in Sec. 2.2.3
- **Hadron Cut:** $\text{quality} > 15$ and $n_0 < 0$ (RICH veto) cut is applied to select hadron for the charged particles with $0.4 < p_T < 5.0$ GeV/ c . The selected hadron tracks are analyzed with the kaon hypothesis, that is, the selected particles have kaon mass.
- **Acceptance Filter:** Since the acceptance (phase space) for positive charged particles and negative charged particles is different due to the detector geometry of PHENIX, the effect of the difference in the phase space needs to be corrected for the subtraction of the like charge sign pairs. The fiducial cut is applied to make the phase space of negative and positive charged tracks identical as the correction for the phase space effect. Figure 5.3 shows the phase spaces of associated negative charged particle and positive charged particle with the geometrical cut.
- **Electron Pair Cut:** RICH veto cut ($n_0 < 0$) used in hadron cut does not reject electron contamination in the selected hadrons completely due to dead area and limited acceptance of RICH. Since about a half of the measured electrons above 2 GeV/ c is produced via the $e^+ e^-$ pair creation, there are strong charge correlation of electron pairs in the events where the trigger electron is found. It is found that the effect of such electron contamination in the hadron tracks is not negligible. The electron contamination is rejected using M_{ee} , which is the invariant mass between identified trigger electrons and the associated tracks where their mass is assigned to be electron mass (0.511MeV). Most of the electron pairs are produced from π^0 Dalitz decay and γ conversion at the beam pipe. They could be

identified via the reconstructed invariant mass distribution of $e^+ e^-$ pair as the peaks at the low mass region. Figure 5.4 shows the M_{ee} distribution of unlike and like pairs of the selected electron and hadron in RUN6. In Fig 5.4, black points show unlike charge sign pairs and red points show like charge sign pairs. The clear peak is shown at the low mass region and $M_{ee} > 0.08\text{GeV}$ is required for the rejection of these electron pairs.

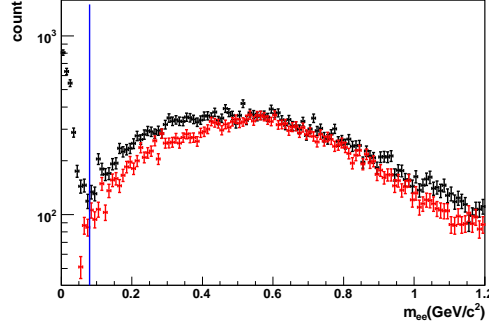


Figure 5.4: M_{ee} distribution of unlike sign and like sign pairs of the selected electron and hadron in RUN6. Black points show unlike charge sign pairs and red points show like charge sign pairs.

5.5 Calculation of ϵ_{data}

Tagging efficiency in the real data, ϵ_{data} is calculated with the trigger electron for $2.0 < p_T < 7.0 \text{ GeV}/c$.

5.5.1 Count of N_{tag}

M_{eh} is defined as the invariant mass of particle pairs when the trigger particle is assumed to be electron and the associated particle is assumed to be kaon. Figure 5.5 and Figure 5.6 show invariant mass distributions (M_{eh}) of unlike and like sign pairs of the trigger electrons and the associated hadrons at each electron p_T range in RUN5 and RUN6, respectively. In Fig .5.5 and 5.6, black lines are unlike charge sign pairs and red lines are like charge sign pairs. Title in each panel shows the trigger electron p_T range. Clear excess of unlike sign pairs can be seen. The excess indicates the existence of the $D^0 \rightarrow e^+ K^- \nu_e$ signals. The distributions of like sign pairs are subtracted from the distributions of unlike sign pairs to utilize the effect of semi-leptonic decay of D and B hadrons.

Subtracted invariant mass distributions still include the contribution of the remaining electron pairs which have $M_{ee} > 0.08 \text{ GeV}$. These remaining electron pairs must be estimated and subtracted to count signals. Identified electron pairs are used to estimate the amount of the remaining electron pairs. One of the electron pair is the trigger electron and the other is associated electron with $0.4 < p_T < 5.0 \text{ GeV}/c$. The contribution of the remaining electron pairs is

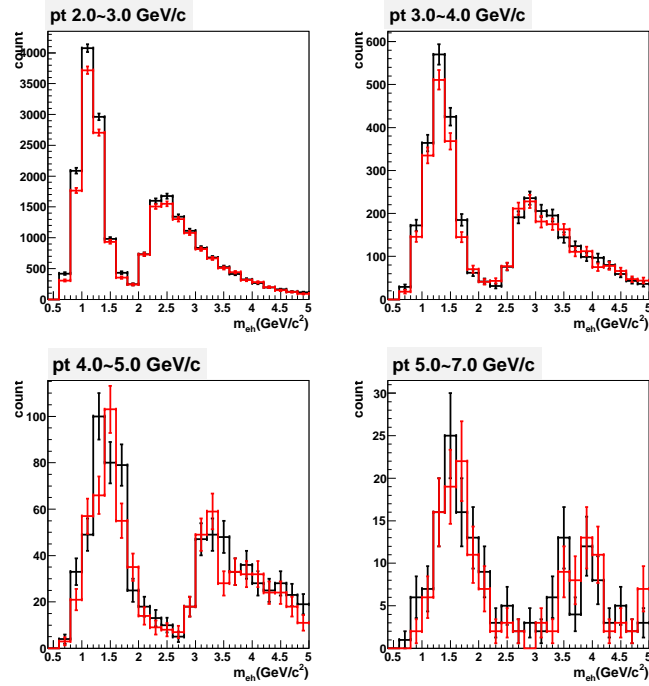


Figure 5.5: Invariant mass distribution from trigger electrons and associated hadrons in RUN5. Black lines are unlike charge sign pairs and red lines are like charge sign pairs.

estimated by the normalized M_{eh} distribution of the identified electron pairs in $M_{ee} > 0.08$ GeV. Normalization of the M_{eh} distribution of the identified electron pairs, where the associated electron is assigned as kaon mass, is determined by the number of entries in $M_{ee} < 0.08$ GeV of the electron and hadron pairs (the number of entries in the peaks from π^0 Dalitz and beam pipe conversion). Figure 5.7 and 5.8 show the subtracted M_{eh} distributions of electron hadron pairs and the estimated M_{eh} distributions of the remaining electron pairs at each electron p_T range in RUN5 and RUN6, respectively. In Fig 5.7 and 5.8, black points show the subtracted M_{eh} distributions and red points show the estimated M_{eh} distributions of the remaining electron pairs.

The estimated M_{eh} distributions of the remaining electron pairs are subtracted from the M_{eh} distributions of electron hadron pairs. After this subtraction, the M_{eh} distributions are regarded as the extracted signals. Figure 5.9 and 5.10 show the extracted reconstruction signals in RUN5 and RUN6 respectively. In Fig 5.9 and 5.10, numbers of entries in $0.4 < M_{eh} < 1.9$ GeV are counted as N_{tag} , since this analysis is partial reconstruction of D^0 and it is not necessary to require tight mass cut around D^0 region. The results of N_{tag} are summarized in Table 5.2 and Table 5.3.

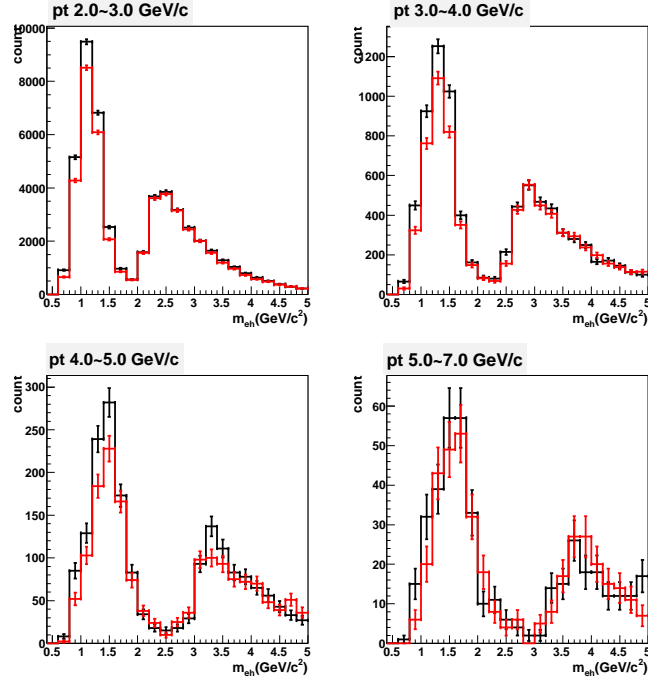


Figure 5.6: Invariant mass distribution from trigger electrons and associated hadrons in RUN6. Black lines are unlike charge sign pairs and red lines are like charge sign pairs.

5.5.2 Number of Electrons from Heavy Flavor

The number of single non-photonic electrons, $N_{e(HF)}$ in Eq. 5.1 is counted according to the following equation.

$$N_{e(HF)} = \int dp_T N_e(p_T) \times R_{HF}(p_T), \quad (5.4)$$

where, $N_e(p_T)$ is the number of measured electrons and $R_{HF}(p_T)$ is the fraction of single non-photonic electrons in measured inclusive electrons as a function of electron p_T . $R_{HF}(p_T)$ is determined as the ratio of the spectrum of single non-photonic electrons obtained at Section 4.4.2 over the sum of spectrum of single non-photonic electrons and the background electrons in the cocktail. Figure 5.11 and Figure 5.12 show the obtained $R_{HF}(p_T)$ in RUN5 and RUN6, respectively. The obtained $R_{HF}(p_T)$ is fitted, which is shown black line in Fig. 5.11 and 5.12. The number of single non-photonic electrons is calculated from the fitted line.

5.6 Systematic Error of ϵ_{data}

The following factors are considered.

- The subtraction of like sign pairs
- The subtraction of the remaining electron pairs
- The counting of single non-photonic electrons

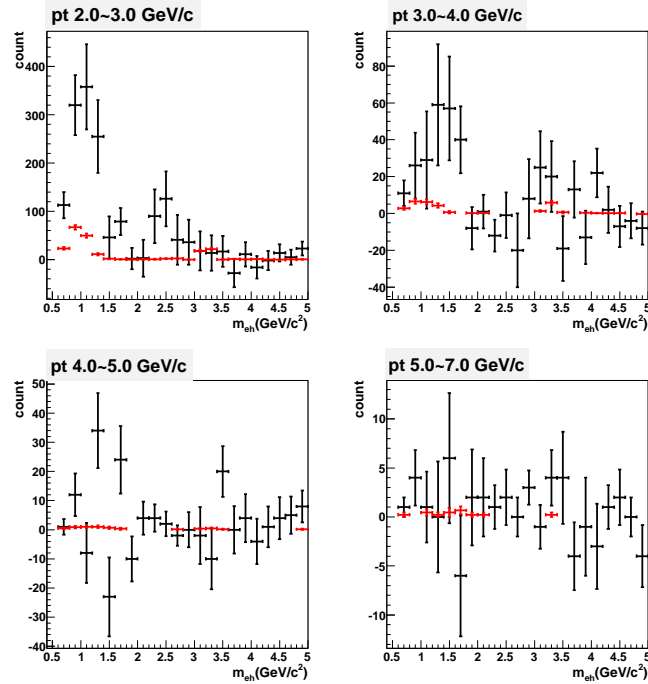


Figure 5.7: Subtracted M_{eh} distribution of electron-hadron pairs (black points) and estimated M_{eh} distributions of the remaining electron pairs (red points) in RUN5.

- Other contributions to N_{tag} background

5.6.1 Subtraction of Like Sign Entries

Systematic error associated with the subtraction of like sign entries is determined based on the effect of the difference in the phase space with the acceptance filter described in Sec. 5.4. The effect of the difference in the phase space on the extracted signals (N_{tag}) is evaluated by using un-correlated electron hadron pairs. Event mixing method is used to create the pairs of un-correlated electrons and hadrons.

The M_{eh} distributions of the un-correlated like sign pairs are expected to be identical as these of the un-correlated unlike sign pairs, if the phase space of negative and positive charged tracks is identical. Therefore, the discrepancy between unity and the ratio of (unlike sign)/(like sign) M_{eh} distribution in mixing events is used for the estimation of the systematic error. Figure 5.13 shows the ratio of (unlike sign)/(like sign) M_{eh} distribution in mixing events in RUN5. The ratios of (unlike sign)/(like sign) M_{eh} distributions are fitted by a constant as shown at Fig. 5.13. Result of fit is summarized at Table 5.1.

When the fit result is consistent with unity within the fitting error, (error of the fit) \times (M_{eh} distribution of like sign pairs) is assigned as the systematic error for the subtraction of like sign entries. When the fit result is not consistent with unity within fitting error, (the deviation of the fitted value from unity) \times (M_{eh} distribution) is assigned as the systematic error for the subtraction.

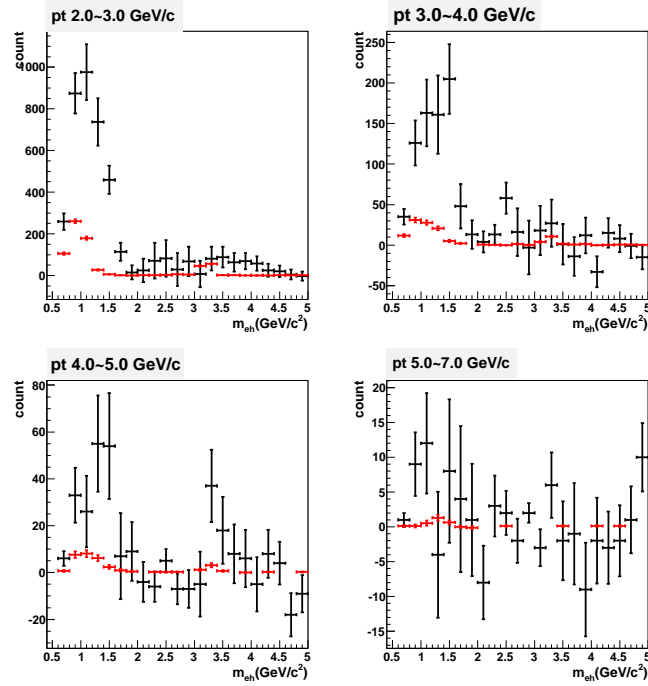


Figure 5.8: Subtracted M_{eh} distribution of electron-hadron pairs (black points) and estimated M_{eh} distributions of the remaining electron pairs (red points) in RUN6.

Table 5.1: Result of fit for (mixing unlike sign)/(mixing like sign) by constant electron p_T range

electron p_T range	mean(RUN5)	error(RUN5)	mean(RUN6)	error(RUN6)
2.0-3.0 GeV/c	0.9995	0.0005	1.0009	0.0002
3.0-4.0 GeV/c	1.006	0.001	1.002	0.0004
4.0-5.0 GeV/c	1.005	0.003	1.002	0.001
5.0-7.0 GeV/c	0.998	0.004	1.002	0.001

5.6.2 Subtraction of Remaining Electron Pairs

The systematic error for the subtraction of the remaining electron pairs is evaluated by the error of the normalization factors for the M_{ee} distribution of identified electron pairs. The error of the normalization factors is determined by the statistical uncertainty of the numbers of entries of identified electron pairs and electron hadron pairs in $M_{ee} < 0.08$ GeV. The uncertainty of normalization is assigned as the systematic error for subtraction of the remaining electron pairs.

5.6.3 Count of Electrons from Heavy Flavor

This uncertainty is the largest source of the systematic error of N_{tag} . Systematic error for the number of electrons from heavy flavor is calculated based on the systematic error of spectra of

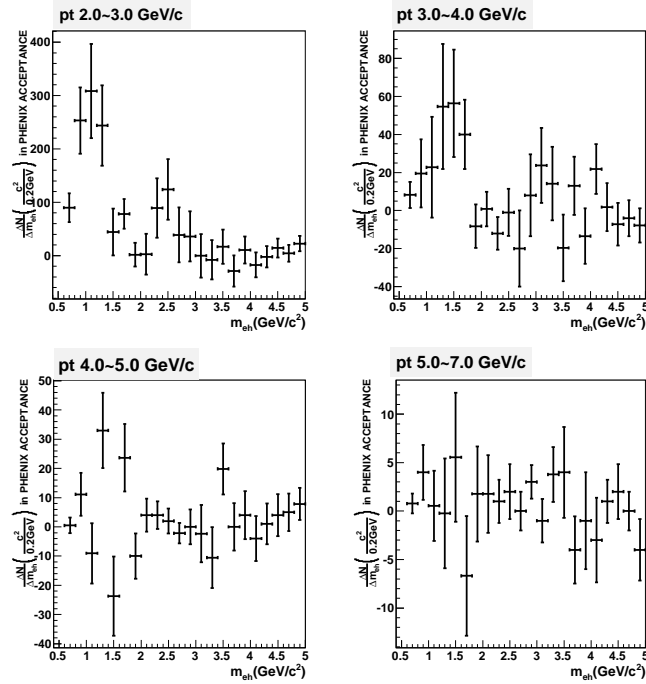


Figure 5.9: Subtracted invariant mass distribution of electron-hadron pairs after subtraction of estimated remaining electron pairs in RUN5.

electrons from heavy flavor decay. The systematic error of spectra are shown in Fig.5.11 and 5.12.

5.6.4 Other Contributions to N_{tag} Background

Following sources are possible to make correlation of electrons and hadrons.

- **K_{e3} decay:**

Since $K_L \rightarrow e^\pm \pi^\mp$ is weak decay, the subtraction of like sign entries can not cancel out this contribution. Therefore, $K_L \rightarrow e^\pm \pi^\mp$ is possible to be background source of charge correlation of electrons and hadrons. This contribution is estimated by the PISA simulation which is used at the cocktail calculation. It is found the contribution of K_{e3} decay to N_{tag} is 0.5% level. Therefore, this contribution can be neglected.

- **Hadron-hadron correlation:**

The charge correlation of hadron hadron pairs becomes the background source of charge correlation of electron and hadron pairs, since there is small hadron contamination in trigger electrons .

The amount of hadron contamination in the trigger electrons is less than 0.5% at $2.0 < p_T < 5.0$ GeV/c, which is estimated in Sec. 3.3.3. The tagging efficiency of hadron hadron pairs correlation (ϵ_{had}) is determined from real data analysis. As a result, the

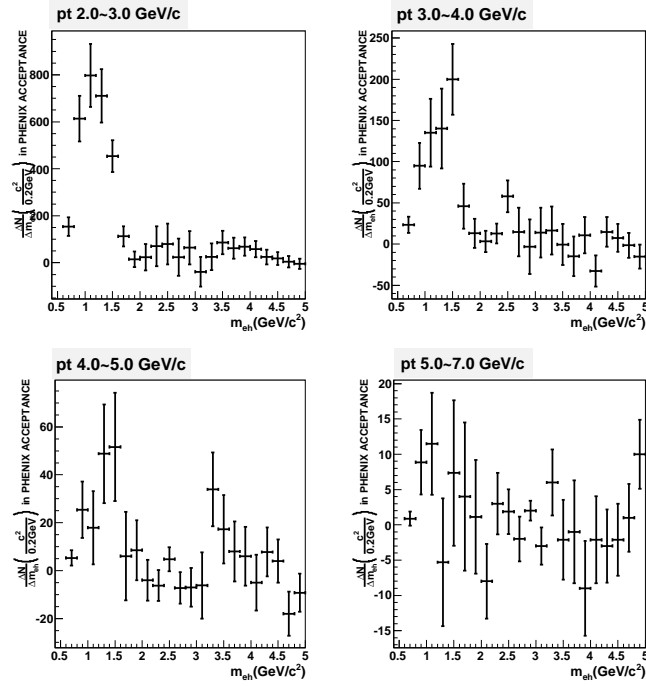


Figure 5.10: Subtracted invariant mass distribution of electron-hadron pairs after subtraction of estimated remaining electron pairs in RUN6.

contribution of hadron hadron correlation to N_{tag} is 0.5% level at $2.0 < p_T < 5.0$ GeV/ c . This contribution can be also neglected at $2.0 < p_T < 5.0$ GeV/ c .

Hadron background is not negligible at high p_T (>5.0 GeV/ c) as estimated in Sec. 3.3.3, while tight eID cut is applied. The number of hadron contamination is calculated according to Table 3.3. The tagging efficiency of hadron hadron pairs (ϵ_{had}) at high p_T is also determined from real data analysis. The amount of hadron contamination is calculated from the estimated number of hadron contamination in the trigger electrons and the tagging efficiency of hadron hadron pairs. This contribution is subtracted from extracted signals (N_{tag}) at high p_T (>5.0 GeV/ c) region. Tagging efficiency of hadrons depends on the distribution of hadron p_T . The p_T distribution of hadron with above cuts may differ from that of hadron background in electrons with tight eID cut. 50% systematic error is assigned for this subtraction.

5.7 Results of ϵ_{data}

ϵ_{data} is calculated from N_{tag} and the number of electrons from heavy flavor decay. ϵ_{data} and used values are summarized in Table 5.2 and 5.3.

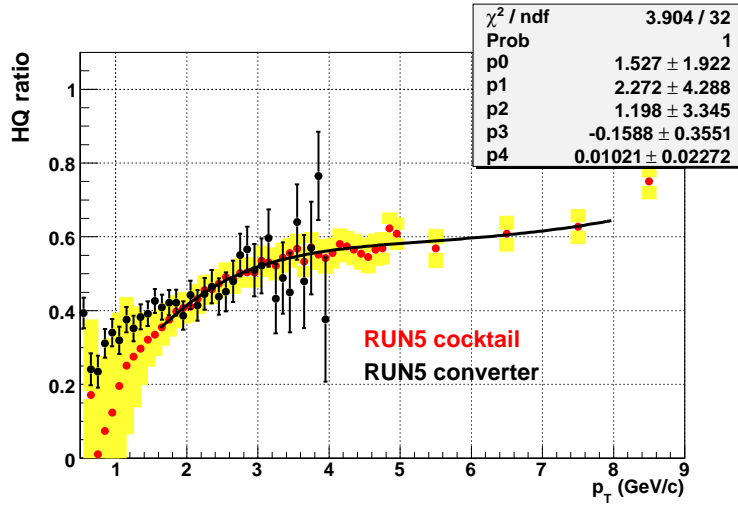


Figure 5.11: The fraction of electron from heavy flavor decay in inclusive electrons in RUN5 as a function of electron p_T .

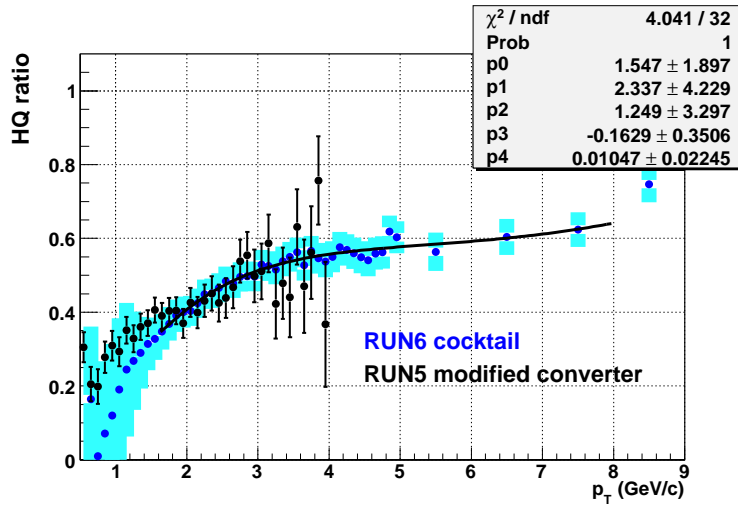


Figure 5.12: The fraction of electron from heavy flavor decay in inclusive electrons in RUN6 as a function of electron p_T .

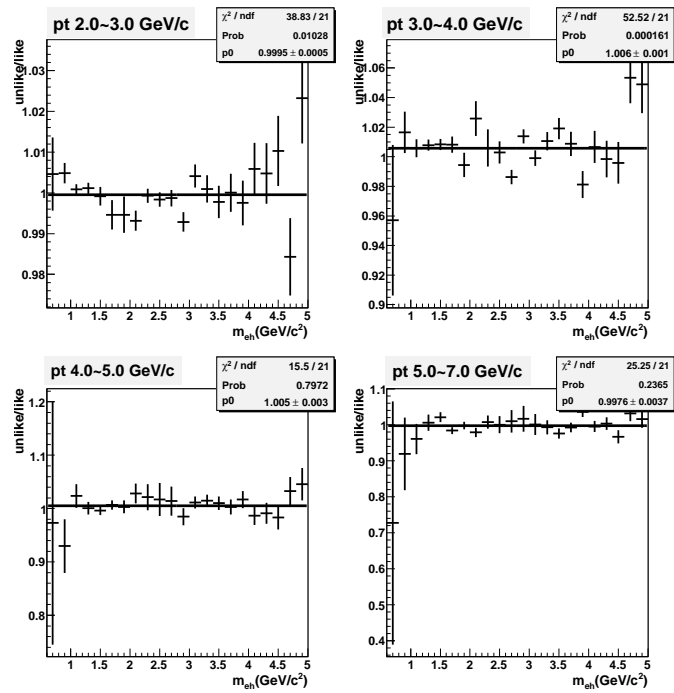


Figure 5.13: The ratio of (unlike sign)/(like sign) M_{eh} distribution in mixing events in RUN5.

Table 5.2: ϵ_{data} and used values at each electron p_T range(RUN5)

electron p_T 2.0-3.0 GeV/ c	
number of unlike sign entries	11050.
number of like sign entries	9872.
number of (unlike -like)	$1178.0 \pm 144.6 \pm 5.0$
remaining e-e pair	$153.3 \pm 7.4 \pm 6.1$
N_{tag}	$1024.7 \pm 144.8 \pm 7.9$
number of heavy flavor electron	$31402.2 \pm 262.5 \pm 2783.$
ϵ_{data}	$0.0326 \pm 0.0046 \pm 0.0029$
electron p_T 3.0-4.0 GeV/ c	
number of unlike sign entries	1770.
number of like sign entries	1548.
number of (unlike -like)	$222.0 \pm 57.6 \pm 9.3$
remaining e-e pair	$20.7 \pm 2.5 \pm 2.5$
N_{tag}	$201.3 \pm 57.7 \pm 9.6$
number of heavy flavor electron	$5310.1 \pm 99.4 \pm 402.5$
ϵ_{data}	$0.0379 \pm 0.0109 \pm 0.0034$
electron p_T 4.0-5.0 GeV/ c	
number of unlike sign entries	353.
number of like sign entries	323.
number of (unlike -like)	$30.0 \pm 26.00 \pm 1.6$
remaining e-e pair	$4.5 \pm 0.9 \pm 1.2$
N_{tag}	$25.5 \pm 26.0 \pm 2.0$
number of heavy flavor electron	$1181.9 \pm 45.5 \pm 89.2$
ϵ_{data}	$0.0216 \pm 0.0220 \pm 0.0023$
electron p_T 5.0-7.0 GeV/ c	
number of unlike sign entries	78.
number of like sign entries	71.
number of (unlike -like)	$7. \pm 12.2 \pm 0.3$
remaining e-e pair	$2.0 \pm 0.7 \pm 1.1$
number of background hadron	$17.8 \pm 3.7(\text{sys})$
signal from hadron	$1.5 \pm 0.8(\text{sys})$
N_{tag}	$3.5 \pm 12.2 \pm 1.4$
number of heavy flavor electron	$269.9 \pm 21.8 \pm 23.5$
ϵ_{data}	$0.0131 \pm 0.0457 \pm 0.0052$

Table 5.3: ϵ_{data} and used values at each electron p_T range(RUN6)

electron p_T 2.0-3.0 GeV/ c	
number of unlike sign entries	26066.
number of like sign entries	22630.
number of (unlike -like)	$3436. \pm 220.7 \pm 5.0$
remaining e-e pair	$578.4 \pm 13.6 \pm 15.5$
N_{tag}	$2857.6 \pm 221.1 \pm 16.1$
number of heavy flavor electron	$76408. \pm 412.5 \pm 6763.9$
ϵ_{data}	$0.0374 \pm 0.0029 \pm 0.0033$
electron p_T 3.0-4.0 GeV/ c	
number of unlike sign entries	4191.
number of like sign entries	3447.
number of (unlike -like)	$744.0 \pm 87.4 \pm 7.0$
remaining e-e pair	$98.3 \pm 5.5 \pm 7.2$
N_{tag}	$645.7 \pm 87.6 \pm 7.2$
number of heavy flavor electron	$12897.0 \pm 155.7 \pm 977.4$
ϵ_{data}	$0.0501 \pm 0.0068 \pm 0.0039$
electron p_T 4.0-5.0 GeV/ c	
number of unlike sign entries	951.
number of like sign entries	774.
number of (unlike -like)	$177.0 \pm 41.5 \pm 0.5$
remaining e-e pair	$26.2 \pm 2.6 \pm 4.5$
N_{tag}	$150.8 \pm 41.9 \pm 4.7$
number of heavy flavor electron	$2933.0 \pm 72.0 \pm 222.$
ϵ_{data}	$0.0514 \pm 0.0142 \pm 0.0042$
electron p_T 5.0-7.0 GeV/ c	
number of unlike sign entries	216.00
number of like sign entries	183.0
number of (unlike -like)	$33.0 \pm 20.0 \pm 0.4$
remaining e-e pair	$2.7 \pm 0.7 \pm 1.1$
number of background hadron	$51.5 \pm 10(\text{sys})$
signal from hadron	$4.5 \pm 2.3(\text{sys})$
N_{tag}	$25.8 \pm 20.0 \pm 2.6$
number of heavy flavor electron	$638.4 \pm 33.6 \pm 54.6$
ϵ_{data}	$0.0404 \pm 0.0314 \pm 0.0057$

5.8 Simulation Study for Correlation Analysis

. This section describes the evaluation of ϵ_c and ϵ_b . ϵ_c and ϵ_b is determined by using Monte-Carlo event generator as outlined in Sec. 5.1.

5.9 Simulation Overview

Figure 5.14 shows a conceptual view of the simulation study. The simulation is performed in three steps. First, p+p collision at 200 GeV in the center of mass system is generated by PYTHIA event generator. As a next step, the decay of D and B hadrons in the generated event is simulated by using EvtGen event generator [19, 20]. Therefore, the event which contains D and B hadrons is generated by the combination of PYTHIA and EvtGen. Finally, all stable particles in the generated event are put into the PISA simulation to evaluate the detector response.

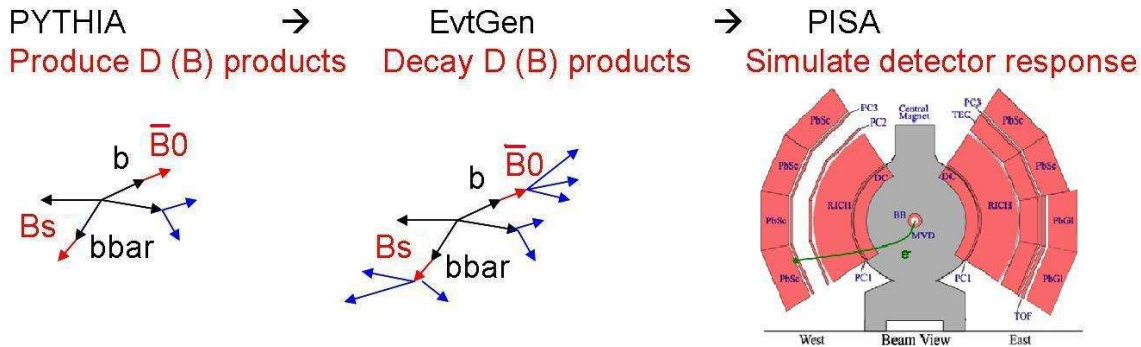


Figure 5.14: A conceptual view of the simulation study

5.9.1 PYTHIA Simulation

PYTHIA simulation (version 6.403) is used to generate p+p collision at 200 GeV in the center of mass system. PYTHIA parameters are tuned to reproduce previous results of heavy flavor production measured by PHENIX [15] and jet production measured by CDF [3]. Since ϵ_c and ϵ_b contain inclusive signals from various heavy flavored hadrons, the production ratios of D or B mesons and baryons ($D^+/D^0, B^+/B^0$ etc) are most important parameters to determine ϵ_c and ϵ_b . Therefore, the production ratios are also tuned according to the experimental results [16, 17, 18]. Tuning parameters of PYTHIA are summarized at Table 5.4. Tuning status of PYTHIA is described in Appendix. C

5.9.2 EvtGen Simulation

EvtGen (version alpha-00-14-05) is used to simulate the decay of D and B hadrons. EvtGen simulation provides a framework for implementation of the decay process of D and B hadrons.

Table 5.4: PYTHIA tuning parameters

parameter name	value
charm mass	1.25 GeV
bottom mass	4.3 GeV
k_T	1.5 GeV/ c
PDF	CTEQ5L
PARJ(13) (charm production)	0.55
PARJ(2) (charm production)	0.36
PARJ(2) (bottom production)	0.44
MSTP(82)	4
PARP(81)	1.9
PARP(82)	2.0
PARP(83)	0.5
PARP(84)	0.4
PARP(85)	0.9
PARP(86)	0.95
PARP(89)	1800
PARP(90)	0.25
PARP(67)	4.0

EvtGen simulation is tuned to reproduce the results of heavy flavor decay at CLEO, BaBar and Belle. Semi-leptonic decay of D and B hadrons is main interest in this analysis. Most of semi-leptonic decay is simulated based on the ISGW2 model in EvtGen. For example, Figure 5.15 shows the electron energy spectrum of inclusive semi-leptonic decay of B meson ($B \rightarrow e\nu X$) in EvtGen simulation and that in CLEO data.

5.9.3 PISA Simulation

All stable particles in the generated event are put into the PISA simulation to evaluate the detector response. The PISA simulation is tuned for the RUN5 and RUN6 detector response as described in Sec. 2.2.3.

5.10 Calculation of ϵ_c and ϵ_b

ϵ_c and ϵ_b are determined via the simulation as outlined in the previous subsection. PYTHIA with MSEL of 4 and 5 are used to produce charm and bottom and to determine ϵ_c and ϵ_b , respectively. For the calculation of ϵ_c and ϵ_b , electron hadron pairs in the simulation are

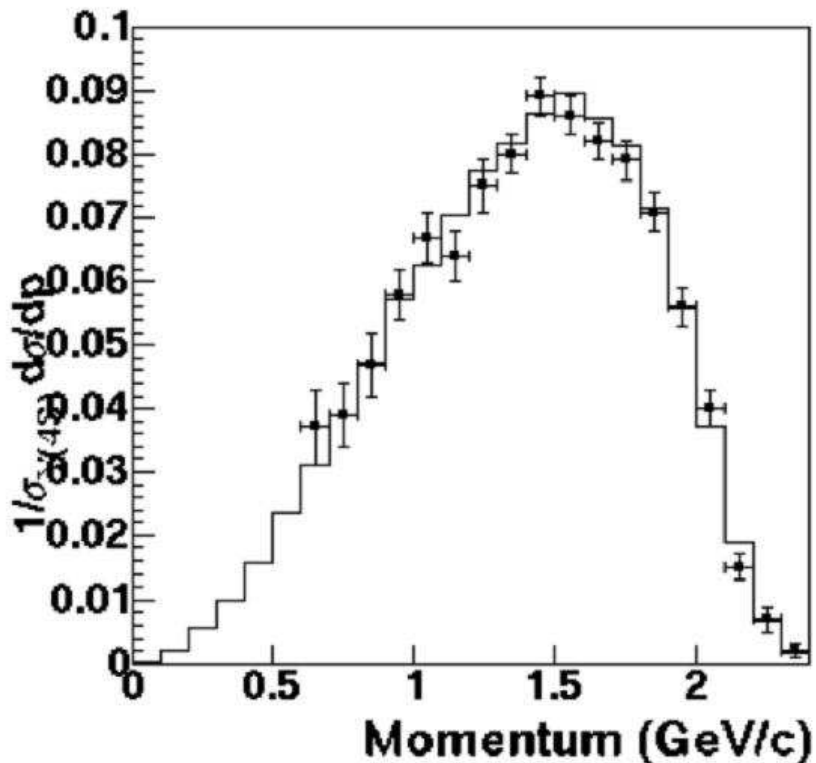


Figure 5.15: Electron energy spectrum at $B \rightarrow e\nu X$ of EvtGen and CLEO [23].

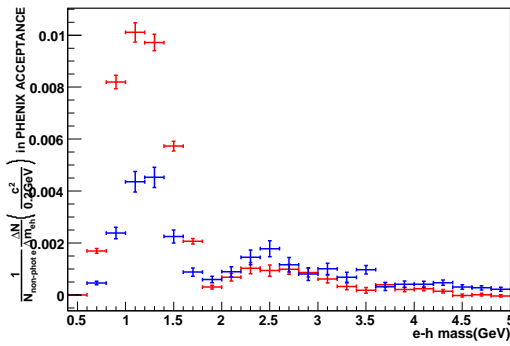
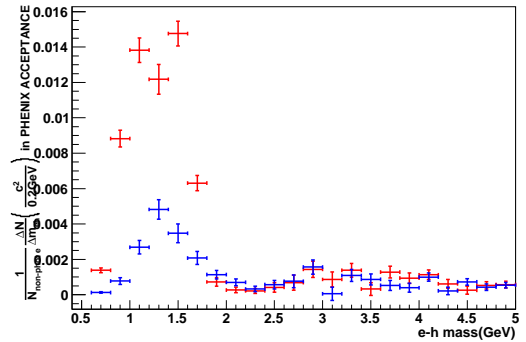
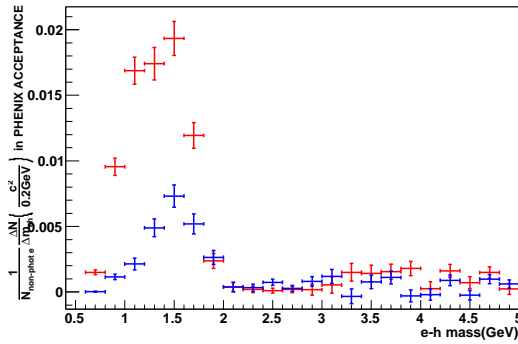
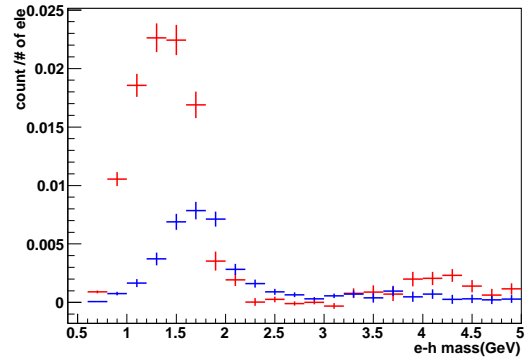
processed in a similar way to evaluate ϵ_{data} in the real data analysis. In the simulation, the rejection of the estimated remaining electron pairs and the calculation of the number of single non-photonic electrons are not performed, since we can reject background for the trigger electron by looking the parent particle in the simulation. Only the subtraction of the M_{eh} distribution of like sign pairs is performed to extract signals from heavy flavor. As a next step, the M_{eh} distribution is normalized by the number of trigger electrons.

Figure 5.16 to 5.19 show the normalized reconstruction signals in charm and bottom production at each electron p_T range in RUN5 configuration. Red points show reconstruction signals in charm production and blue points show these in bottom production.

ϵ_c and ϵ_b at each electron p_T range are determined as the number of entries in $0.4 < M_{eh} < 1.9$ GeV in Fig.5.16 to 5.19. Results of ϵ_c and ϵ_b are summarized in Table 5.5. ϵ_c increases as electron p_T increases by kinematic reason.

Table 5.5: Result of ϵ_c

electron p_T range	ϵ_c		ϵ_b	
	RUN5	RUN5	RUN6	RUN6
2.0-3.0 GeV/c	0.0378	0.0162	0.0371	0.156
3.0-4.0 GeV/c	0.0566	0.0160	0.0563	0.0168
4.0-5.0 GeV/c	0.0810	0.0210	0.0781	0.0198
5.0-7.0 GeV/c	0.0921	0.0275	0.0913	0.0270

**Figure 5.16:** Subtracted and normalized invariant mass distributions of electron-hadron pairs in charm and bottom production. Red points show charm case and blue points show bottom case. p_T range of trigger electrons is 2.0-3.0 GeV/c.**Figure 5.17:** Subtracted and normalized invariant mass distributions of electron-hadron pairs in charm and bottom production. p_T range of trigger electrons is 3.0-4.0 GeV/c.**Figure 5.18:** Subtracted and normalized invariant mass distributions of electron-hadron pairs in charm and bottom production. p_T range of trigger electrons is 4.0-5.0 GeV/c.**Figure 5.19:** Subtracted and normalized invariant mass distributions of electron-hadron pairs in charm and bottom production. p_T range of trigger electrons is 5.0-7.0 GeV/c.

5.11 Systematic Errors for ϵ_c and ϵ_b

Systematic error for ϵ_c and ϵ_b can be categorized into two components. One is systematic error of the difference in reconstruction efficiency including geometrical acceptance between real data and PISA simulation. This component is common factor for ϵ_c and ϵ_b . The other is from the uncertainty of the event generator (PYTHIA and EvtGen). The uncertainty of ϵ_c and ϵ_b originated from the uncertainty of PYTHIA and EvtGen needs to be assigned as systematic error. These errors are estimated for ϵ_c and ϵ_b separately. The following factors are considered.

- Production ratios of charmed and bottomed hadrons
- Branching ratios of charmed and bottomed hadrons
- Momentum distribution of charmed and bottomed hadrons
- PYTHIA parameters

5.11.1 Geometrical Acceptance

3% systematic error is assigned for geometrical acceptance, as described in Sec. 3.2.1 for RUN5 and RUN6 configuration.

5.11.2 Production Ratios of Charmed and Bottomed Hadrons

Production ratios of D and B hadrons (D^+/D^0 , D_s/D^0 , B^+/B^0 , B_s/B^0 ...) are one of the most important parameters to determine ϵ_c and ϵ_b . Although the production ratios in the generated events are tuned based on the experimental results as already described, the ratios have considerable uncertainty. Therefore, the uncertainty of the production ratios should be considered as the systematic error source.

D^+/D^0 , D_s/D^0 and Λ_c/D^0 ratios in PYTHIA are summarized in Table 5.6. The assigned uncertainties of D^+/D^0 , D_s/D^0 , Λ_c/D^0 based on experimental results are also listed in Table 5.6. B^+/B^0 , B_s/B^0 and B baryons/ B^0 ratios and uncertainty are summarized in Table 5.7. B^+/B^0

Table 5.6: $D^+/D^0, D_s/D^0, \Lambda_c/D^0$ ratios from other experiments [16, 17, 18] and PYTHIA (default and tuned)

	PYTHIA (default)	CDF (p+p)	P.D.G (e^+e^- @ $\sqrt{s} = 91\text{GeV}$)	PYTHIA (tuned)
D^+/D^0	0.3	0.45		0.45 ± 0.1
D_s/D^0	0.2	0.23	0.29	0.25 ± 0.1
Λ_c/D^0	0.1		0.17	0.1 ± 0.05

is fixed to 1, since there are no reason to break isospin symmetry. B_s/B^0 and B baryons/ B^0 ratios and their uncertainty are summarized in Table 5.7. Since there are little experimental

Table 5.7: $B^+/B^0, B_s/B^0, B$ baryons/ B^0 ratios from other experiment [17] and PYTHIA (tuned)

	P.D.G ($e^+e^-@ \sqrt{s} = 91\text{GeV}$)	PYTHIA (tuned)
B^+/B^0	1	1
B_s/B^0	0.35	0.4 ± 0.2
B baryons/ B^0	0.2	0.2 ± 0.15

results of B_s/B^0 and B baryons/ B^0 ratios, 50% uncertainty is assigned for B_s/B^0 ratio and 75% uncertainty is assigned for B baryons/ B^0 ratio.

The effect of the assigned uncertainty on the tagging efficiency is regarded as the systematic error of the tagging efficiency. For the study of this effect, details of ϵ_c and ϵ_b are evaluated for each decay channel at each trigger electron p_T range. For example, the results at the trigger electron with $2 < p_T < 3$ GeV/ c are summarized in Table 5.8. For the results at other electron p_T are shown in Appendix. D.

The effect on the ϵ_c and ϵ_c are calculated by changing the production ratios of D and B hadrons according to the assigned uncertainties. The results are summarized in Table 5.9 and 5.10.

5.11.3 Branching Ratio

Branching ratios in EvtGen simulation are implemented according to P.D.G and the results from CLEO, BarBar etc. However, branching ratios listed in P.D.G have uncertainty and there is small discrepancy in the branching ratios between P.D.G values and implemented values in EvtGen for some decay channels. For these decay channels, these discrepancy are taken as the uncertainty of the branching ratios for corresponding channel. The implemented and P.D.G values of branching ratios are summarized in Table 5.11. The assigned uncertainty of branching ratios are also summarized in Table 5.11.

We calculate the effect of the uncertainty of the branching ratios on the ϵ_c and ϵ_c by the similar way used to estimate the systematic errors of the production ratio. That is, the effect on the ϵ_c and ϵ_c are calculated when the branching ratios of D and B hadrons are changed according to the assigned uncertainty. The results are summarized in Table 5.11 and assigned as a systematic error for the branching ratio.

5.11.4 $b \rightarrow c \rightarrow e$ Process

There is discrepancy in the production ratios of D hadrons which originates from inclusive $b \rightarrow c$ process between P.D.G and EvtGen, which is the known problem of EvtGen. The production ratios of D hadrons in inclusive $b \rightarrow c$ process in P.D.G and EvtGen are summarized at Table 5.12. As a result, D^+/D^0 in B decay are 0.30 and 0.41 in P.D.G value and EvtGen, respectively. The effect of this discrepancy in $b \rightarrow c \rightarrow e$ needs to be considered as systematic error of tagging efficiency of ϵ_b . The difference in D^+/D^0 in B decay makes $\sim 4\%$ effect on

the tagging efficiency in $c \rightarrow e$ process, which is estimated in the same way to estimate the uncertainty from the production ratio. The 4% effect of the tagging efficiency in $c \rightarrow e$ process changes the tagging efficiency of bottom production via $b \rightarrow c \rightarrow e$ process, which is evaluated from Table 5.8. It is found that such effect is less than 2%.

5.11.5 Momentum Distribution of Charmed and Bottomed Hadrons

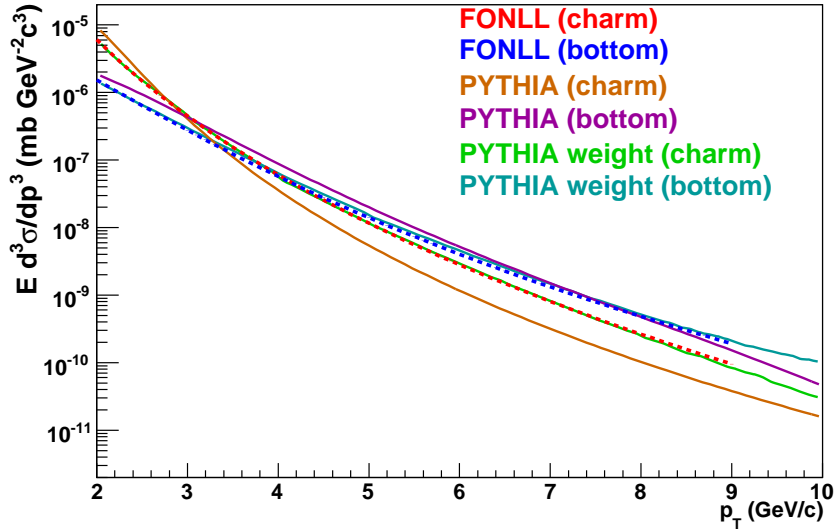


Figure 5.20: The spectra of the single electrons from charm and bottom at PYTHIA and FONLL [38]. Dark orange line and magenta line show the spectra from charm and bottom at PYTHIA. Green line and cyan line show the spectra of the electrons from charm and bottom at PYTHIA with weighting factor. Red line and blue lines show the spectra from charm and bottom at FONLL.

D and B hadrons in the PYTHIA simulation have the uncertainty in their momentum distribution. Tagging efficiency as a function of trigger electron p_T depends on the momentum distributions of parent D and B hadrons. Therefore, the systematic error for the momentum distribution of the parent particles should be estimated.

The shape of the p_T spectra of the electrons from charm and bottom reflects the momentum distribution of the parent particles. The difference of the momentum distribution of the parent particles between PYTHIA and the experimental results can be estimated by comparing the shape of electron p_T spectra obtained by PYTHIA and real data. Figure 5.20 shows the p_T spectra of the electrons from charm (Dark Orange) and bottom (Magenta) at PYTHIA. The spectra of the electrons from PYTHIA are compared with the spectra from FONLL, where the shape of the spectra from FONLL almost agrees with the experimental results including PHENIX.

Weighting factor, $w(p_T)$, is defined as follows.

$$w(p_T) = \text{FONLL}(p_T) / \text{PYTHIA}(p_T). \quad (5.5)$$

This weighting factor is used to correct the difference of the momentum distribution. In Fig 5.20, green line and cyan line show the spectra of the electrons from charm and bottom produced at PYTHIA with weighting factor. The difference of ϵ_c and ϵ_b between with and without the weighting reflects the correction of the momentum distribution. As a result, about 1.5% systematic error is assigned for ϵ_c and about 2% systematic error is assigned for ϵ_b .

5.11.6 PYTHIA Uncertainty

N_{tag} includes the remaining contribution from the associated hadron which is not from heavy flavor decay (jet fragmentation). Such effect has the dependence of the PYTHIA parameters and this dependence should be included into the systematic error. Study is done to estimate the amount of the contribution from the associated hadron which is from jet fragmentation.

ϵ_c and ϵ_b are calculated in the two cases for all stable particles and only decay daughters of D and B hadrons in generated events. Figure 5.21 shows a conceptual view of this procedure. In Fig.5.21, blue particles are decay daughters of D and B hadrons and green particles are from jet fragmentation simulated with PYTHIA. The contribution of jet fragmentation generated by PYTHIA can be estimated by comparison between the above two cases (with and without hadron from jet fragmentation). It is found that the contribution of jet fragmentation to ϵ_c and ϵ_b is less than 15%. Therefore, the effect of uncertainty of jet fragmentation on the tagging efficiency is expected to be small. For a example, if the uncertainty of the contribution of jet fragmentation in PYTHIA is 20%, the uncertainty of ϵ_c and ϵ_b becomes $15\% \times 20\% = 3\%$.

More precisely, the uncertainty from the PYTHIA dependence on the contribution of jet fragmentation is estimated by looking at the measured yield of associated hadrons as a function of azimuthal angle between the trigger non-photonic electrons and the associated hadron (correlation function) in charm and bottom production. Since the contribution of jet fragmentation is not canceled out for the inclusive multiplicity, the inclusive multiplicity is a good observable to study the PYTHIA dependence of the jet fragmentation. The multiplicity in RUN5 is obtained in Appendix. C. Some parameter sets, which are expected to affect the contribution of jet fragmentation, are prepared to estimate the effect of PYTHIA uncertainty on the ϵ_c and ϵ_b as follows.

- default PYTHIA (1)
- PARP(90) 0.25→0.16 (2)
- P.D.F CTEQ5L→GRV94L (3)
- charm mass 1.2→1.4GeV/ c^2 , bottom mass 4.3→4.5GeV/ c^2 (4)

Figure 5.22 shows the inclusive multiplicity as a function of azimuthal angle between the trigger single non-photonic electrons and the associated hadron. Black points show the result in RUN5 data obtained at Appendix. C and various lines show the results from PYTHIA with the parameter sets. Since (1) and (2) parameter sets are NOT consistent with real data, the deviation of ϵ_c and ϵ_b with the (1) and (2) parameter sets from tuned PYTHIA gives enough conservative systematic error. We assign 6% systematic error as PYTHIA uncertainty, since the deviations are 5% for ϵ_c and ϵ_b .

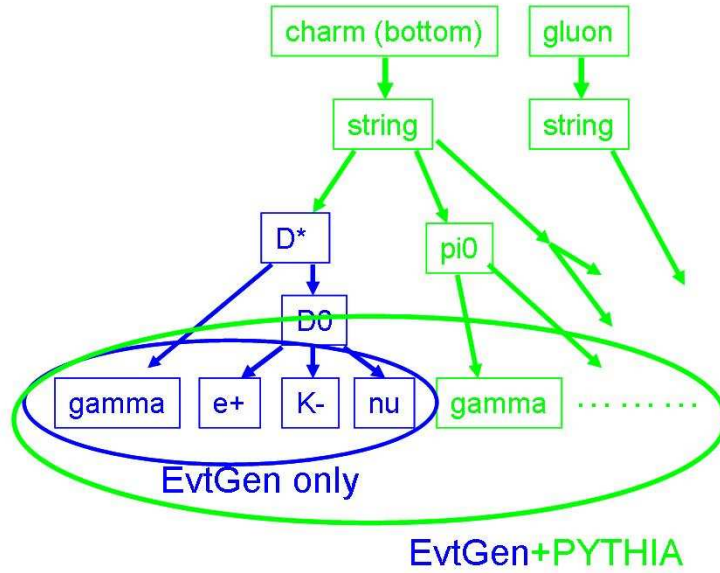


Figure 5.21: Conceptual view of the procedure to estimate contribution of jet fragmentation simulated by PYTHIA. Blue particles are D mesons and baryons simulated by EvtGen and green particles are jet fragmentation simulated by PYTHIA.

5.11.7 Summary of Systematic Error for PYTHIA and EvtGen

Systematic error of ϵ_c and ϵ_b are summarized in Table 5.13.

5.12 ϵ_{data} , ϵ_c and ϵ_b

ϵ_{data} , ϵ_c and ϵ_b are obtained in Sec. 5.3 and 5.8. The location of effective bin center of electron p_T at each p_T range is determined as weighted mean of electron p_T at each p_T range. Since the bin center of $\epsilon_{c(b)}(p_T)$ is different from the bin center of $\epsilon_{data}(p_T)$, it is necessary to correct to $\epsilon_{c(b)}(p_T)$ the value at the same p_T as used in ϵ_{data} . This is done as follows.

$$\epsilon_{c(b)}(p_T^{real}) = \frac{f_{c(b)}(p_T^{real})}{f_{c(b)}(p_T^{c(b)})} \times \epsilon_{c(b)}(p_T^{c(b)}), \quad (5.6)$$

where

- p_T^{real} and $p_T^{c(b)}$ are the effective bin center of electron p_T in real data and simulation for charm (bottom) production.
- $f_{c(b)}(p_T)$ is the fit function for the obtained $\epsilon_{c(b)}$.

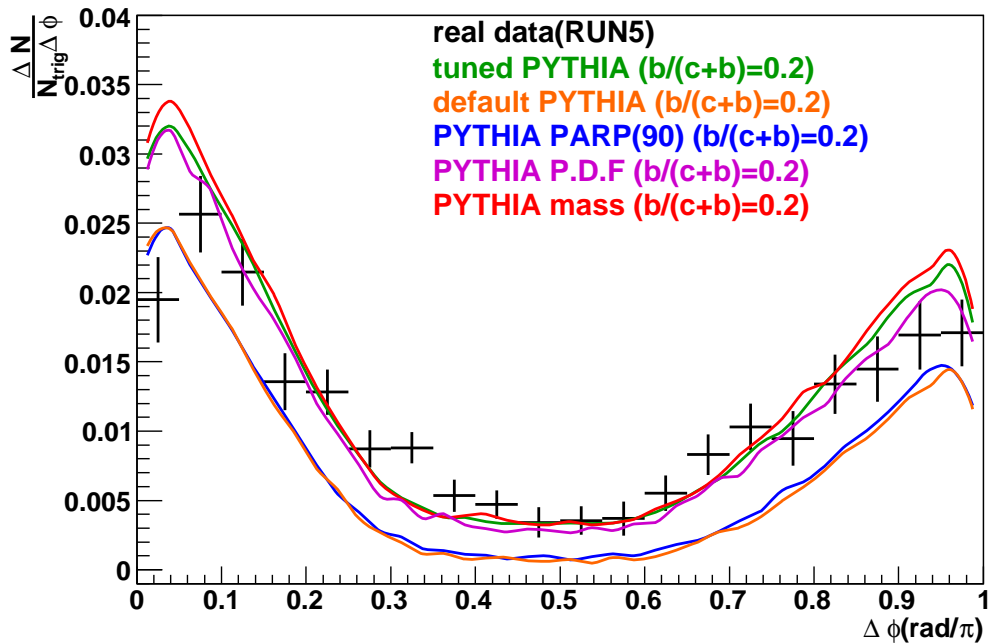


Figure 5.22: The correlation function of electrons and hadrons, when the trigger electrons were from heavy flavor. Black points show the result in RUN5 data obtained at SectionC and various lines show the result at PYTHIA with the parameter sets.

Figure 5.23 and 5.24 show ϵ_{data} , ϵ_c and ϵ_b as a function of electron p_T in RUN5 and RUN6, respectively. Here, black points correspond to ϵ_{data} , red points correspond to ϵ_c and blue points correspond to ϵ_b . In Fig. 5.23 and 5.24, data points move near bottom values as electron p_T increases. This fact indicates the fraction of the electrons from bottom increases with electron p_T . Results are summarized in Table 5.14

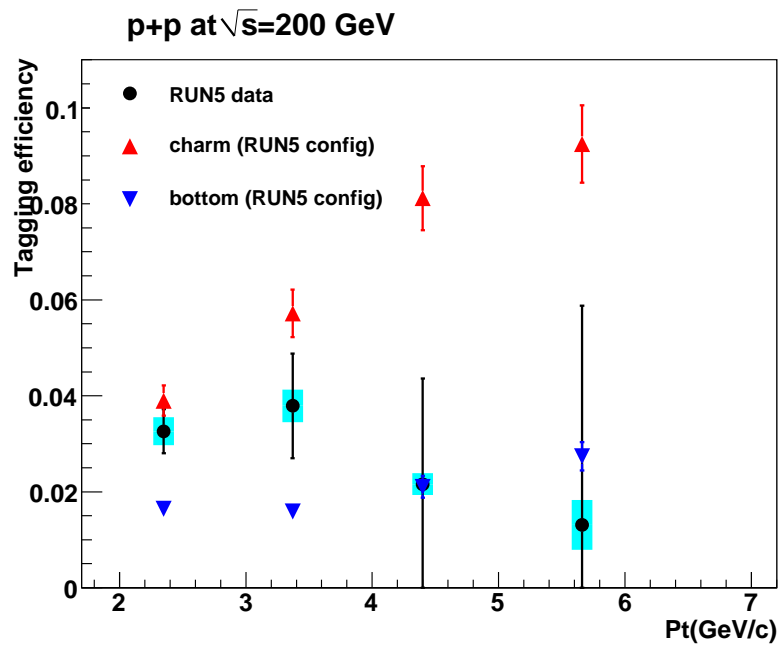


Figure 5.23: ϵ_c , ϵ_b and ϵ_{data} as a function of electron p_T in RUN5.

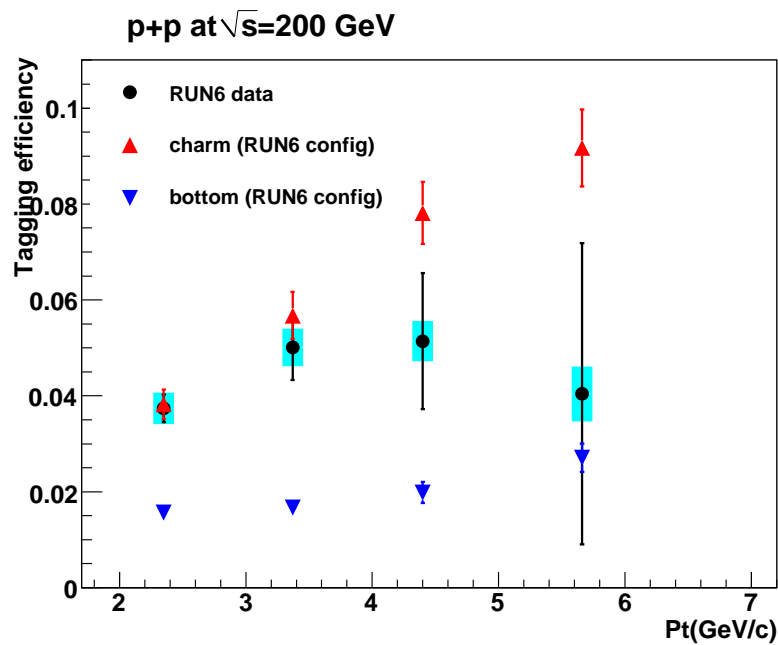


Figure 5.24: ϵ_c , ϵ_b and ϵ_{data} as a function of electron p_T in RUN6.

Table 5.8: Detail of charm and bottom decay for electron p_T 2-3 GeV/c

channel	N_{tag} (part)/(all)	N_{ele} (part)/(all)	ϵ
D^0			
$D^0 \rightarrow e^+ K^- \nu_e$	38.96%	29.64%	$4.68 \pm 0.09\%$
$D^0 \rightarrow e^+ K^{*-} \nu_e$	15.24%	3.73%	$14.57 \pm 0.34\%$
$D^0 \rightarrow e^+ \pi^- \nu_e$	4.34%	5.24%	$2.95 \pm 0.19\%$
$D^0 \rightarrow e^+ \rho^- \nu_e$	2.04%	0.52%	$13.88 \pm 0.81\%$
$D^0 \rightarrow e^+ other$	1.23%	0.51%	$8.67 \pm 0.83\%$
D^+			
$D^+ \rightarrow e^+ \bar{K}^0 \nu_e$	25.23%	38.55%	$2.33 \pm 0.07\%$
$D^+ \rightarrow e^+ \bar{K}^{*0} \nu_e$	6.00%	4.70%	$4.55 \pm 0.31\%$
$D^+ \rightarrow e^+ \pi^0 \nu_e$	2.00%	3.32%	$2.15 \pm 0.21\%$
$D^+ \rightarrow e^+ \rho^0 \nu_e$	0.25%	0.36%	$2.52 \pm 1.14\%$
$D^+ \rightarrow e^+ other$	1.91%	2.02%	$3.37 \pm 0.37\%$
D_s			
$D_s \rightarrow e^+ \phi \nu_e$	0.45%	0.89%	$1.80 \pm 0.73\%$
$D_s \rightarrow e^+ \eta \nu_e$	3.70%	7.66%	$1.72 \pm 0.14\%$
$D_s \rightarrow e^+ \eta' \nu_e$	0.30%	0.67%	$1.60 \pm 0.69\%$
$D_s \rightarrow e^+ other$	0.35%	0.82%	$1.52 \pm 0.47\%$
Λ_c			
$\Lambda_c \rightarrow e^+ \Lambda \nu_e$	-0.40%	0.31%	$-4.63 \pm 2.67\%$
$\Lambda_c \rightarrow e^+ other$	-1.60%	1.05%	$-5.44 \pm 1.25\%$
B^0			
$B^0 \rightarrow e^+ D^- \nu_e$	3.27%	6.20%	$0.89 \pm 0.15\%$
$B^0 \rightarrow e^+ D^{*-} \nu_e$	0.50%	21.21%	$0.04 \pm 0.09\%$
$B^0 \rightarrow e^+ other$	4.39%	5.88%	$1.26 \pm 0.17\%$
B^+			
$B^+ \rightarrow e^+ D^0 \nu_e$	7.16%	6.72%	$1.80 \pm 0.15\%$
$B^+ \rightarrow e^+ D^{*0} \nu_e$	21.30%	22.93%	$1.57 \pm 0.08\%$
$B^+ \rightarrow e^+ other$	2.95%	6.47%	$0.77 \pm 0.17\%$
B_s			
$B_s \rightarrow e^+ total$	15.87 %	10.81%	$2.49 \pm 0.12\%$
$Bhad \rightarrow e^+$	10.51%	10.10%	$1.76 \pm 0.12\%$
$B \rightarrow c \rightarrow e$	34.05%	9.69%	$5.95 \pm 0.18\%$

Table 5.9: The effect of $D^+/D^0, D_s/D^0, \Lambda_c/D^0$ changes on ϵ_c

electron p_T	$\Delta(\epsilon_c)/\epsilon_c$ $2 < p_T < 3 \text{ GeV}/c$	$\Delta(\epsilon_c)/\epsilon_c$ $3 < p_T < 4 \text{ GeV}/c$	$\Delta(\epsilon_c)/\epsilon_c$ $4 < p_T < 5 \text{ GeV}/c$	$\Delta(\epsilon_c)/\epsilon_c$ $5 < p_T < 7 \text{ GeV}/c$
D^\pm/D^0	2.7%	3.6%	3.3%	4%
D_s/D^0	2.0%	1.9%	2.0%	2.0%
Λ_c/D^0	1.7%	1.5%	1.0%	0.4%

Table 5.10: The effect of B_s/B^0 and B baryons/ B^0 changes on ϵ_b

electron p_T	$\Delta(\epsilon_c)/\epsilon_c$ $2 < p_T < 3 \text{ GeV}/c$	$\Delta(\epsilon_c)/\epsilon_c$ $3 < p_T < 4 \text{ GeV}/c$	$\Delta(\epsilon_c)/\epsilon_c$ $4 < p_T < 5 \text{ GeV}/c$	$\Delta(\epsilon_c)/\epsilon_c$ $5 < p_T < 7 \text{ GeV}/c$
B_s/B^0	2.5%	2.5%	3.7 %	4.5 %
B baryons/ B^0	0.5%	1%	2.5 %	3 %

Table 5.11: Branching ratio of D and B hadrons in P.D.G and EvtGen. The assigned uncertainties for the branching ratios and these effect on the ϵ_c and ϵ_b electron p_T 2-3 GeV/c

charmed hadrons channel	Branching Ratio EvtGen	Branching ratio P.D.G	$\delta(Br)/Br$	$\delta(\epsilon_c)/\epsilon_c$
D^0				
$D^0 \rightarrow e^+ K^- \nu_e$	$3.50 \pm 0.11\%$	$3.51\% \pm 0.11\%$	3.10%	0.29%
$D^0 \rightarrow e^+ K^{*-} \nu_e$	$2.25 \pm 0.16\%$	$2.17\% \pm 0.16\%$	7.10%	0.81%
$D^0 \rightarrow e^+ \pi^- \nu_e$	$0.34 \pm 0.06\%$	$0.28\% \pm 0.02\%$	17.60%	0.16%
$D^0 \rightarrow e^+ \rho^- \nu_e$	$0.22 \pm 0.03\%$	$0.19\% \pm 0.04\%$	13.60%	0.21%
$D^0 \rightarrow e^+ other$	$0.45 \pm 0.35\%$	$0.56\% \pm 0.35\%$	77.80%	0.56%
$D^0 \rightarrow e^+ total$				1.06%
D^+				
$D^+ \rightarrow e^+ \bar{K}^0 \nu_e$	$9.00 \pm 0.50\%$	$8.60\% \pm 0.50\%$	5.60%	0.73%
$D^+ \rightarrow e^+ \bar{K}^{*0} \nu_e$	$5.50 \pm 0.50\%$	$8.60\% \pm 0.50\%$	5.40%	0.07%
$D^+ \rightarrow e^+ \pi^0 \nu_e$	$0.44 \pm 0.07\%$	$0.44\% \pm 0.07\%$	16.30%	0.21%
$D^+ \rightarrow e^+ \rho^0 \nu_e$	$0.28 \pm 0.06\%$	$0.22\% \pm 0.04\%$	21.40%	0.02%
$D^+ \rightarrow e^+ other$	$1.46 \pm 0.7\%$	$1.12\% \pm 0.7\%$	48.70%	0.05%
$D^+ \rightarrow e^+ total$				0.77%
D_s				
$D_s \rightarrow e^+ \phi \nu_e$	$2.42 \pm 0.50\%$	$2.50\% \pm 0.30\% (l^+)$	20.70%	0.09%
$D_s \rightarrow e^+ \eta \nu_e$	$3.07 \pm 0.8\%$	$3.10\% \pm 0.60\%$	26.10%	1.01%
$D_s \rightarrow e^+ \eta' \nu_e$	$1.06 \pm 0.4\%$	$1.08\% \pm 0.35\%$	47.20%	0.17%
$D_s \rightarrow e^+ other$	$0.37 \pm 0.37\%$	100.00%	0.46%	
$D_s \rightarrow e^+ total$				1.13%
Λ_c				
$\Lambda_c \rightarrow e^+ \Lambda \nu_e$	$1.8 \pm 0.6\%$	$2.1\% \pm 0.6\%$	33.30%	0.24%
$\Lambda_c \rightarrow e^+ other$	$2.7 \pm 1.8\%$	$2.4\% \pm 1.8\%$	66.70%	1.76%
$\Lambda_c \rightarrow e^+ total$				1.77%
$total$				2.48%
bottomed hadrons channel	Branching Ratio EvtGen	Branching ratio P.D.G	$\delta(Br)/Br$	$\delta(\epsilon_b)/\epsilon_b$
B^0				
$B^0 \rightarrow e^+ D^- \nu_e$	$2.07 \pm 0.2\%$	$2.12\% \pm 0.2\%$	9.70%	0.28%
$B^0 \rightarrow e^+ D^{*-} \nu_e$	$5.70 \pm 0.35\%$	$5.35\% \pm 0.2\%$	6.10%	1.25%
$B^0 \rightarrow e^+ other$	$2.6 \pm 0.5\%$	$2.93\% \pm 0.5\%$	19.20%	0.28%
$B^0 \rightarrow e^+ total$				1.31%
B^+				
$B^+ \rightarrow e^+ D^0 \nu_e$	$2.24 \pm 0.22\%$	$2.15\% \pm 0.22\%$	10.20%	0.04%
$B^+ \rightarrow e^+ D^{*0} \nu_e$	$6.17 \pm 0.5\%$	$6.50\% \pm 0.5\%$	7.70%	0.12%
$B^+ \rightarrow e^+ other$	$2.49 \pm 0.7\%$	$2.25\% \pm 0.67\%$	26.90%	0.93%
$B^+ \rightarrow e^+ total$				0.94%
B_s				
$B_s \rightarrow e^+ total$	$7.9 \pm 3\%$	$7.9\% \pm 2.4\%$	37.00%	1.80%
$Bhad \rightarrow e^+ others$	$7.5 \pm 4.0\%$	$8.5\% \pm 4.0\%$	40.0%	0.2 %
$total$				2.42%

Table 5.12: Inclusive resonance D production in B decays at PDG and EvtGen

	P.D.G 06 (%)	EvtGen (%)
$B \rightarrow e\nu X$	10.24 ± 0.15	10.6
$B \rightarrow D^\pm X$	22.8 ± 1.4	32.4
$B \rightarrow D^0 X$	63.7 ± 1.4	68.2
$B \rightarrow D^{*\pm} X$	22.5 ± 1.5	26.2
$B \rightarrow D^{*0} X$	26.0 ± 2.7	25.7
$B \rightarrow D^{(*)} D^{(*)} \bar{X}$	$7.1 + 2.7 - 1.7$	7.7

Table 5.13: Summary of ϵ_c and ϵ_b

ϵ_c electron p_T	simulation statistics	EvtGen+PYTHIA	geometrical acceptance	total
2.0-3.0 GeV/c	1.7%	7.6%	3%	8.3%
3.0-4.0 GeV/c	2.2%	7.9%	3%	8.7%
4.0-5.0 GeV/c	1.6%	7.5%	3%	8.3%
5.0-7.0 GeV/c	2.1%	8.0%	3%	8.8%

ϵ_b electron p_T	simulation statistics	EvtGen+PYTHIA	geometrical acceptance	total
2.0-3.0 GeV/c	3.5%	7.5%	3%	8.8%
3.0-4.0 GeV/c	5.0%	7.3%	3%	9.4%
4.0-5.0 GeV/c	4.8%	9.1%	3%	10.7%
5.0-7.0 GeV/c	3.8%	9.6%	3%	10.7%

Table 5.14: ϵ_{data} , ϵ_c and ϵ_b

electron p_T	ϵ_{data}	ϵ_c	ϵ_b
RUN5			
2.35GeV/c	$0.0326 \pm 0.0046 \pm 0.0029$	0.0390 ± 0.0031	0.0164 ± 0.0014
3.37GeV/c	$0.0379 \pm 0.0109 \pm 0.0034$	0.0571 ± 0.0050	0.0159 ± 0.0015
4.40GeV/c	$0.0216 \pm 0.0220 \pm 0.0023$	0.0812 ± 0.0067	0.0210 ± 0.0023
5.66GeV/c	$0.0131 \pm 0.0457 \pm 0.0052$	0.0924 ± 0.0081	0.0274 ± 0.0030
RUN6			
2.35GeV/c	$0.0374 \pm 0.0029 \pm 0.0033$	0.0382 ± 0.0031	0.0156 ± 0.0014
3.37GeV/c	$0.0501 \pm 0.0068 \pm 0.0039$	0.0567 ± 0.0049	0.0167 ± 0.0015
4.40GeV/c	$0.0514 \pm 0.0142 \pm 0.0042$	0.0781 ± 0.0065	0.0198 ± 0.0022
5.66GeV/c	$0.0404 \pm 0.0314 \pm 0.0057$	0.0917 ± 0.0080	0.0271 ± 0.0029

Chapter 6

Result

The spectrum of electrons from semi-leptonic decay of heavy flavor and tagging efficiency, ϵ_{data} , ϵ_c and ϵ_b are obtained as described in the previous chapter. In this chapter, the spectrum of single electrons of charm and that of bottom are obtained.

6.1 $(b \rightarrow e)/(c \rightarrow e + b \rightarrow e)$ Results

The fraction of the contribution of bottom quark in the single non-photonic electrons ($(b \rightarrow e)/(c \rightarrow e + b \rightarrow e)$) is obtained from ϵ_{data} , ϵ_c and ϵ_b using following equation.

$$\frac{b \rightarrow e}{c \rightarrow e + b \rightarrow e} = \frac{\epsilon_c - \epsilon_{data}}{\epsilon_c - \epsilon_b}. \quad (6.1)$$

The obtained values of $(b \rightarrow e)/(c \rightarrow e + b \rightarrow e)$ in RUN5 and RUN6 are combined. When the results in RUN5 and RUN6 are combined, following two issues should be taken carefully. First, a part of systematic errors of RUN5 and RUN6 are correlated. Second, a physical boundary exists in the value of $(b \rightarrow e)/(c \rightarrow e + b \rightarrow e)$, that is $0 < (b \rightarrow e)/(c \rightarrow e + b \rightarrow e) < 1$. BLUE (Best Linear Unbiased Estimate) method and Bayes' principle are applied to take into account such conditions. The combined mean values and standard deviations are determined using the BLUE method under the condition that there is no physical boundary. Then, Bayes' principle is applied to take into account the physical constraint.

6.1.1 BLUE Method in Correlation Analysis

The BLUE method is applied to combine the results in RUN5 and RUN6. Error sources are summarized in Table 6.1. The definition of the types of errors is described in Sec.4.4.2. In Table 6.1, the correlated systematic errors is tagged as B and they are assumed to have 100% correlation. With this assumption, the relation between correlated and uncorrelated errors in BLUE to become simple as follows.

$$(\sigma^{corr})^2 = \rho \sigma_{run5} \sigma_{run6}, \quad (6.2)$$

$$\sigma^{corr} = \sqrt{\sigma_{run5}^{sys-B} \sigma_{run6}^{sys-B}}, \quad (6.3)$$

$$\sigma_{runi}^{uncorr} = \sqrt{(\sigma_{runi})^2 - (\sigma^{corr})^2}. \quad (6.4)$$

Table 6.1: Summary of error source

error source	run5/6 correlation (Type)
statistics	0 % (A)
signal count	0% (A)
cocktail calculation	100%(B)
PISA geometry	0% (B)
simulation statistics	0% (A)
Event generator	100%(B)

From the above equations, the weighted average and combined error are obtained as follows.

$$\langle r \rangle = \frac{r_{run5}(\sigma_{run6}^{uncorr})^2 + r_{run6}(\sigma_{run5}^{uncorr})^2}{(\sigma_{run5}^{uncorr})^2 + (\sigma_{run6}^{uncorr})^2}, \quad (6.5)$$

$$\sigma = \sqrt{\frac{\sigma_{run5}^2 \sigma_{run6}^2 - (\sigma^{corr})^4}{(\sigma_{run5}^{uncorr})^2 + (\sigma_{run6}^{uncorr})^2}}, \quad (6.6)$$

$$\sigma^{stat} = \frac{\sqrt{(\sigma_{run6}^{stat})^2 (\sigma_{run5}^{uncorr})^4 + (\sigma_{run5}^{stat})^2 (\sigma_{run6}^{uncorr})^4}}{(\sigma_{run5}^{uncorr})^2 + (\sigma_{run6}^{uncorr})^2}, \quad (6.7)$$

$$\sigma^{sys} = \sqrt{\sigma^2 - (\sigma^{stat})^2}. \quad (6.8)$$

(χ^2/ndf) of the combination is 3.0/4, which indicates that the results in RUN5 and RUN6 are consistent.

6.1.2 Physical Constraint

The ratio, $(b \rightarrow e)/(c \rightarrow e + b \rightarrow e)$ which we want to determine in this analysis has physical boundary, $0 \leq (b \rightarrow e)/(c \rightarrow e + b \rightarrow e) \leq 1$. Bayes' principle is applied to take into account the effect of the physical constraint. Bayes' principle is

$$f(r | \epsilon) = \frac{L(\epsilon | r)g(r)}{\int_{r'} L(\epsilon | r')g(r')dr'}. \quad (6.9)$$

Here, ϵ is the outcome of experiment (tagging efficiency in this analysis) and r is an unknown parameter that we want to determine ($(b \rightarrow e)/(c \rightarrow e + b \rightarrow e)$ in this analysis). $f(r | \epsilon)$ is the posterior probability density function when experimental value ϵ is given. Since $f(r | \epsilon)$ includes all knowledge about r , we can determine the error of r when we get $f(r | \epsilon)$. $L(\epsilon | r)$ is the likelihood function, that is the joint probability density function for the data given a certain value of r . $g(r)$ is the prior probability density function. Since the statistics does not give us any information about $g(r)$, we must assume the distribution of $g(r)$ reasonably. We assume that $(b \rightarrow e)/(c \rightarrow e + b \rightarrow e)$ has uniform distribution from 0 to 1 in this analysis. Since the obtained error for ϵ obey Gaussian, $f(r | \epsilon)$ becomes

$$f(r | \epsilon) = A \times \exp\{-(r - r_0)/2\sigma_r^2\} \quad (0 \leq r \leq 1), \quad (6.10)$$

$$f(r | \epsilon) = 0 \quad (0 > r \parallel r > 1).$$

Here, r_0 is the obtained r from the combination of RUN5 and RUN6 analysis and σ_r is the obtained deviation from r the combination. A is a normalization factor so that the integral value of $f(r | \epsilon)$ becomes 1.

The variables, x_1 and x_2 are defined as following equations.

$$\begin{aligned} \int_0^{x_1} f(r | \epsilon) dr &= \int_{x_2}^1 f(r | \epsilon) dr = (1 - \alpha)/2, \\ \int_{x_1}^{x_2} f(r | \epsilon) dr &= \alpha. \\ \alpha &= 0.6827 \end{aligned} \quad (6.11)$$

Deviation from x_1 and x_2 to mean value are considered as the standard deviation.

6.1.3 Lower and Upper Limit

90% C.L is determined for the highest and the lowest electron p_T range ($2.0 < p_T < 3.0$ GeV/ c and $5.0 < p_T < 7.0$ GeV/ c), since the mean value obtained by the BLUE analysis is close to the boundary.

Probability density function is defined as bellow.

$$f(r) = A \times \exp(-(r - r_0)^2/2\sigma^2) \quad (0 < r < 1), \quad (6.12)$$

$$r_0 = \frac{\epsilon_c - \epsilon_{data}}{\epsilon_c - \epsilon_b}, \quad (6.13)$$

$$\sigma = \sqrt{\sigma_{stat}^2 + \sigma_{sys}^2}. \quad (6.14)$$

Here, A is a normalization factor to have integrated value becomes 1. σ_{stat} is statistical error of ϵ_{data} without the consideration of the boundary. σ_{sys} is also systematic errors of ϵ_{data} , ϵ_c and ϵ_b without the consideration of the boundary.

90% C.L is determined from this probability density function. The values at which integrated probability density function becomes 50% from the boundary are also determined as the mean values.

6.1.4 The Combined Result

Figure 6.1 shows the combined result about the bottom fraction, $(b \rightarrow e)/(c \rightarrow e + b \rightarrow e)$ as a function of electron p_T with FONLL prediction [38]. In this figure, black points show the the obtained $(b \rightarrow e)/(c \rightarrow e + b \rightarrow e)$. Red line show the central value in FONLL prediction and pink solid and dotted lines show the uncertainty of FONLL calculation. Pink solid lines in Fig. 6.1 show $(b \rightarrow e)/(c \rightarrow e + b \rightarrow e)$ of the FONLL prediction when the correlation of the uncertainty about cross sections of charm and bottom are maximum. Pink dotted lines show $(b \rightarrow e)/(c \rightarrow e + b \rightarrow e)$ of the FONLL prediction when the correlation of the uncertainty about cross sections of charm and bottom are anti-maximum. The results are also summarized

in Table 6.2. FONLL is almost consistent with the obtained result within the theoretical uncertainty.

It is worth to note that the point at lowest p_T has a small value. This suggests majority of interested yield of 'single non-photonic electron', that is the electron after the subtraction of all possible background and what we have been measured, can be explained as semi-leptonic $c \rightarrow e$ decay. It provides the proof that the indirect measurement of heavy flavor via electrons performed at PHENIX is really measurement of heavy flavor.

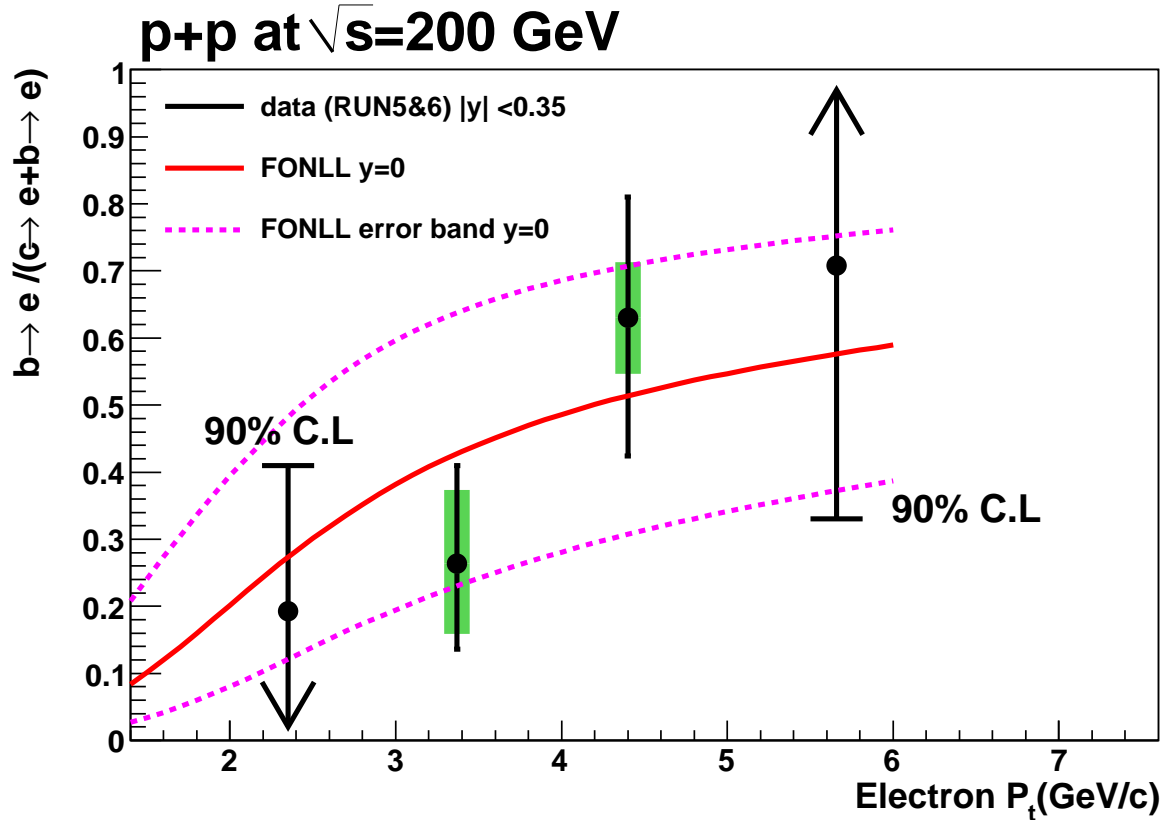


Figure 6.1: $(b \rightarrow e)/(c \rightarrow e + b \rightarrow e)$ in the electrons from heavy flavor as a function of electron p_T in RUN6 and RUN5 with FONLL calculation. Black points show the result in RUN6 and RUN5. Red lines are FONLL prediction and pink solid and dotted lines are uncertainty of FONLL prediction.

6.2 Comparison of the Data with Simulation

The invariant mass (M_{eh}) distributions of extracted signals in the data shown at Fig 5.9 and 5.10 are compared with those generated by PYTHIA and EvtGen simulation. The distributions are normalized by number of the single non-photonic electrons. An agreement of the simulation results with the data provide the confidence for this analysis method and the result.

Table 6.2: Result of $(b \rightarrow e)/(c \rightarrow e + b \rightarrow e)$ in RUN5 and RUN6

electron p_T	$(b \rightarrow e)/(c \rightarrow e + b \rightarrow e)$
2.35 GeV/ c	< 0.41 (90% C.L) 0.19 (50% point)
3.37 GeV/ c	$0.26_{0.13}^{+0.14}(stat)_{0.11}^{+0.11}(sys)$
4.40 GeV/ c	$0.63_{-0.21}^{+0.18}(stat) \pm 0.08(sys)$
5.66 GeV/ c	> 0.33 (90% C.L) 0.71 (50% point)

Figure 6.2 to 6.7 show the invariant mass distributions of extracted signals in the data and the simulation at each electron p_T range in RUN5 and RUN6. In these figures, black points are the data points. Red points show the result of PYTHIA and EvtGen simulation only for charm production and blue points show the result of PYTHIA and EvtGen simulation only for bottom production. Green points show the result of the simulation which is obtained by combining the charm and bottom contributions according to the obtained $(b \rightarrow e)/(c \rightarrow e + b \rightarrow e)$ values.

The agreement of simulation (green) and real data is good. χ^2/ndf values which are calculated in $0.4 < M_{eh} < 5.0$ GeV/ c^2 are summarized in Table 6.3. Uncertainty of simulation is NOT included in these (χ^2/ndf).

Table 6.3: χ^2/ndf (theoretical uncertainty is NOT included)

electron p_T	χ^2/ndf (RUN5)	χ^2/ndf (RUN6)
2.0-3.0 GeV/ c	20.5/22	15.8/22
3.0-4.0 GeV/ c	15.9/22	21.2/22
4.0-5.0 GeV/ c	28.0/22	23.3/22

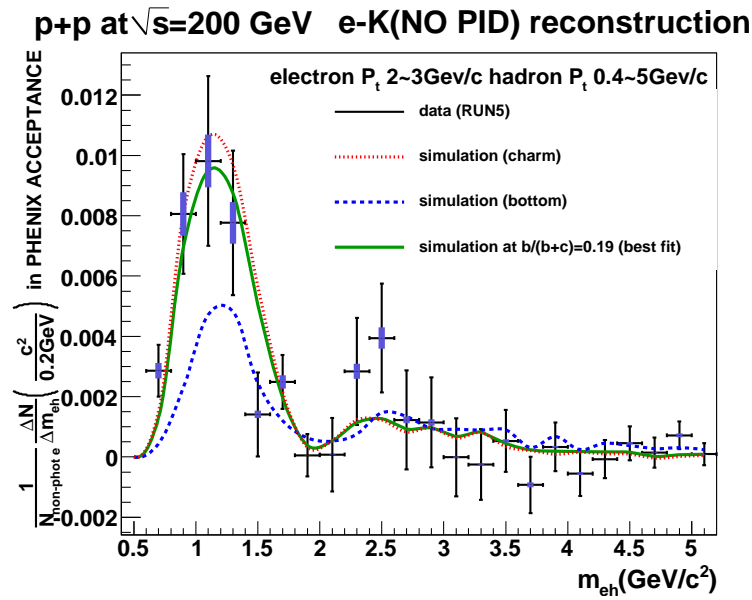


Figure 6.2: Comparison of the data with PYTHIA and EvtGen simulation about substracted invariant mass distributions in RUN5. Electron p_T range is 2.0-3.0 GeV/c.

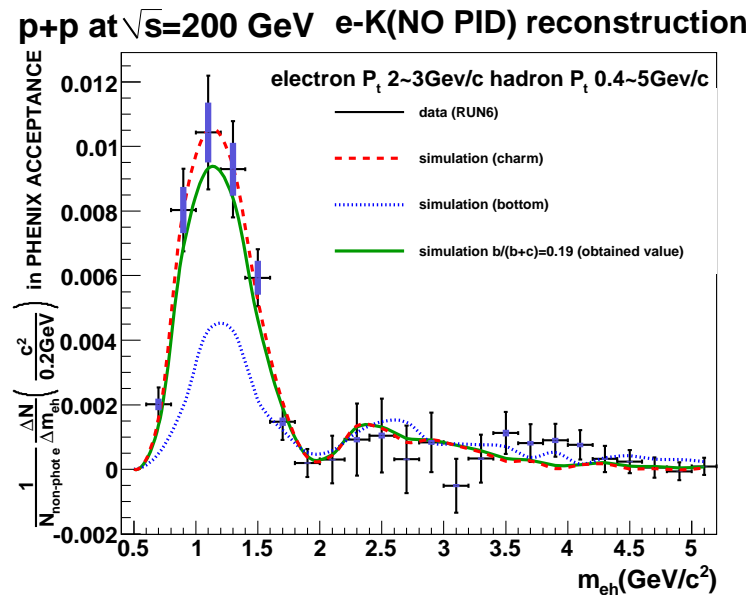


Figure 6.3: Comparison of the data with PYTHIA and EvtGen simulation about substracted invariant mass distributions in RUN5. Electron p_T range is 2.0-3.0 GeV/c.

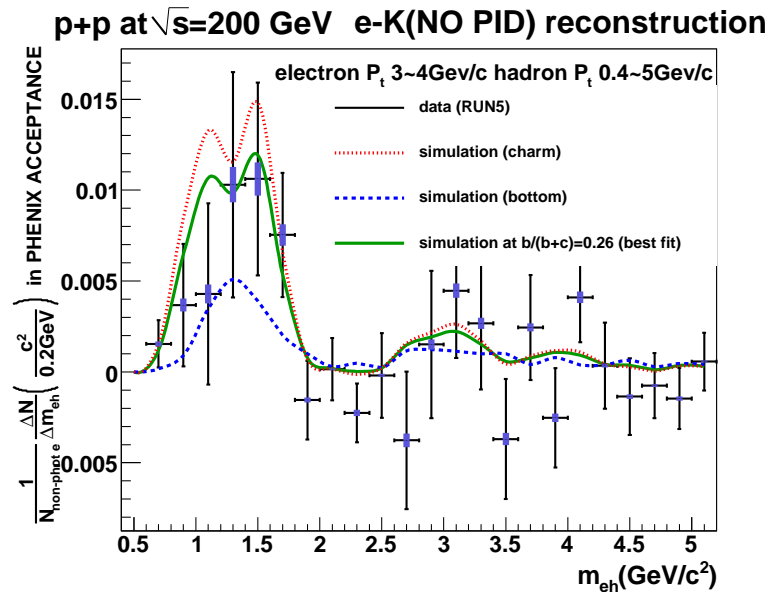


Figure 6.4: Comparison of the data with PYTHIA and EvtGen simulation about subtracted invariant mass distributions in RUN5. Electron p_T range is 3.0-4.0 GeV/c.

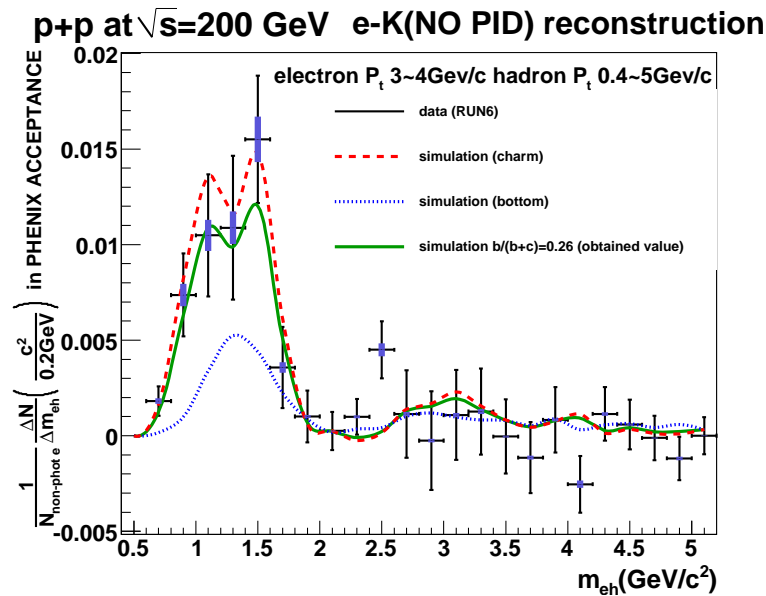


Figure 6.5: Comparison of the data with PYTHIA and EvtGen simulation about subtracted invariant mass distributions in RUN5. Electron p_T range is 3.0-4.0 GeV/c.

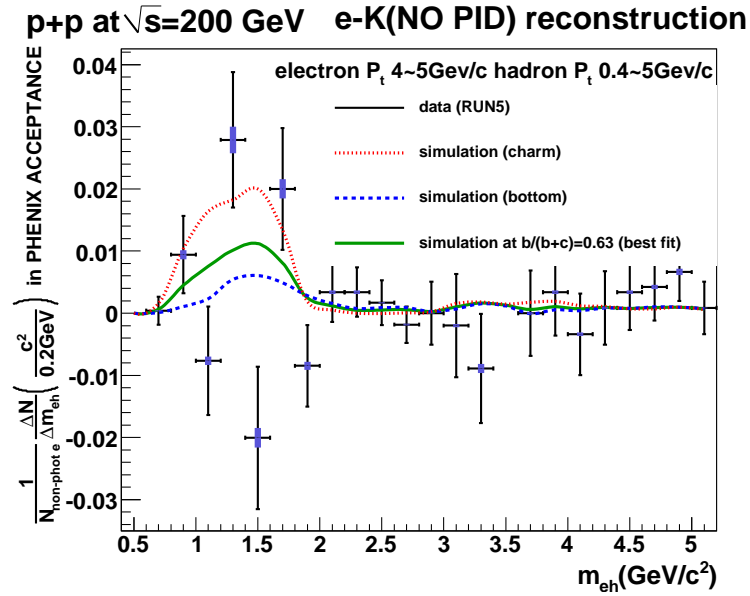


Figure 6.6: Comparison of the data with PYTHIA and EvtGen simulation about subtracted invariant mass distributions in RUN5. Electron p_T range is 4.0-5.0 GeV/c.

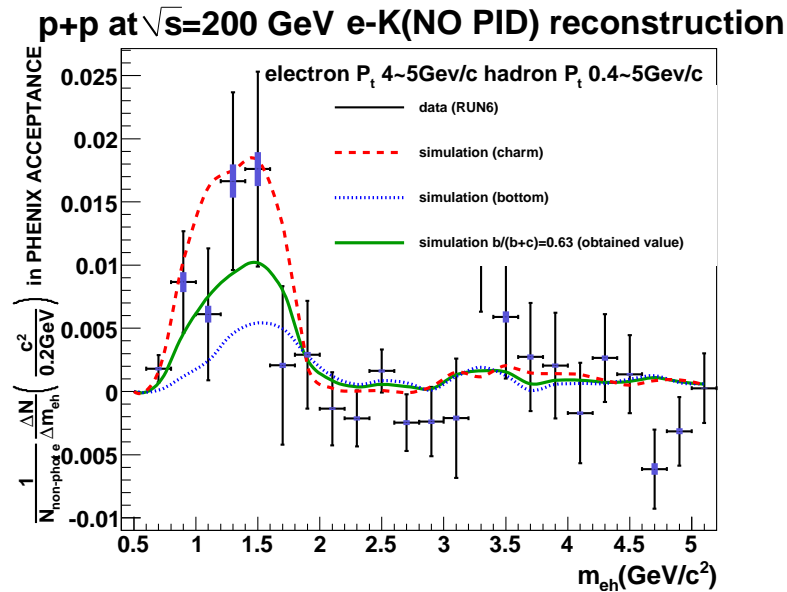


Figure 6.7: Comparison of the data with PYTHIA and EvtGen simulation about subtracted invariant mass distributions in RUN5. Electron p_T range is 4.0-5.0 GeV/c.

6.3 Cross Section of Bottom

Cross section of bottom is obtained using the spectrum of the electrons from heavy flavor and the ratio, $(b \rightarrow e)/(c \rightarrow e + b \rightarrow e)$.

6.3.1 Invariant Cross Section of Electrons from Charm and Bottom

The differential invariant cross section of the electrons from semi-leptonic decay of charm and that from bottom are obtained by (electron spectrum from heavy flavor) $\times (c(b) \rightarrow e)/(c \rightarrow e + b \rightarrow e)$. $(b \rightarrow e)/(c \rightarrow e + b \rightarrow e)$ is obtained in the four electron p_T range, 2-3GeV/ c , 3-4GeV/ c , 4-5GeV/ c and 5-7GeV/ c . The spectrum of the single non-photon electrons is merged into these electron p_T range to make the same bin width as $(b \rightarrow e)/(c \rightarrow e + b \rightarrow e)$. The yield at the electron p_T , where $(b \rightarrow e)/(c \rightarrow e + b \rightarrow e)$ is obtained, is calculated as follows.

$$Y(p_T^{real}) = \frac{f(p_T^{real})}{f(p_T^0)} \times Y(p_T^0). \quad (6.15)$$

Here, p_T^{real} is the bin values of electron p_T where $(b \rightarrow e)/(c \rightarrow e + b \rightarrow e)$ is obtained, p_T^0 is the bin values where the electron spectrum is rebinned, $f(p_T)$ is the fit function of the electron spectrum and $Y(p_T)$ is the electron yield.

Figure 6.8 shows the invariant cross section of single electrons from charm and those from bottom with FONLL calculation. The spectrum of single electrons (circles) is also shown as a reference. The results are also summarized in Table 6.4.

Table 6.4: Invariant cross section of electrons from charm and bottom

electron p_T	cross section (mb GeV ⁻² c ³)	data/FONLL
charm		
2.35 GeV/ c	> 3.30 (90% C.L) 4.52 (50%) $\times 10^{-6}$	> 1.49 (90% C.L) 2.03 (50%)
3.37 GeV/ c	$4.17_{-0.83-0.46}^{+0.73+0.41} \times 10^{-7}$	$2.05_{-0.41-0.22}^{+0.36+0.20}$
4.40 GeV/ c	$3.49_{-1.70}^{+1.95} \pm 0.66 \times 10^{-8}$	$1.16_{-0.56}^{+0.65} \pm 0.22$
5.66 GeV/ c	< 1.11 (90% C.L) 0.48 (50%) $\times 10^{-8}$	< 2.48 (90% C.L) 1.08 (50%)
bottom		
2.35 GeV/ c	< 2.30 (90% C.L) 1.08 (50%) $\times 10^{-6}$	< 2.74 (90% C.L) 1.29 (50%)
3.37 GeV/ c	$1.49_{-0.73-0.66}^{+0.83+0.73} \times 10^{-7}$	$0.99_{-0.48-0.43}^{+0.55+0.48}$
4.40 GeV/ c	$5.95_{-1.95}^{+1.70} \pm 1.10 \times 10^{-8}$	$1.87_{-0.61}^{+0.54} \pm 0.34$
5.66 GeV/ c	> 0.54 (90% C.L) 1.17 (50%) $\times 10^{-8}$	> 0.90 (90% C.L) 1.93 (50%)

6.3.2 Total Cross Section of Bottom

Total cross section of bottom is obtained from the spectrum of the electron from bottom. The procedure to get total cross section of bottom can be written by following equations.

$$\left. \frac{d\sigma_{b\bar{b}}}{dy} \right|_{y=0} = \frac{1}{BR(b \rightarrow e)} \frac{1}{C_{e/B}} \frac{d\sigma_{b \rightarrow e}}{dy}, \quad (6.16)$$

$$\sigma_{b\bar{b}} = \int_y dy \frac{d\sigma_{b\bar{b}}}{dy} \sim R \times \left. \frac{d\sigma_{b\bar{b}}}{dy} \right|_{y=0}. \quad (6.17)$$

The procedures to calculate above equations are following.

- $b \rightarrow c \rightarrow e$ subtraction and p_T extrapolation to obtain $d\sigma_{b \rightarrow e}/dy$.
- Kinematical correction ($C_{e/B}$)
- Branching ratio correction.
- Rapidity extrapolation. R is a correction factor for rapidity extrapolation

Differential cross section of single electrons from bottom shown in Fig 6.8 is integrated from $p_T = 3$ GeV/ c to $p_T = 5$ GeV/ c . The points at $2 < p_T < 3$ GeV/ c and $5 < p_T < 7$ GeV/ c is dropped off for this integral, since confidence level is only determined at these region.

$$\left. \frac{d\sigma^{b \rightarrow e + b \rightarrow c \rightarrow e}}{dy} \right|_{y=0} (3 < p_T < 5 \text{ GeV}/c) = 0.0048_{-0.0016}^{+0.0018}(\text{stat})_{-0.0018}^{+0.0019}(\text{sys})\mu b. \quad (6.18)$$

p_T Extrapolation

$b \rightarrow c \rightarrow e$ subtraction and p_T extrapolation are done by using PYTHIA and FONLL calculation. Figure 6.9 shows invariant cross sections of the electrons from bottom with FONLL calculation and PYTHIA with $1.5 < k_T < 10$ GeV/ c . Solid lines show the electron from $b \rightarrow c \rightarrow e$ and $b \rightarrow e$ and dotted lines show the electron from $b \rightarrow e$. In Fig 6.9 black line show FONLL calculation and other lines show PYTHIA with $1.5 < k_T < 10$ GeV/ c . The distribution of the simulations are normalized at 4-5 GeV/ c points. Correction factor is determined from the simulation as follows.

$$\frac{(d\sigma^{b \rightarrow e})/(dy)|_{y=0}}{(d\sigma^{b \rightarrow e + b \rightarrow c \rightarrow e})/(dy)|_{y=0}(3 < p_T < 5 \text{ GeV}/c)}. \quad (6.19)$$

Obtained correlation factors from simulation are summarized in Table 6.5. We take 16.8 as the correction factor for the p_T extrapolation and $b \rightarrow c \rightarrow e$ subtraction. We assigned 2.0 as systematic error to cover PYTHIA simulation and FONLL results.

Kinematical Correction

The kinematical correlation factor, $C_{e/B}$ is applied to account for the difference in rapidity distribution of the electron from bottom and B hadron.

PYTHIA simulation is used to determine a kinematical correction factor, $C_{e/B}$.

Figure 6.10 shows the rapidity distribution of B hadron and the electrons from bottom at PYTHIA. Black points show the rapidity distribution of the electrons and red points show that of B hadron. Figure 6.11 shows the ratios of the rapidity distributions of the electrons over that of B hadron shown at Fig.6.10. $C_{e/B}$ is determined by straight line fit of this ratios. We use 0.88 as $C_{e/B}$.

Systematic error is not assigned for this correction, since this correction factor is determined by pure kinematics.

Table 6.5: Correction factors for p_T extrapolation and $b \rightarrow c \rightarrow e$ subtraction

simulation	Correction factor
PYTHIA $k_T1.5$	18.6
PYTHIA $k_T2.5$	16.9
PYTHIA $k_T3.5$	15.9
PYTHIA $k_T5.0$	15.3
PYTHIA $k_T7.5$	14.9
PYTHIA $k_T10.0$	14.7
FONLL p_T scaling	18.1
FONLL p_T scaling (max)	18.8
FONLL p_T scaling (min)	17.0

Table 6.6: Electron branching ratios of bottom hadrons

hadron	BR(e)
$B^{+(-)}$	10.8 ± 0.4
B^0	10.1 ± 0.4
B_s	7.9 ± 2.4
B baryons	8.6 ± 2.5

Branching ratio

Inclusive $BR(b \rightarrow e)$ is calculated from the production ratios of B hadron and their exclusive electron branching ratios. Their exclusive electron branching ratios are summarized in Table 6.6. As a result, inclusive $BR(b \rightarrow e)$ is determined to be $10.0\% \pm 1\%$. This assignment is conservative and also cover LEP result, 10.8% .

$d\sigma_{b\bar{b}}/dy|_{y=0}$ and $d\sigma^{b \rightarrow e}/dy|_{y=0}$ are obtained from above correction factors. The results are as follows.

$$\left. \frac{d\sigma^{b \rightarrow e}}{dy} \right|_{y=0} = 0.081^{+0.030}_{-0.027}(\text{stat})^{+0.034}_{-0.027}(\text{sys})\mu b. \quad (6.20)$$

$$\left. \frac{d\sigma_{b\bar{b}}}{dy} \right|_{y=0} = 0.92^{+0.035}_{-0.031}(\text{stat})^{+0.39}_{-0.36}(\text{sys})\mu b. \quad (6.21)$$

Figure 6.12 shows $d\sigma^{b \rightarrow e}/dy|_{y=0}$ with FONLL prediction as a function of rapidity. Figure 6.13 shows $d\sigma_{b\bar{b}}/dy|_{y=0}$ with FONLL prediction as a function of rapidity. The FONLL prediction is very consistent with the experimental result.

Rapidity Extrapolation

Total cross section of bottom is obtained by extrapolating rapidity of B hadron. The correction factor for rapidity extrapolation is determined by using the simulation as follows

$$R = \frac{\int dy \frac{d\sigma}{dy}(B \text{ hadron})}{\int_{-0.5}^{0.5} dy \frac{d\sigma}{dy}(B \text{ hadron})}. \quad (6.22)$$

The correction factor by rapidity distribution of B hadron at PYTHIA is 3.30. NLO calculation for heavy quark production (HVQMNR) is also used for rapidity extrapolation [8], since PYTHIA is just LO calculation. Figure 6.14 show rapidity distribution of bottom quark at HVQMNR using CTEQ5M as parton distribution function for example.

Generated rapidity distribution at HVQMNR is that of bare b quark, while we should integrate cross section for rapidity of B hadron. Generated rapidity distribution of bare b quark is expected to differ from that of bare b quark slightly by the fragmentation process.

The correction factor for the difference in the rapidity distribution between bare b quarks and B hadrons is estimated by the similar way to determine $C_{e/B}$. 0.96 is used for the correction for the fragmentation of bare b into B hadrons.

Therefore the rapidity correction is done as follows.

$$R = \frac{\int dy \frac{d\sigma}{dy}(B \text{ hadron})}{\int_{-0.5}^{0.5} dy \frac{d\sigma}{dy}(B \text{ hadron})} = \frac{\int dy \frac{d\sigma}{dy}(\text{bare } b)}{\int_{-0.5}^{0.5} dy \frac{d\sigma}{dy}(\text{bare } b)} \times \frac{1}{0.96}. \quad (6.23)$$

The correction factor is calculated by using HVQMNR at various conditions. Results are summarized in Table 6.7. CTEQ5M value, 3.44 is used as the correction factor. Systematic error for the correction factor is assigned 0.25 to cover the results at various conditions. σ_{bb} is obtained from the correction factor for rapidity extrapolation. The result is:

$$\sigma_{bb} = 3.16_{-1.07}^{+1.19}(\text{stat})_{-1.27}^{+1.37}(\text{sys})\mu b. \quad (6.24)$$

The FONLL predicts $\sigma_{bb} = 1.87_{-0.67}^{+0.99}\mu b$ and agrees with the experimental result.

Table 6.7: Correction factors for rapidity extrapolation

simulation condition	Correction factor(bare b)	Correction factor(B hadron)
CTEQ4M(PDF)	3.37	3.51
CTEQ5M1(PDF)	3.22	3.35
CTEQ5M(PDF)	3.30	3.44
CTEQ5HQ(PDF)	3.37	3.51
GRVHO(PDF)	3.44	3.58
CTEQ5M(PDF) b mass 4.5 GeV	3.20	3.33
PYTHIA		3.30

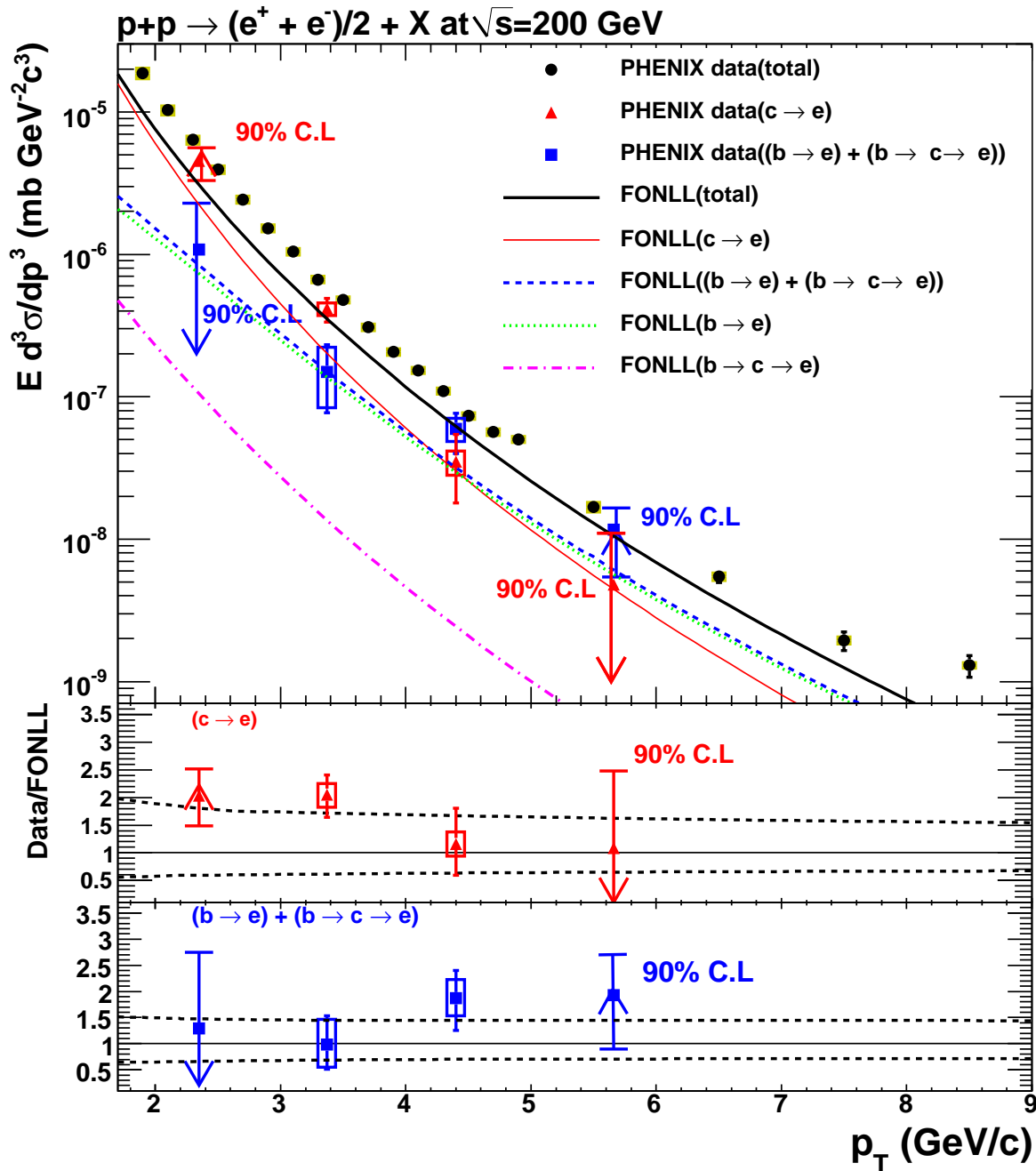


Figure 6.8: Upper panel: Invariant cross sections of electrons from charm and bottom with FONLL calculation. Lower panel: The ratios of data points over FONLL prediction as a function of electron p_T .

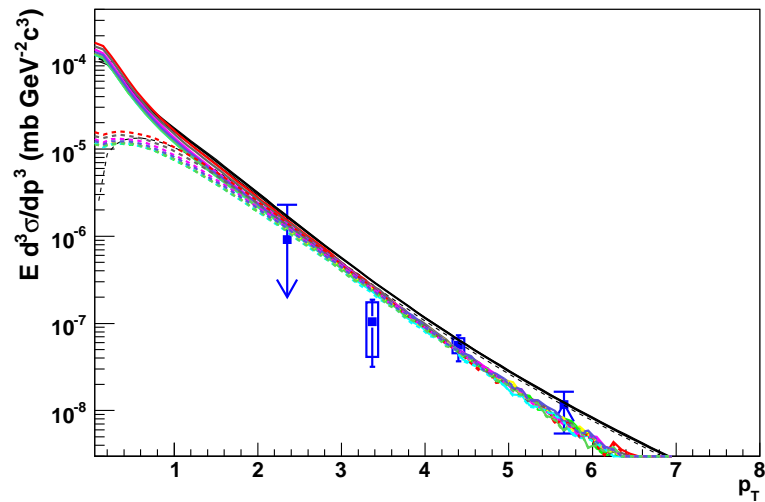


Figure 6.9: Invariant cross sections of electrons from bottom from FONLL calculation and PYTHIA. The simulations include electron from $b \rightarrow c \rightarrow e$ and $b \rightarrow e$. Black line show FONLL calculation. Other lines show PYTHIA with $1.5 < k_T < 10$ GeV/c. Dotted lines show electron from $b \rightarrow e$.

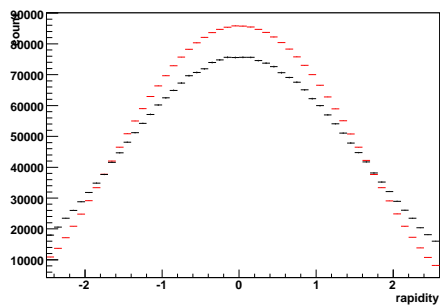


Figure 6.10: Rapidity distribution of B hadron and electrons from bottom at PYTHIA. Black points show the distribution of electrons and blue points show that of B hadron.

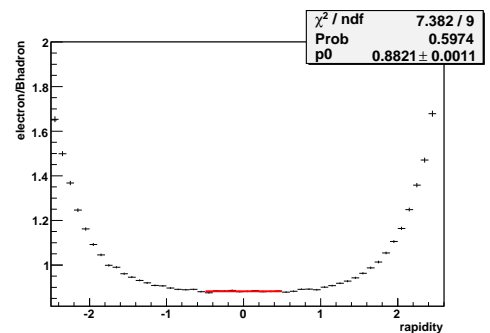


Figure 6.11: Ratios of the rapidity distributions shown at Fig.6.10

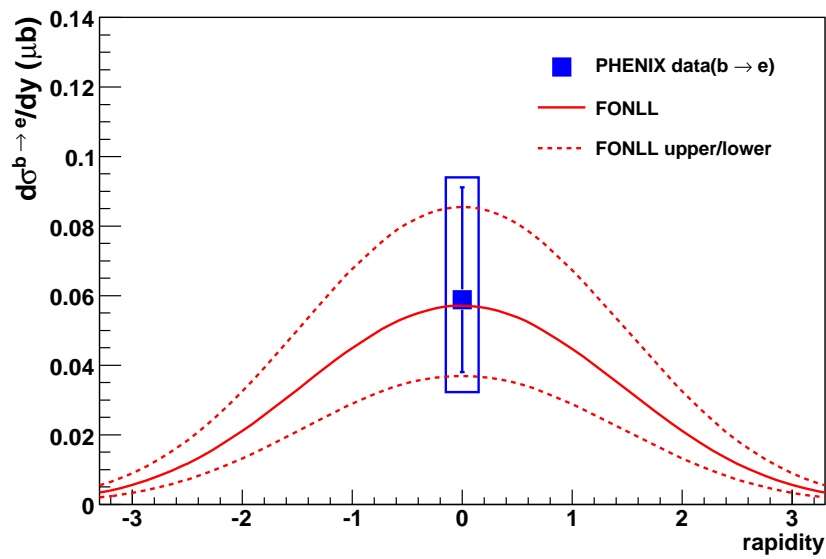


Figure 6.12: $d\sigma^{b \rightarrow e}/dy|_{y=0}$ with FONLL prediction as a function of rapidity.

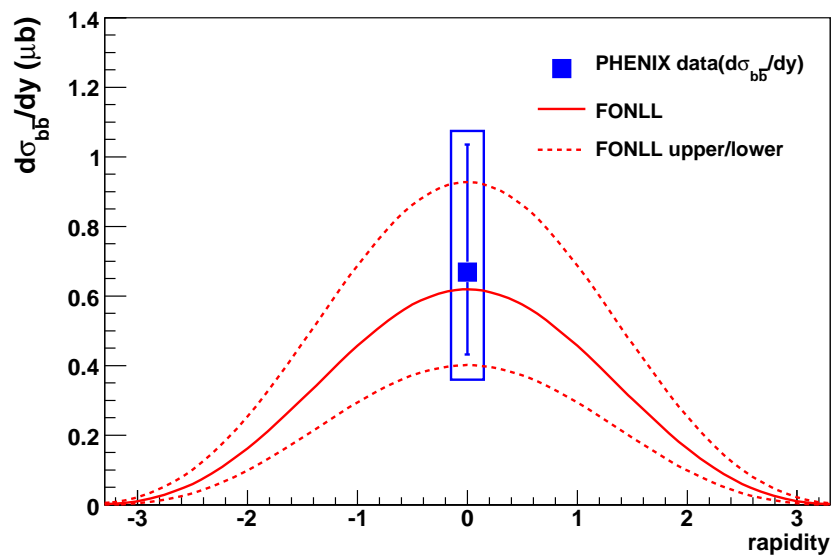


Figure 6.13: $d\sigma_{b\bar{b}}/dy|_{y=0}$ with FONLL prediction as a function of rapidity.

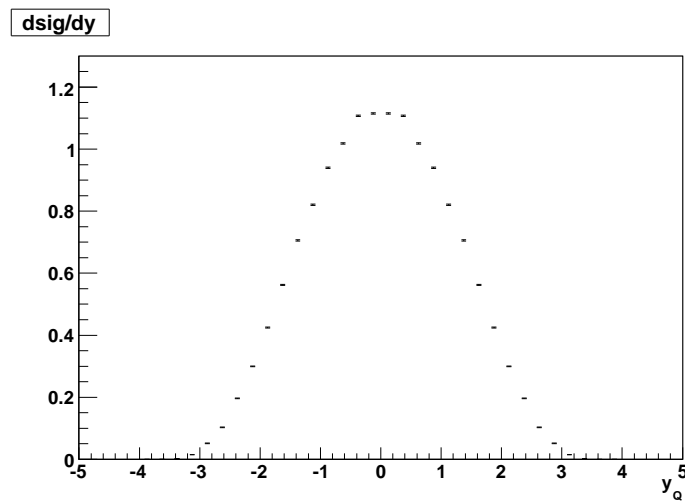


Figure 6.14: Rapidity distribution of bottom quark at HVQMNR using CTEQ5M as parton distribution function.

Bibliography

- [1] analysis note 615
- [2] analysis note 656
- [3] R.Field Acta Phys Polon B **36**,167(2005)
- [4] analysis note 380
- [5] analysis note 622
- [6] analysis note 632
- [7] Y.S Tsai, Mod. Phys. **46**,(1974) 815
- [8] <http://www.ge.infn.it/ridolfi/>
- [9] analysis note ppg065
- [10] analysis note ppg349
- [11] analysis note ppg066
- [12] GEANT4 home page
<http://geant4.web.cern.ch/>
- [13] Review of Mordern Physics **46**,815(1974)
- [14] Eur.Phys.J.C **17** 137(2000)
- [15] analysis note ppg011
- [16] D.Acosta et al Phys Rev Lett **91**,241804(2003)
- [17] Particle Data Group 2007
- [18] G. Alves et al Phys Rev Lett**77**,2388(1996)
- [19] EvtGen home page
<http://www.slac.stanford.edu/lange/EvtGen/>

- [20] EvtGen documentation
http://www.slac.stanford.edu/lange/EvtGen/rel_alpha-00-14-05/Evt.ps.gz
- [21] CLEO collaboration Phys Rev Lett **76**,1570(1996)
- [22] Analysis Note 486
- [23] CLEO collaboration B. Barish *et al.*, Phys. Rev. Lett **76** (1996) 1570
- [24] HERA-B collaboration Phys.Rev.D **73**,052005(2006)
- [25] E789 collaboration Phys.Rev.Lett **74**,3118(1995)
- [26] E789 collaboration Phys.Rev.Lett **82**,41(1999)
- [27] UA1 collaboration Phys.Lett.B **256**,121(1991)
- [28] CDF collaboration Phys.Rev.D **71**,032001(2005)
- [29] M.Cacciari Phys.Rev.Lett **95**,122001 (2005)
- [30] PHENIX Collaboration S. S. Adler *et al.*, Phys. Rev. Lett **91**, (2003) 241803.
- [31] PHENIX Collaboration S. S. Adler *et al.*, Phys. Rev. Lett. **96**, (2006) 202301.
- [32] R. Averbeck *et al.*, PHENIX Internal Analysis Note **89** (2001)
- [33] PHENIX Collaboration S. S. Adler *et al.*, nucl-ex/0611031 (2006).
- [34] PHENIX Collaboration S. S. Adler *et al.*, Phys. Rev. Lett. **96**, (2006) 032001.
- [35] R. Vogt, Private communication.
- [36] M. J. Leitch for the PHENIX Collaboration J. Phys. G **32** (2006) S391.
- [37] D. Das for the STAR Collaboration J. Phys. G **35** (2008) 104153.
- [38] M. Cacciari *et al.*, Phys.Rev.Lett **95** (2005) 122001

Appendix A

Data Tables

Table A.1: Invariant cross section of single non-photonic electrons from heavy flavor decays at $y=0$.

p_T (GeV/ c)	cross section (mb GeV $^{-2}$ c 3)	stat error	sys error
0.55	0.00433	0.000404	0.00111
0.65	0.00218	0.000237	0.000542
0.75	0.00132	0.000148	0.000275
0.85	0.000911	9.87e-005	0.000149
0.95	0.000572	6.87e-005	8.47e-005
1.1	0.00033	3e-005	3.82e-005
1.3	0.000141	1.71e-005	1.53e-005
1.5	6.51e-005	1.04e-005	6.7e-006
1.7	3.29e-005	2.92e-007	4.41e-006
1.9	1.87e-005	1.55e-007	2.06e-006
2.1	1.03e-005	9.17e-008	1.01e-006
2.3	6.36e-006	6.32e-008	5.66e-007
2.5	3.94e-006	4.56e-008	3.31e-007
2.7	2.43e-006	3.36e-008	2e-007
2.9	1.52e-006	2.52e-008	1.23e-007
3.1	1.05e-006	1.93e-008	7.97e-008
3.3	6.65e-007	1.48e-008	5.12e-008
3.5	4.8e-007	1.16e-008	3.5e-008
3.7	3.08e-007	9.05e-009	2.32e-008
3.9	2.07e-007	7.22e-009	1.6e-008
4.1	1.54e-007	5.87e-009	1.15e-008
4.3	1.1e-007	4.82e-009	8.28e-009
4.5	7.35e-008	3.84e-009	5.91e-009
4.7	5.66e-008	3.28e-009	4.42e-009
4.9	5.03e-008	2.85e-009	3.58e-009
5.5	1.69e-008	1.02e-009	1.69e-009
6.5	5.45e-009	5.09e-010	4.64e-010
7.5	1.95e-009	2.91e-010	1.54e-010
8.5	1.3e-009	2.24e-010	8.82e-011

Table A.2: The Data/FONLL ratios of single non-photonic electron yield at $y=0$.

p_T (GeV/ c)	cross section	stat error	sys error
0.55	2.21	0.206	0.567
0.65	1.75	0.19	0.435
0.75	1.68	0.189	0.35
0.85	1.84	0.199	0.3
0.95	1.81	0.217	0.268
1.1	2.04	0.185	0.236
1.3	1.92	0.233	0.208
1.5	1.83	0.293	0.189
1.7	1.79	0.0159	0.24
1.9	1.86	0.0155	0.205
2.1	1.78	0.0159	0.175
2.3	1.84	0.0183	0.164
2.5	1.84	0.0213	0.155
2.7	1.78	0.0246	0.146
2.9	1.71	0.0283	0.138
3.1	1.76	0.0324	0.134
3.3	1.65	0.0367	0.127
3.5	1.72	0.0416	0.126
3.7	1.58	0.0463	0.119
3.9	1.49	0.0521	0.115
4.1	1.54	0.0589	0.115
4.3	1.52	0.0666	0.114
4.5	1.38	0.0722	0.111
4.7	1.44	0.0831	0.112
4.9	1.71	0.0967	0.121
5.5	1.3	0.0788	0.13
6.5	1.45	0.135	0.123
7.5	1.56	0.233	0.124
8.5	2.83	0.488	0.192

Table A.3: Result of $(b \rightarrow e)/(c \rightarrow e + b \rightarrow e)$ in RUN5 and RUN6

electron p_T	$(b \rightarrow e)/(c \rightarrow e + b \rightarrow e)$
2.35 GeV/ c	< 0.41 (90% C.L) 0.19 (50% point)
3.37 GeV/ c	$0.26^{+0.14}_{-0.13}(stat)^{+0.11}_{-0.11}(sys)$
4.40 GeV/ c	$0.63^{+0.18}_{-0.21}(stat) \pm 0.08(sys)$
5.66 GeV/ c	> 0.33 (90% C.L) 0.71 (50% point)

Table A.4: Invariant cross section of electrons from charm and bottom

electron p_T	cross section (mb GeV ⁻² c ³)	data/FONLL
charm		
2.35 GeV/ c	> 3.30 (90% C.L) 4.52 (50%) $\times 10^{-6}$	> 1.49 (90% C.L) 2.03 (50%)
3.37 GeV/ c	$4.17^{+0.73+0.41}_{-0.83-0.46} \times 10^{-7}$	$2.05^{+0.36+0.20}_{-0.41-0.22}$
4.40 GeV/ c	$3.49^{+1.95}_{-1.70} \pm 0.66 \times 10^{-8}$	$1.16^{+0.65}_{-0.56} \pm 0.22$
5.66 GeV/ c	< 1.11 (90% C.L) 0.48 (50%) $\times 10^{-8}$	< 2.48 (90% C.L) 1.08 (50%)
bottom		
2.35 GeV/ c	< 2.30 (90% C.L) 1.08 (50%) $\times 10^{-6}$	< 2.74 (90% C.L) 1.29 (50%)
3.37 GeV/ c	$1.49^{+0.83+0.73}_{-0.73-0.66} \times 10^{-7}$	$0.99^{+0.55+0.48}_{-0.48-0.43}$
4.40 GeV/ c	$5.95^{+1.70}_{-1.95} \pm 1.10 \times 10^{-8}$	$1.87^{+0.54}_{-0.61} \pm 0.34$
5.66 GeV/ c	> 0.54 (90% C.L) 1.17 (50%) $\times 10^{-8}$	> 0.90 (90% C.L) 1.93 (50%)

Appendix B

Comparison Between Real Data and Simulation in RUN6

B.1 eID variables

The distributions of the variables used for the electron identification from the PISA simulation are compared to these of the real data in RUN6. The used cuts for each variable comparison are described in Sec. 3.2.1.

Figure B.1, B.2 and B.3 show the distributions of RICH variables, n_0 , $disp$ and chi^2/npe_0 at each RICH sector, respectively. In addition, Figure B.4, B.5 and B.6 show the distributions of EMCal variables at each sector, $emcsdphi_e$, $emcsdz_e$ and $prob$, respectively. Figure B.7 and B.8 show mean and sigma values of $ecore/mom$ distributions as a function of electron p_T . In Fig. B.1-B.8, black squares show the results from the real data in RUN6 and red circles show these from the PISA simulation with RUN6 tuning parameters and CM++ field. The distribution in simulation is normalized by the number of entries at each sector. The distributions of the simulation and these of the real data match well.

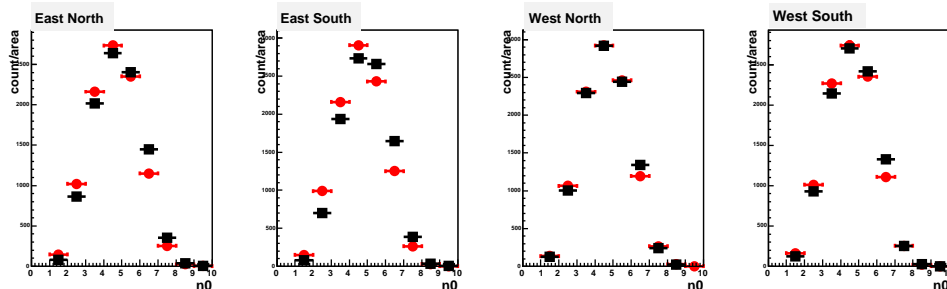


Figure B.1: The distribution of n_0 with the standard eID cut without n_0 cut and the $0.5 < p_T < 5$ GeV/ c cut in the real data (square) and simulation (circle).

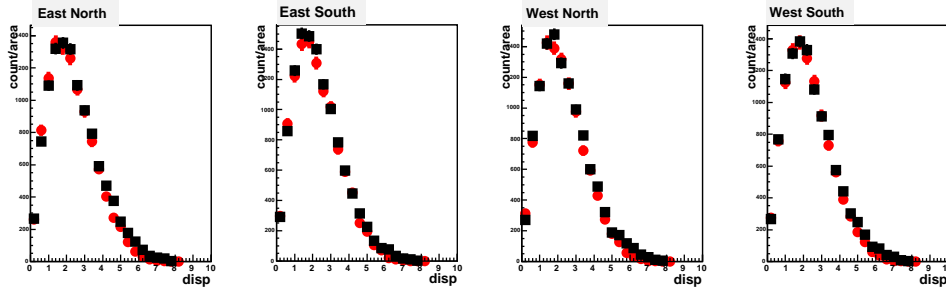


Figure B.2: The distribution of disp with the standard eID cut without disp cut and the $0.5 < p_T < 5 \text{ GeV}/c$ cut in the real data (square) and simulation (circle).

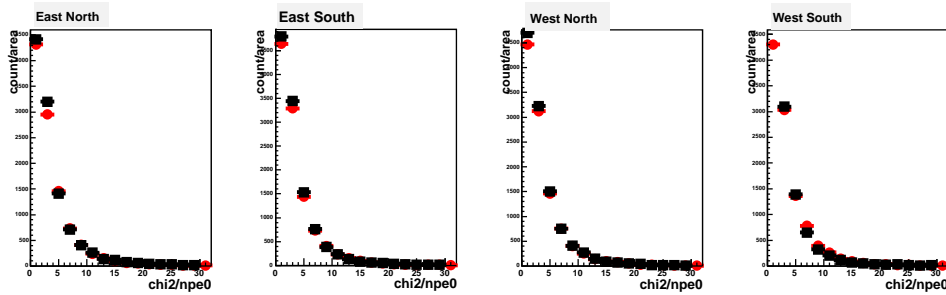


Figure B.3: The distribution of $\text{chi}^2/\text{npe}0$ with the standard eID cut without $\text{chi}^2/\text{npe}0$ cut and the $0.5 < p_T < 5 \text{ GeV}/c$ cut in the real data (square) and simulation (circle).

B.2 Geometrical Acceptance

The distributions of phi , zed of the simulation are compared with these of the real data for the electron samples selected by the standard eID and a transverse momentum with $0.5 < p_T < 5 \text{ GeV}/c$. Figure B.9 shows the distributions of phi at North (top panel) and South (bottom panel) sector, and Figure B.10 shows the distributions of zed at East (top panel) and West (bottom panel) sector. In Fig. B.9 and B.10, black squares show the real data in RUN6 and red circles show the PISA simulation with RUN6 tuning parameters and CM++ field. The distributions of simulation are normalized by number of entries in the reference regions, where are little low efficiency, dead or noisy area. In Fig B.9 and B.10, the used reference region to normalize is region 1.

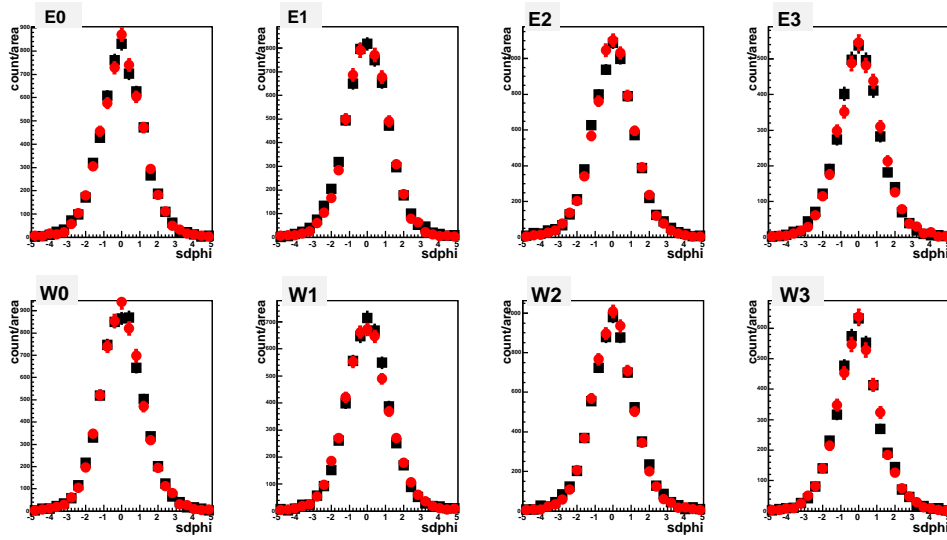


Figure B.4: The distribution of emcsdphi_e with the standard eID cut without $\text{emcsdphi}(z)_e$ cut and the $0.5 < p_T < 5 \text{ GeV}/c$ cut in the real data (square) and simulation (circle).

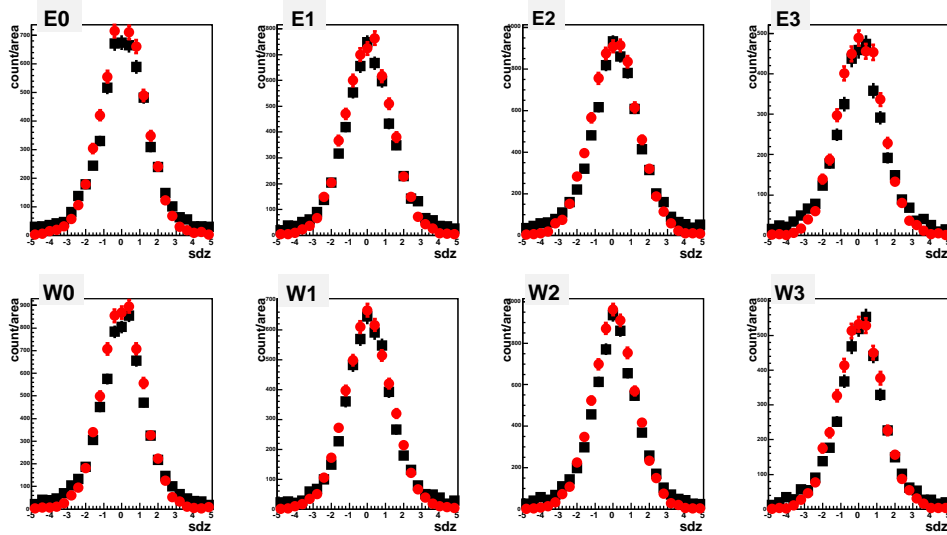


Figure B.5: The distribution of emcsdz_e with the standard eID cut without $\text{emcsdphi}(z)_e$ cut and the $0.5 < p_T < 5 \text{ GeV}/c$ cut in the real data (square) and simulation (circle).

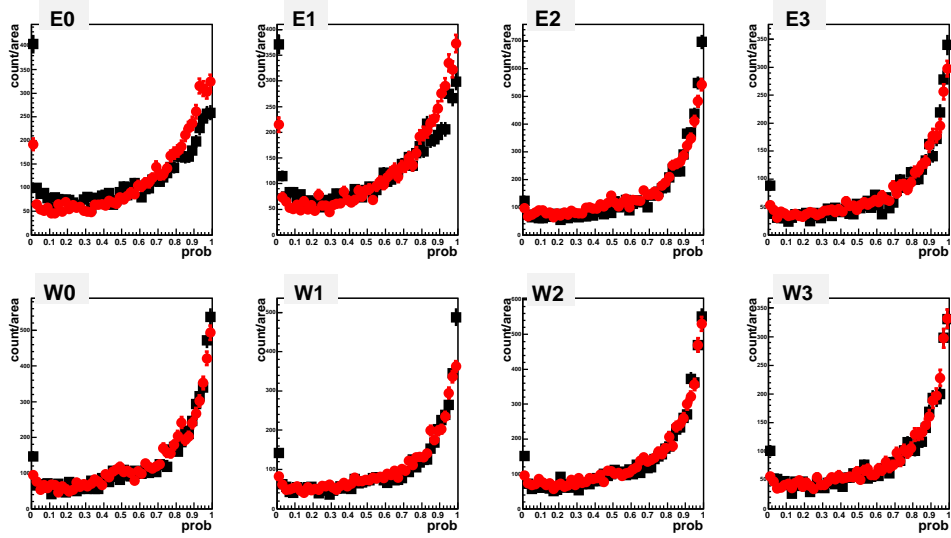


Figure B.6: The distribution of prob with the standard eID cut without prob cut and the $0.5 < p_T < 5$ GeV/c cut in the real data (square) and simulation (circle).

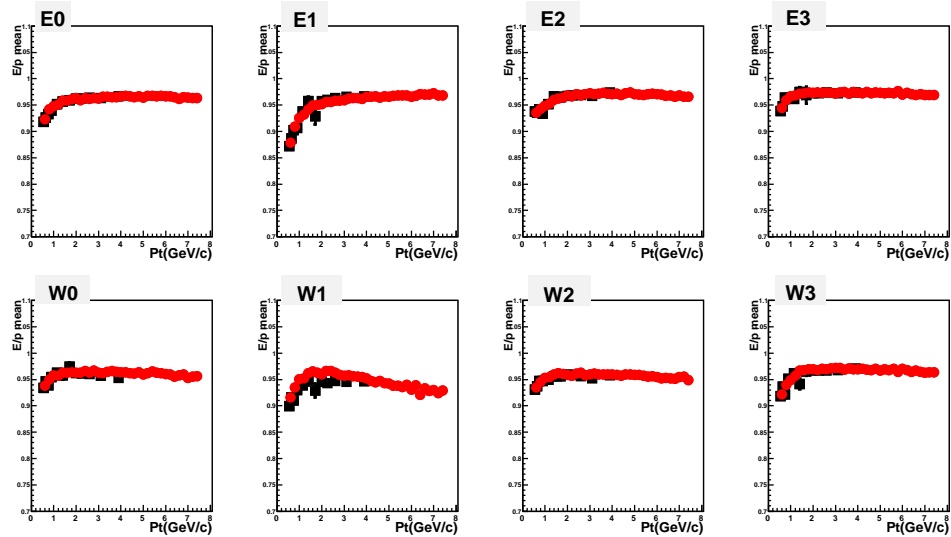


Figure B.7: The mean value of ecore/mom distribution with the standard eID cut as a function of electron p_T in the real data (square) and simulation (circle).

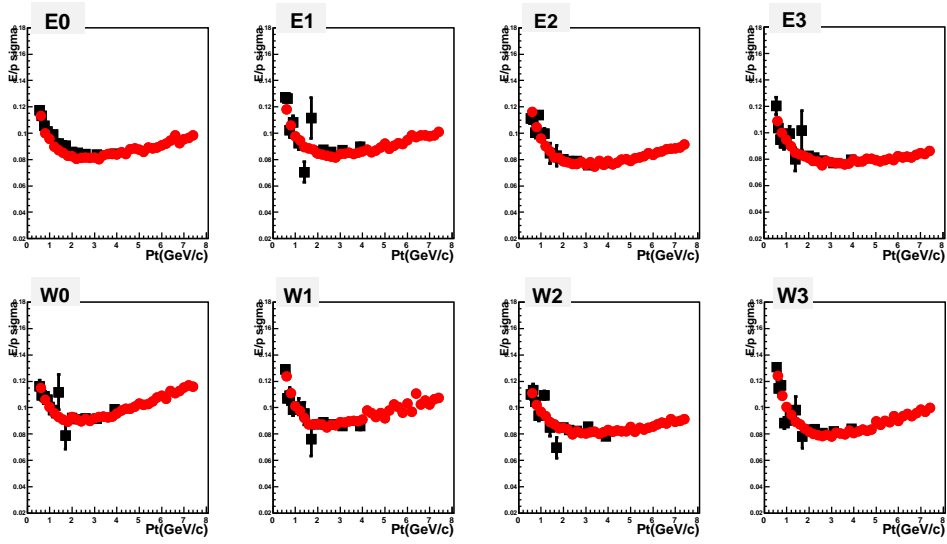


Figure B.8: The sigma value of ecore/mom distribution with the standard eID cut as a function of electron p_T in the real data (square) and simulation (circle).

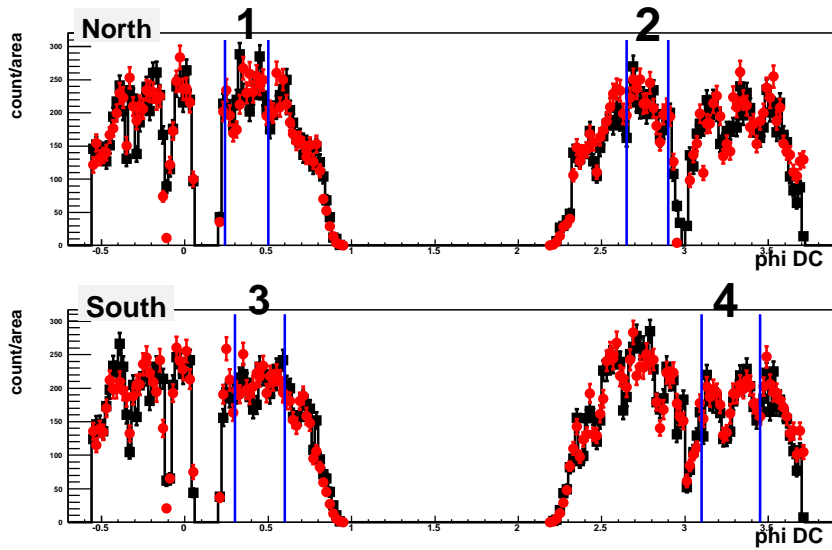


Figure B.9: The distribution of phi with the standard eID cut and the $0.5 < p_T < 5$ GeV/c cut in the real data in RUN6 (square) and simulation (circle).

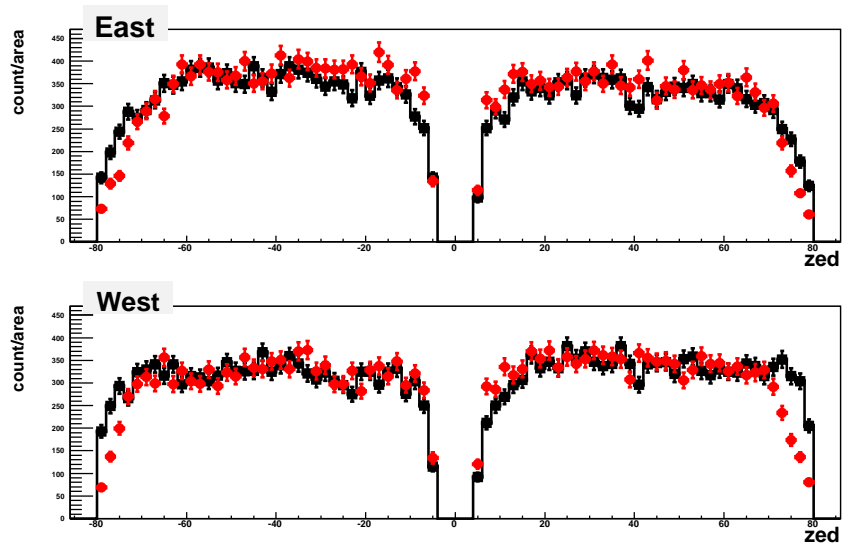


Figure B.10: The distribution of zed with the standard eID cut and the $0.5 < p_T < 5$ GeV/ c cut in the real data in RUN6 (square) and simulation (circle).

Appendix C

Correlation Function of Electron and Hadron

C.1 Correlation Function in Real Data

Acceptance filter is NOT applied when we study the correlation function

Two particle correlations with respect to the azimuthal angular difference, which is called 'correlation function' is studied in this chapter. The one of two particle is called 'trigger particle' and the other is called 'associated particle'. Correlation function is defined as the measured yield of the associated particles as a function of the azimuthal angular difference. Correlation function of trigger electrons and associated hadrons is studied to compare with PYTHIA simulation. Since charge asymmetry of electing hadron pairs have little PYTHIA parameter dependence, the comparison with real data between PYTHIA should be done for other observables to study the tuning status of PYTHIA. For this purpose, we choose the correlation function between the trigger non-photonic electrons and the associated hadrons.

The condition of analysis cut for trigger electrons is described at Sec 2.2.3. p_T range of the selected trigger electrons is $2.0 < p_T < 5.0$ GeV/ c and that of the selected associated hadrons is $0.4 < p_T < 5.0$ GeV/ c .

Figure C.1 shows the raw number of the associated hadrons as a function of the azimuthal angle with respect to the trigger electron, $\Delta N/\Delta\phi$, per the number of the trigger electrons, where the trigger electrons are inclusive electrons. Black points shows the $\Delta N/\Delta\phi$ in ERT triggered events in RUN5. Red points show the $\Delta N/\Delta\phi$ in mixing events. $\Delta N/\Delta\phi$ in mixing events is considered as the background to take into account the effect of geometrical acceptance. $\Delta N/\Delta\phi$ in mixing events is normalized by the number of the trigger electrons.

Figure C.2 shows the $\Delta N/\Delta\phi$ distribution per the number of the trigger electrons, where the trigger electrons are the photonic electrons. Black points show the $\Delta N/\Delta\phi$ in ERT triggered events in RUN5 and red points show the background used by the mixing event method. The photonic electrons are identified by the invariant mass distribution of di-electron. When the associated electron is found in the associated particles, we calculate the invariant mass of the trigger electrons and the associated electrons. The trigger electrons is identified as the photonic

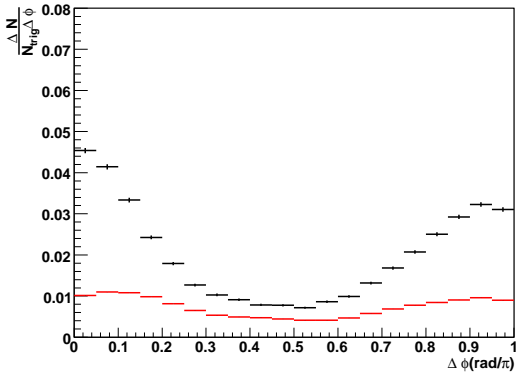


Figure C.1: The $\Delta N/\Delta\phi$ distribution per the number of the trigger electrons, when the trigger electrons were the inclusive electrons. Black points shows the $\Delta N/\Delta\phi$ in real events and red points show the background.

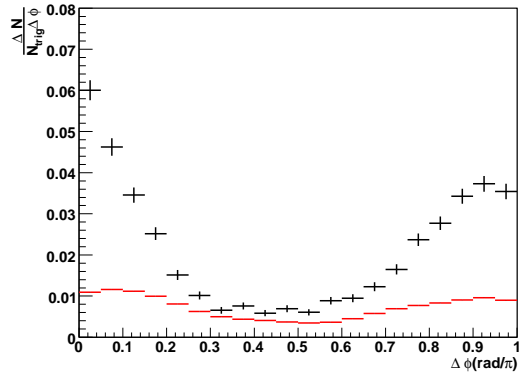


Figure C.2: The $\Delta N/\Delta\phi$ distribution per the number of the trigger electrons, when the trigger electrons were the photonic electrons. Black points shows the $\Delta N/\Delta\phi$ in real events and red points show the background.

electron trigger, when the invariant mass is below $0.08 \text{ GeV}/c^2$. When we make the background for the photonic electron trigger by mixing events, the photonic trigger electrons are selected by the above method to take account for the acceptance bias by the selection of the photonic electrons.

The correlation functions of the inclusive and the photonic electron-hadrons are obtained by the subtraction of the background $\Delta N/\Delta\phi$ distribution. The correlation function of electrons from heavy flavor - hadrons is obtained as follows.

$$C_{HQ}(\Delta\phi) = (C_{incl}(\Delta\phi) - (1 - R_{HQ}) \times C_{phot}(\Delta\phi))/R_{HQ}.$$

Here,

- $C_{HQ}(\Delta\phi)$ is the correlation function, where the trigger electrons are from heavy flavor.
- $C_{incl}(\Delta\phi)$ is the correlation function, where the trigger electrons are inclusive electrons
- $C_{phot}(\Delta\phi)$ is the correlation function, where the trigger electrons are photonic electrons
- R_{HQ} is the fraction of electrons from heavy flavor in the inclusive electrons.

Figure C.3 shows the correlation functions of electron-hadrons, where the trigger electrons are inclusive (black), photonic (red) and heavy flavor (blue).

C.2 PYTHIA tuning status

The PYTHIA tuning status is studied by the comparison of the correlation function of heavy flavor electrons and hadrons between in RUN5 data and PYTHIA simulation. The correlation function is obtained in PYTHIA simulation by the similar way in the analysis at real data.

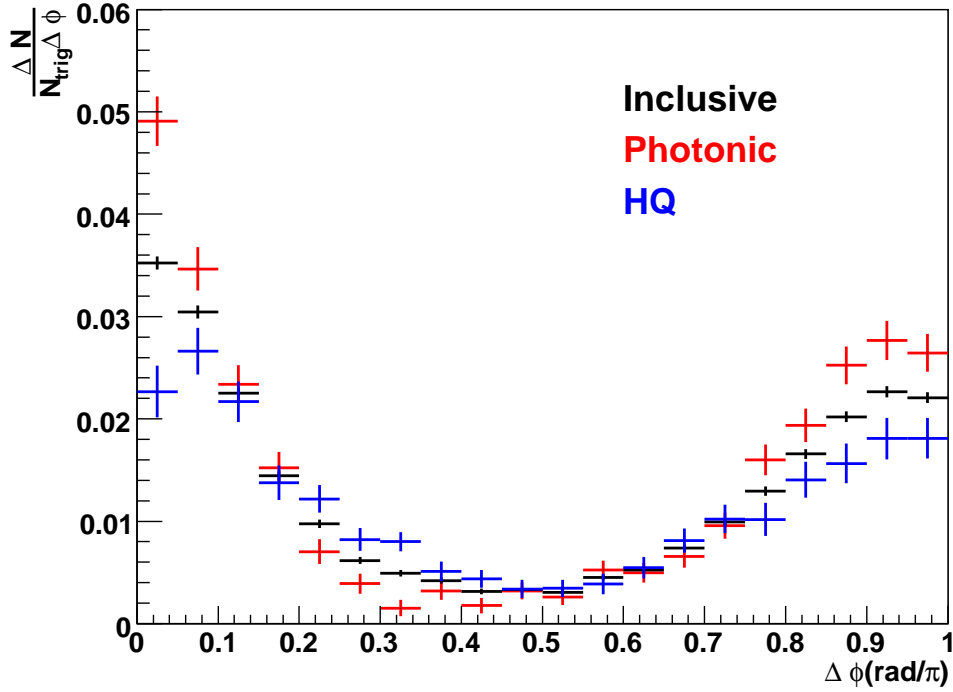


Figure C.3: The correlation function of electron-hadrons when the trigger electrons are inclusive (black), photonic (red) and heavy flavor (blue).

Figure C.4 shows the correlation function of electrons and hadrons in the PYTHIA simulation, where the trigger electrons are from charm and bottom. Red line shows the correlation function in the case of charm production and blue line shows that in the case of bottom production. For the comparison with real data and PYTHIA, the obtained PYTHIA results are mixed up as follows.

$$C_{HQ}(\Delta\phi) = R_b(C_b(\Delta\phi) + (1 - R_b)C_c(\Delta\phi)).$$

Here,

- $C_{HQ}(\Delta\phi)$ is the correlation function, where the trigger electrons are from heavy flavor.
- $C_{c(b)}(\Delta\phi)$ is the correlation function, where the trigger electrons are from charm (bottom)
- R_b is $\frac{N_{b \rightarrow e}}{N_{c \rightarrow e} + N_{b \rightarrow e}}$.

We set R_b to 0.15 from this analysis for the comparison with real data. Figure C.5 shows the correlation function of electrons and hadrons, where the trigger electrons are from heavy flavor. Black points show the result in RUN5 data and green line shows the result in PYTHIA. The PYTHIA simulation agrees with the real data. This indicated the tuning for PYTHIA simulation is well.

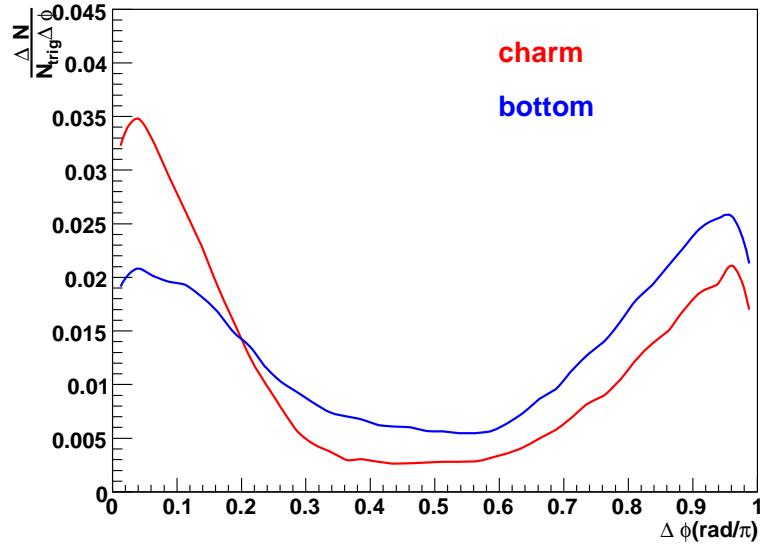


Figure C.4: The correlation function of electrons and hadrons at the tuned PYTHIA, when the trigger electrons were from charm and bottom. Red line shows the correlation function in the case of charm production and blue line shows that in the case of bottom production.

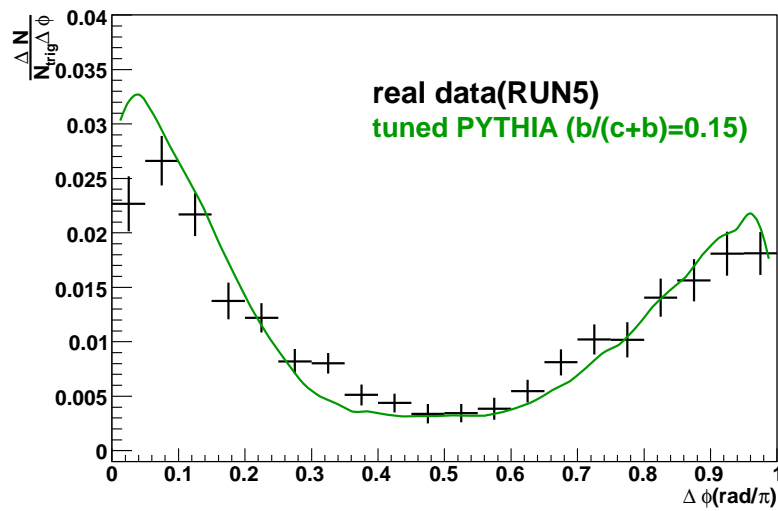


Figure C.5: The correlation function of electrons and hadrons, where the trigger electrons are from heavy flavor. Black points show the result at RUN5 data obtained and green line shows the result at PYTHIA when we set R_b to 0.15.

Appendix D

Details of ϵ_c and ϵ_b

Table D.1: Detail of charm and bottom decay for electron p_T 3-4 GeV/c

channel	N_{tag} (part)/(all)	N_{ele} (part)/(all)	ϵ
D^0			
$D^0 \rightarrow e^+ K^- \nu_e$	46.71%	29.46%	$8.06 \pm 0.18\%$
$D^0 \rightarrow e^+ K^{*-} \nu_e$	11.84%	3.11%	$19.31 \pm 0.73\%$
$D^0 \rightarrow e^+ \pi^- \nu_e$	4.65%	5.77%	$4.10 \pm 0.36\%$
$D^0 \rightarrow e^+ \rho^- \nu_e$	1.29%	0.45%	$14.63 \pm 1.70\%$
$D^0 \rightarrow e^+ other$	0.91%	0.44%	$10.39 \pm 1.74\%$
D^+			
$D^+ \rightarrow e^+ \bar{K}^0 \nu_e$	21.57%	39.47%	$2.78 \pm 0.13\%$
$D^+ \rightarrow e^+ \bar{K}^{*0} \nu_e$	6.08%	4.05%	$7.64 \pm 0.64\%$
$D^+ \rightarrow e^+ \pi^0 \nu_e$	1.84%	3.79%	$2.47 \pm 0.35\%$
$D^+ \rightarrow e^+ \rho^0 \nu_e$	0.14%	0.32%	$2.20 \pm 2.31\%$
$D^+ \rightarrow e^+ other$	1.60%	1.92%	$4.23 \pm 0.72\%$
D_s			
$D_s \rightarrow e^+ \phi \nu_e$	0.44%	0.73%	$3.04 \pm 1.56\%$
$D_s \rightarrow e^+ \eta \nu_e$	3.91%	7.80%	$2.55 \pm 0.26\%$
$D_s \rightarrow e^+ \eta' \nu_e$	0.58%	0.57%	$5.18 \pm 1.49\%$
$D_s \rightarrow e^+ other$	0.16%	0.82%	$0.98 \pm 0.90\%$
Λ_c			
$\Lambda_c \rightarrow e^+ \Lambda \nu_e$	-0.57%	0.26%	$-11.24 \pm 5.15\%$
$\Lambda_c \rightarrow e^+ other$	-1.15%	1.04%	$-5.63 \pm 2.34\%$
B^0			
$B^0 \rightarrow e^+ D^- \nu_e$	4.56%	5.93%	$1.41 \pm 0.22\%$
$B^0 \rightarrow e^+ D^{*-} \nu_e$	0.76%	23.28%	$0.06 \pm 0.12\%$
$B^0 \rightarrow e^+ other$	5.48%	5.29%	$1.90 \pm 0.26\%$
B^+			
$B^+ \rightarrow e^+ D^0 \nu_e$	8.31%	6.55%	$2.33 \pm 0.22\%$
$B^+ \rightarrow e^+ D^{*0} \nu_e$	29.43%	25.17%	$2.14 \pm 0.12\%$
$B^+ \rightarrow e^+ other$	3.64%	5.86%	$1.14 \pm 0.26\%$
B_s			
$B_s \rightarrow e^+ total$	16.69 %	11.62%	$2.63 \pm 0.16\%$
$Bhad \rightarrow e^+ others$	11.41%	10.82%	$1.93 \pm 0.17\%$
$B \rightarrow c \rightarrow e$	19.71%	5.48%	$6.60 \pm 0.34\%$

Table D.2: Detail of charm and bottom decay for electron p_T 4-5 GeV/c

channel	N_{tag} (part)/(all)	N_{ele} (part)/(all)	ϵ
D^0			
$D^0 \rightarrow e^+ K^- \nu_e$	46.18%	29.62%	$10.79 \pm 0.18\%$
$D^0 \rightarrow e^+ K^{*-} \nu_e$	10.54%	3.42%	$21.30 \pm 0.69\%$
$D^0 \rightarrow e^+ \pi^- \nu_e$	3.97%	5.52%	$4.97 \pm 0.38\%$
$D^0 \rightarrow e^+ \rho^- \nu_e$	1.02%	0.49%	$14.53 \pm 1.62\%$
$D^0 \rightarrow e^+ other$	1.14%	0.47%	$16.78 \pm 1.76\%$
D^+			
$D^+ \rightarrow e^+ \bar{K}^0 \nu_e$	23.71%	39.07%	$4.20 \pm 0.13\%$
$D^+ \rightarrow e^+ \bar{K}^{*0} \nu_e$	5.62%	4.40%	$8.83 \pm 0.60\%$
$D^+ \rightarrow e^+ \pi^0 \nu_e$	2.03%	3.58%	$3.93 \pm 0.34\%$
$D^+ \rightarrow e^+ \rho^0 \nu_e$	0.21%	0.34%	$4.33 \pm 2.23\%$
$D^+ \rightarrow e^+ other$	1.33%	1.95%	$4.73 \pm 0.71\%$
D_s			
$D_s \rightarrow e^+ \phi \nu_e$	0.37%	0.80%	$3.20 \pm 1.49\%$
$D_s \rightarrow e^+ \eta \nu_e$	3.71%	7.70%	$3.33 \pm 0.27\%$
$D_s \rightarrow e^+ \eta' \nu_e$	0.32%	0.62%	$3.63 \pm 1.49\%$
$D_s \rightarrow e^+ other$	0.37%	0.81%	$3.16 \pm 0.90\%$
Λ_c			
$\Lambda_c \rightarrow e^+ \Lambda \nu_e$	-0.36%	0.32%	$-7.89 \pm 4.81\%$
$\Lambda_c \rightarrow e^+ other$	-0.16%	0.88%	$-1.30 \pm 2.55\%$
B^0			
$B^0 \rightarrow e^+ D^- \nu_e$	5.79%	5.84%	$2.08 \pm 0.28\%$
$B^0 \rightarrow e^+ D^{*-} \nu_e$	-0.48%	23.89%	$-0.04 \pm 0.15\%$
$B^0 \rightarrow e^+ other$	5.34%	5.09%	$2.20 \pm 0.34\%$
B^+			
$B^+ \rightarrow e^+ D^0 \nu_e$	7.40%	6.40%	$2.43 \pm 0.28\%$
$B^+ \rightarrow e^+ D^{*0} \nu_e$	31.15%	25.89%	$2.53 \pm 0.14\%$
$B^+ \rightarrow e^+ other$	1.61%	5.65%	$0.60 \pm 0.33\%$
B_s			
$B_s \rightarrow e^+ total$	19.83 %	11.97%	$3.48 \pm 0.20\%$
$Bhad \rightarrow e^+ others$	14.67%	10.79%	$2.86 \pm 0.21\%$
$B \rightarrow c \rightarrow e$	14.69%	4.47%	$6.91 \pm 0.46\%$

Table D.3: Detail of charm and bottom decay for electron p_T 5-7 GeV/c

channel	N_{tag} (part)/(all)	N_{ele} (part)/(all)	ϵ
D^0			
$D^0 \rightarrow e^+ K^- \nu_e$	50.38%	29.51%	$13.60 \pm 0.22\%$
$D^0 \rightarrow e^+ K^{*-} \nu_e$	9.46%	3.20%	$23.53 \pm 0.84\%$
$D^0 \rightarrow e^+ \pi^- \nu_e$	2.72%	5.77%	$3.75 \pm 0.44\%$
$D^0 \rightarrow e^+ \rho^- \nu_e$	1.27%	0.48%	$21.16 \pm 1.89\%$
$D^0 \rightarrow e^+ other$	1.03%	0.43%	$19.32 \pm 2.15\%$
D^+			
$D^+ \rightarrow e^+ \bar{K}^0 \nu_e$	22.03%	39.60%	$4.43 \pm 0.15\%$
$D^+ \rightarrow e^+ \bar{K}^{*0} \nu_e$	4.38%	4.10%	$8.51 \pm 0.73\%$
$D^+ \rightarrow e^+ \pi^0 \nu_e$	2.11%	3.77%	$4.46 \pm 0.37\%$
$D^+ \rightarrow e^+ \rho^0 \nu_e$	0.20%	0.33%	$4.87 \pm 2.67\%$
$D^+ \rightarrow e^+ other$	1.33%	1.91%	$5.53 \pm 0.85\%$
D_s			
$D_s \rightarrow e^+ \phi \nu_e$	0.41%	0.74%	$4.42 \pm 1.81\%$
$D_s \rightarrow e^+ \eta \nu_e$	3.46%	7.66%	$3.59 \pm 0.32\%$
$D_s \rightarrow e^+ \eta' \nu_e$	0.46%	0.57%	$6.32 \pm 1.90\%$
$D_s \rightarrow e^+ other$	0.58%	0.80%	$5.79 \pm 1.07\%$
Λ_c			
$\Lambda_c \rightarrow e^+ \Lambda \nu_e$	-0.32%	0.28%	$-9.09 \pm 6.70\%$
$\Lambda_c \rightarrow e^+ other$	0.51%	0.85%	$4.79 \pm 3.30\%$
$\Lambda_c \rightarrow e^+ total$	0.19 %	1.13%	$1.37 \pm 2.98\%$
B^0			
$B^0 \rightarrow e^+ D^- \nu_e$	5.55%	5.81%	$2.59 \pm 0.25\%$
$B^0 \rightarrow e^+ D^{*-} \nu_e$	2.80%	24.29%	$0.31 \pm 0.13\%$
$B^0 \rightarrow e^+ other$	7.30%	5.08%	$3.89 \pm 0.30\%$
B^+			
$B^+ \rightarrow e^+ D^0 \nu_e$	8.80%	6.34%	$3.75 \pm 0.24\%$
$B^+ \rightarrow e^+ D^{*0} \nu_e$	27.02%	26.10%	$2.80 \pm 0.13\%$
$B^+ \rightarrow e^+ other$	1.47%	5.55%	$0.71 \pm 0.29\%$
B_s			
$B_s \rightarrow e^+ total$	21.74 %	12.21%	$4.82 \pm 0.17\%$
$Bhad \rightarrow e^+ others$	14.94%	10.57%	$3.83 \pm 0.20\%$
$B \rightarrow c \rightarrow e$	10.38%	4.04%	$6.95 \pm 0.42\%$

Appendix E

Air Conversion

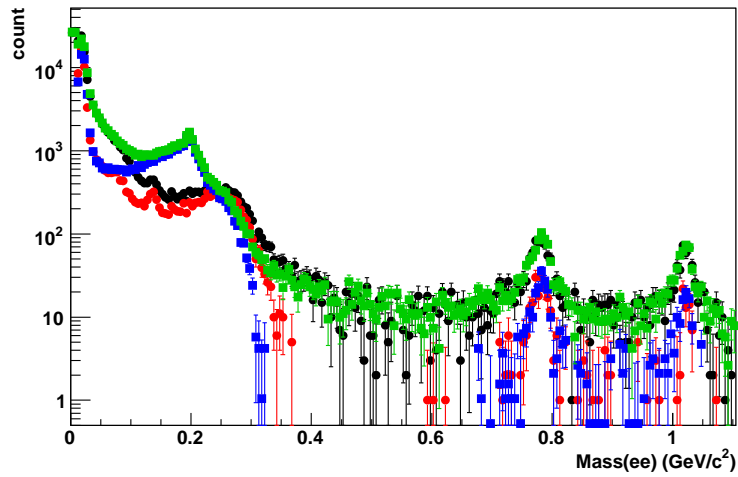


Figure E.1: Di-electron invariant mass distribution in RUN5 and RUN6 CNT ERT.

Figure E.1 shows di-electron invariant mass distribution at RUN6 and RUN5. In Fig.E.1, green points show the distribution at RUN6 and black points show that at RUN5. Blue points show RUN6 result with $\phi_{vj} < 0.2$ cut (selected conversion like pair) and red points show RUN5 result with $\phi_{vj} < 0.2$ cut. The distribution at RUN6 was normalized by number of entries at $M_{ee} < 0.1$ GeV/c. Clear excess from conversion was seen at about 0.2 GeV.

The contribution from air conversion was calculated via PISA simulation to take into account the exact eID cuts, since the reconstructed yield of electrons from air conversion depended on eID cuts. The simulation was done as follows.

1. Generate inclusive photon.
2. Convert inclusive photon into electron pairs at $0 < r < 100$ cm. (r is the distance from collision vertex)

3. Perform PISA simulation for generated electrons pairs.
4. Obtain the contribution of air conversion from simulation outputs.

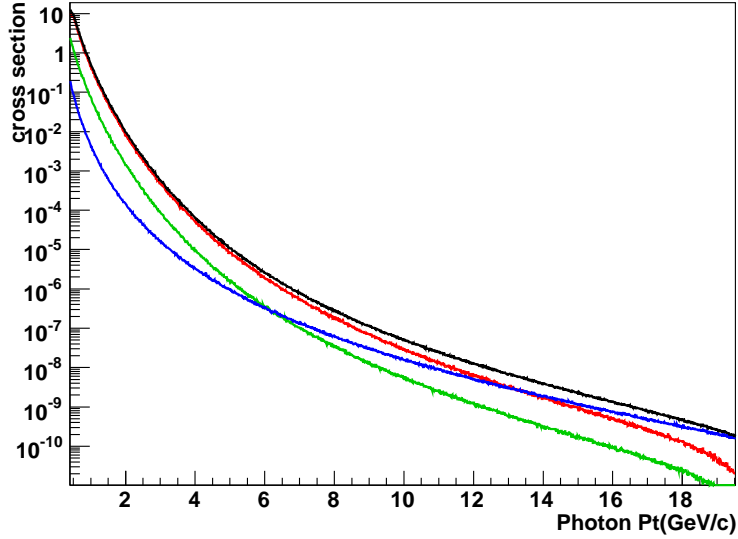


Figure E.2: Invariant cross section of generated inclusive photon (black), photon from $\pi^0 \rightarrow \gamma\gamma$ (red), photon from $\eta \rightarrow \gamma\gamma$ (green) and direct photon (blue).

Step1.

Inclusive photon was obtained as a sum of $\pi^0 \rightarrow \gamma\gamma$, $\eta \rightarrow \gamma\gamma$ and direct photon. Figure E.2 shows invariant cross section of obtained inclusive photon (black), photon from $\pi^0 \rightarrow \gamma\gamma$ (red), photon from $\eta \rightarrow \gamma\gamma$ (green) and direct photon (blue). p_T spectra and yields of π^0 , η and direct photon was obtained from the same formalization and parametrization as RUN5 p+p cocktail. $\pi^0, \eta \rightarrow \gamma\gamma$ process was simulated by exodus generator. Obtained spectrum of inclusive photon was fitted by modified Hagedron function. As a result, inclusive photon was generated by following equation.

$$E \frac{d^3\sigma}{dp^3} = \frac{1173.9}{(\exp(-0.339p_T - 0.299p_T^2) + p_T/0.458)^{7.74}} \quad (\text{E.1})$$

The other condition of photon generation follows.

- $|y| < 0.4$
- $0 < \phi < 2\pi$
- $|z_{\text{vtx}}| < 30 \text{ cm}$

Step2.

Generated photon was converted into electron pairs at $0 < r < 100\text{cm}$ to reproduce air

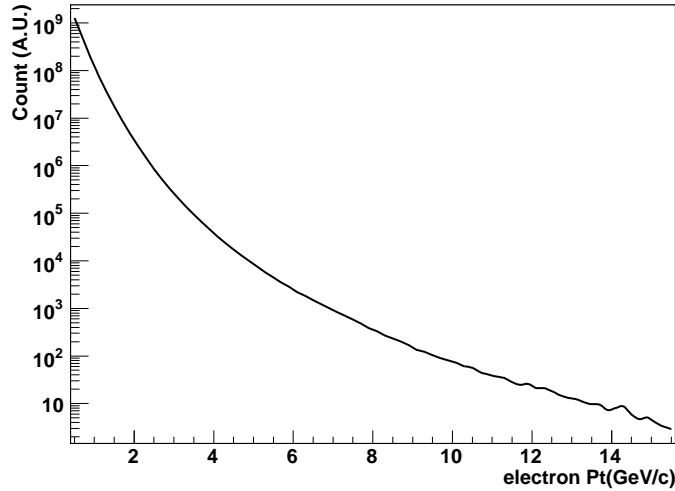


Figure E.3: The p_T distribution of electrons from photon conversion. Normalization of p_T distribution was not done at this step.

conversion. Photon conversion was simulated according to corrected Bethe-Heitler formula, as implemented in GEANT[12]. The distribution of conversion point was flat about r (the distance from collision vertex) Figure E.3 shows the p_T distribution of electrons from photon conversion. Normalization of p_T distribution was not done at this step.

Step3 and 4.

PISA simulation was performed for generated electrons pairs, and generated pDST files were processed by the same code as in the real data. Here, only electrons which generated points were $30 < r < 100\text{cm}$ were plotted in histograms, so that what we obtain was the effect of the absence of He bag. The obtained p_T distribution was converted into invariant cross section by the same procedure as real data.

Conversion probability was calculated as follow.

$$(\text{radiation length}) \times \frac{7}{9} \times \frac{\sigma_{conv}(k)}{\sigma_{conv}(\text{inf})}$$

Here, $\sigma_{conv}(k)$ is the total cross section of photon conversion when photon energy is k GeV/ c . $\frac{7}{9}$ corresponds to conversion probability when photon energy is infinite. The $\sigma_{conv}(k)/\sigma_{conv}(\text{inf})$ was taken from the review article[13]. Figure E.4 shows $1 - \sigma_{conv}(k)/\sigma_{conv}(\text{inf})$. Red points show the value taken from [13]. Black line show interpolate line by the following function.

$$0.0819 - 0.057 \log(k) + 0.0174 \log(k)^2 - 0.00269 \log(k)^3 + 0.000168 \log(k)^4$$

When we filled histograms, histograms were weighted according to the parent photon energy and Eq.E to take into account for energy dependence of the probability of photon conversion. The normalization of p_T distribution was done according to the yield of inclusive photon and

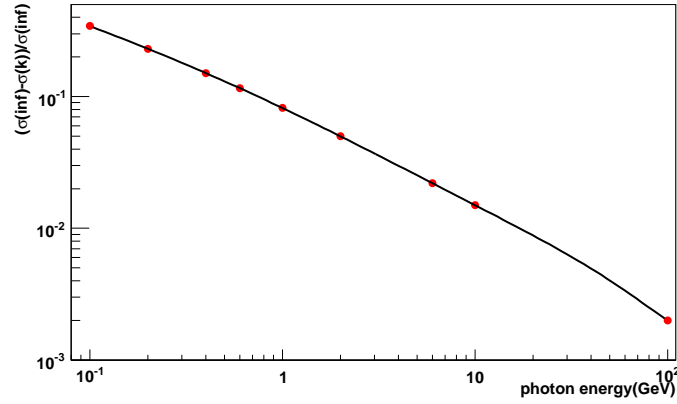


Figure E.4: $1 - \sigma_{conv}(k)/\sigma_{conv}(\text{inf})$. Red points show the value taken from [13]. Black line show interpolate line .

conversion probability in the air. The yield of inclusive photon was obtained from Eq.E.1. Figure E.5 shows the invariant cross section of electrons from increasing air conversion due to the absence of He bag. Blue points show the electrons from increasing air conversion and green line shows the electrons from air conversion at $r < 30\text{cm}$ in Fig.E.5. Black line shows the total background electrons implemented as cocktail.

RUN6 cocktail was obtained as the sum of RUN5 cocktail and the contribution of the increasing electrons from air conversion. Figure E.6 shows invariant cross section of electrons from all sources considered in the RUN6 p+p cocktail.

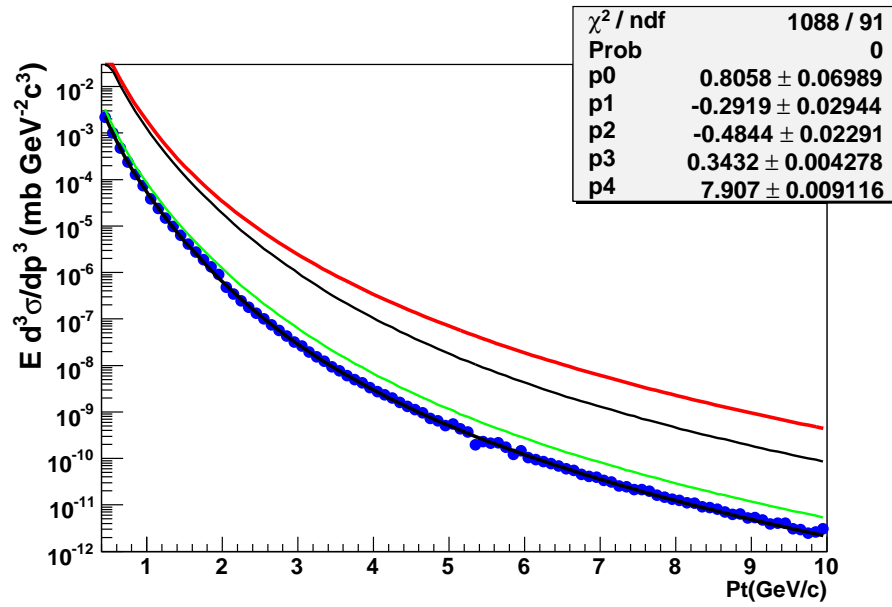


Figure E.5: Invariant cross section of electrons from increasing air conversion due to the absence of He bag. Blue points show the electrons from increasing air conversion and green line shows the electrons from air conversion at $r < 30\text{cm}$. Black line shows the total background electrons implemented as cocktail.

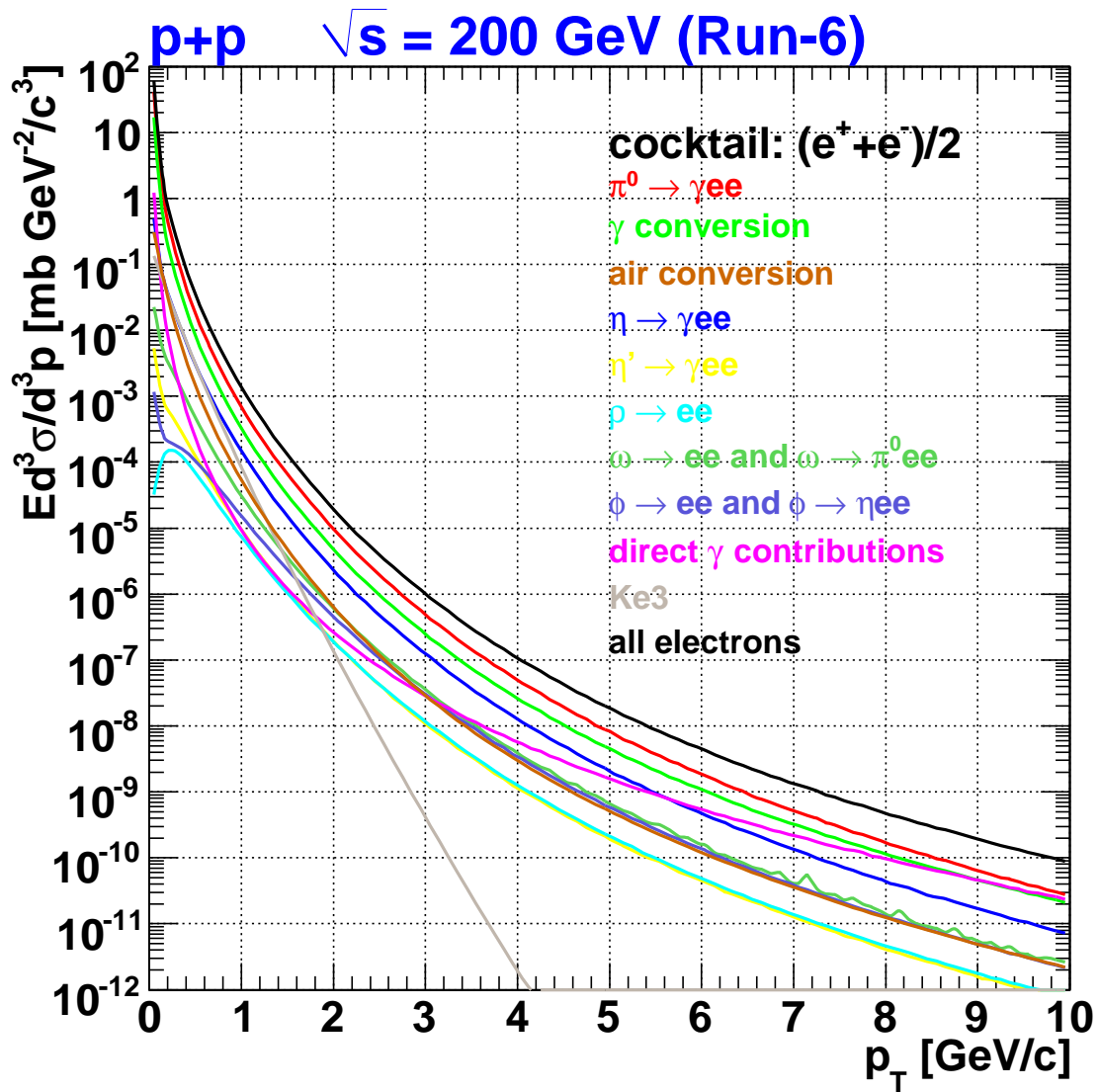


Figure E.6: Invariant cross section of electrons from all sources considered in the RUN6 p+p cocktail

Appendix F

Used RUN

F.1 RUN5

168314 168316 168320 168324 168326 168484 168486 168488
168490 168492 168494 168496 168666 168670 168672 168676
168681 168683 168705 168707 168709 168917 168920 169056
169058 169071 169198 169203 169205 169207 169209 169211
169213 169215 169217 169219 169221 169226 169303 169305
169307 169312 169314 169317 169319 169327 169329 169332
169518 169520 169522 169524 169526 169530 169535 169538
169540 169564 169566 169570 169572 169574 169576 169578
169584 169586 169588 169590 169592 169596 169717 169719
169721 169725 169727 169731 169733 169735 169832 169834
169836 169840 169842 169844 169850 169852 169854 169856
169870 169872 169876 169878 169880 169882 169884 169886
170005 170007 170009 170013 170015 170019 170021 170035
170037 170039 170043 170045 170049 170051 170053 170160
170162 170164 170166 170168 170170 170172 170176 170178
170201 170203 170205 170207 170209 170211 170332 170336
170568 170572 170574 170576 170578 170586 170670 170673
170675 170676 170678 170680 170682 170687 170695 170699
170701 170703 170705 170707 170709 170713 170715 170803
170805 170807 170809 170844 170846 170850 170852 170854
170860 170862 170866 170911 170915 170917 170921 170925
170927 170929 170931 170933 171072 171074 171076 171078
171080 171082 171084 171176 171178 171180 171182 171184
171186 171189 171191 171193 171195 171197 171199 171201
171203 171205 171207 171209 172163 172165 172167 172173
172175 172402 172404 172406 172408 172414 172416 172418
172420 172422 172452 172632 172634 172636 172638 172646
172648 172650 172652 172654 172656 172658 172660 172662

172664 172666 172668 172671 172781 172783 172785 172925
172927 172929 172931 172933 172935 173053 173143 173162
173164 173166 173168 173170 173172 173174 173176 173326
173328 173332 173334 173336 173338 173340 173344 173346
173348 173350 173352 173354 173356 173358 173434 173440
173442 173488 173490 173492 173494 173496 173498 173500
173595 173597 173684 173686 173689 173691 173693 173695
173697 173699 173701 173827 173829 173831 173836 173838
173840 173842 173844 173846 173848 173851 173853 173855
173857 173859 173861 173863 173865 173918 173922 173960
173962 173964 173968 173972 173974 173978 173980 173982
173984 173988 173992 174004 174169 174175 174177 174179
174181 174183 174185 174198 174200 174202 174206 174208
174210 174214 174308 174310 174312 174314 174316 174318
174320 174322 174376 174378 174380 174382 174384 174386
174388 174390 174438 174440 174442 174446 174448 174547
174549 174552 174554 174556 174558 174560 174562 174663
174665 174683 174696 174698 174700 174702 174704 174706
174708 174710 174714 174716 174720 174733 174735 174737
174744 174746 174748 174750 174806 174808 174810 174812
174814 174816 174818 174820 174903 174911 174913 174915
174917 174921 174923 175034 175039 175041 175043 175045
175047 175049 175051 175131 175139 175150 175154 175158
175160 175162 175164 175166 175168 175172 175182 175186
175187 175192 175194 175196 175244 175246 175248 175250
175253 175255 175257 175261 175308 175310 175314 175316
175318 175341 175344 175346 175348 175350 175359 175446
175448 175451 175453 175455 175457 175598 175599 175602
175606 175608 175610 175612 175620 175622 175624 175626
175628 175630 175632 175634 175636 175638 175640 175645
175646 175763 175765 175767 175769 175773 175775 175777
175811 175910 175912 175915 175917 175919 175921 175932
175934 175937 175939 175948 175950 175956 175974 175976
176103 176105 176107 176109 176111 176115 176119 176121
176123 176722 176727 176734 176759 176807 176809 176811
177029 177031 177033 177036 177038 177040 177042 177044
177052 177058 177062 177064 177066 177068 177070 177152
177154 177183 177185 177191 177238 177240 177296 177298
177300 177509 177514 177516 177518 177524 177526 177566
177568 177570 177625 177627 177629 177631 177633 177635
177637 177639 177641 177686 177688 177690 177779 177839
177843 177851 177860 177903 177905 177907 177911 177915
177917 177919 177979 178010 178012 178014 178018 178020

178022 178083 178085 178087 178089 178178 178180 178182
178184 178186 178188 178190 178198 178200 178202 178204
178206 178208 178422 178424 178426 178428 178430 178527
178529 178531 178543 178545 178547 178549 178551 178553
178555 178565 178567 178569 178571 178573 178575 178577
178579 178581 178585 178600 178604 178606 178745 178748
178750 178752 178754 178756 178759 178804 178806 178808
178810 178812 178814 178818 178820 178823 178825 178911
178913 178918 178920 178922 178928 178932 178934

F.2 RUN6

189580 189586 189588 189594 189595 189600 189601 189602
189613 189768 189770 189776 189777 189778 189782 189823
189824 189826 189827 189830 189841 189845 189850 189856
190456 190457 190458 190459 190461 190465 190466 190467
190468 190770 190771 190772 190773 190774 190776 190777
190891 190894 190895 190896 190954 190955 190956 190958
190960 190962 190966 191068 191070 191071 191079 191093
191095 191097 191098 191099 191100 191103 191104 191105
191107 191109 191110 191112 191215 191216 191219 191221
191309 191311 191320 191367 191370 191371 191499 191504
191549 191556 191630 191753 191756 191922 191924 191929
191932 191933 191934 191935 191936 191937 192488 192489
192496 192503 192505 192648 192650 192651 192653 192654
192656 192657 192666 192672 192675 192678 192869 192878
192879 192880 192881 192882 192909 192910 192911 192999
193024 193025 193045 193046 193053 193056 193057 193059
193063 193066 193067 193146 193147 193191 193197 193198
193568 193569 193570 193576 193577 193578 193581 193582
193583 193584 194312 194313 194315 194316 194320 194321
194450 194451 194454 194455 194456 194457 194458 194500
194501 194502 194504 194505 194522 194524 194526 194527
194528 194529 194531 194569 194570 194575 194576 194577
194578 194579 194580 194581 194744 194745 194746 194748
194760 194762 194763 194764 194766 194767 194772 194773
194777 194781 194782 194794 194797 194798 194799 194801
194802 194803 194804 194806 194925 194927 194928 194929
194930 195690 195692 195693 195694 195696 195697 195880
195884 195895 195900 195901 195903 197390 197391 197401
197402 197408 197409 197520 197521 197522 197523 197524
197525 197758 197762 197763 197764 197765 197766 197767
197768 197771 197772 197774 197794 197795 198063 198064

198134 198136 198160 198161 198162 198164 198165 198303
198306 198307 198308 198309 198355 198356 198357 198358
198359 198361 198362 198377 198378 198379 198386 198387
198389 198393 198440 198441 198443 198444 198445 198490
198494 198501 198502 198503 198508 198509 198511 198565
198566 198567 198568 198569 198570 198571 198572 198575
198576 198625 198627 198635 198731 198742 198748 198749
198750 198751 198752 198755 198756 198760 198761 198847
198979 198981 199105 199140 199141 199142 199143 199144
199145 199231 199238 199240 199241 199242 199244 199245
199266 199267 199268 199269 199270 199272 199273 199369
199372 199373 199374 199376 199377 199378 199379 199380
199381 199427 199429 199430 199431 199432 199433 199434
199435 199485 199486 199487 199488 199489 199490 199491
199492 199493 199498 199499 199500 199501 199502 199503
199504 199505 199506 199542 199543 199544 199545 199639
199640 199641 199642 199653 199654 199655 200240 200247
200357 200358 200367 200368 200370 200372 200373 200397
200399 200400 200401 200402 200450 200451 200452 200453
200454 200456 200457 200458 200459 200460 200461 200462
200582 200584 200585 200586 200587 200673 200674 200675
200676 200677 200678 200679 200690 200691 200692 200693
200695 200697 200698 200699 200700 200786 200787 200794
200803 200806 200888 200890 200891 200893 200894 200895
200896 200897 201001 201009 201013 201017 201026 201030
201031 201037 201038 201039 201128 201131 201234 201235
201242 201244 201247 201249 201333 201338 201468 201469
201726 201743 201756 201870 201872 201880 201885 201892
201895 202005 202006 202019 202021 202022 202023 202024
202025 202029 202045 202049 202166 202168 202169 202170
202174 202178 202188 202279 202287 202294 202325 202336
202340 202346 202347 202427 202428